Studies on the Effect of nano Manganous Tungstate and Zinc Sulphide as Potential Fillers for Styrene Butadiene Rubber and its Chlorinated form

Thesis submitted to the
University of Calicut
in partial fulfilment of the requirements
for the award of the degree of

Doctor of Philosophy
in
Chemistry

by

Jasna V.C

DEPARTMENT OF CHEMISTRY
UNIVERSITY OF CALICUT
KERALA

June 2018

DEPARTMENT OF CHEMISTRY
UNIVERSITY OF CALICUT
THENJIPALAM, MALAPPURAM
KERALA-673 635

Dr. M.T Ramesan **Tel: +91-9447837455**
Associate Professor **E-mail: mtramesan@uoc.ac.in**

Date: **…….**

Certificate

Certified that the research work embodied in the thesis entitled **"Studies on the Effect of nano Manganous Tungstate and Zinc Sulphide as Potential Fillers for Styrene Butadiene Rubber and its Chlorinated form"** has been carried out by **Jasna V. C** under my supervision at the Department of Chemistry, University of Calicut, Kerala and the same has not been submitted elsewhere previously for the award of any other degree or diploma.

Calicut University **Dr. M.T Ramesan**

DEPARTMENT OF CHEMISTRY
UNIVERSITY OF CALICUT
THENJIPALAM, MALAPPURAM
KERALA-673 635

Dr. M.T Ramesan **Tel: +91-9447837455**
Associate Professor **E-mail: mtramesan@uoc.ac.in**

Date: **…….**

Certificate

Certified that the research work embodied in the thesis entitled **"Studies on the Effect of nano Manganous Tungstate and Zinc Sulphide as Potential Fillers for Styrene Butadiene Rubber and its Chlorinated form"** has been carried out by **Jasna V. C** under my supervision at the Department of Chemistry, University of Calicut, Kerala and the same has not been submitted elsewhere previously for the award of any other degree or diploma. I also hereby certify that the corrections/suggestions from the adjudicators have been incorporated in the revised thesis.

Calicut University **Dr. M.T Ramesan**

Declaration

I hereby declare that the research work embodied in the thesis entitled **"Studies on the Effect of nano Manganous Tungstate and Zinc Sulphide as Potential Fillers for Styrene Butadiene Rubber and its Chlorinated form"**, is based on the original research work carried out by me under the guidance of **Dr. M.T Ramesan**, Asst. Professor, Department of Chemistry, University of Calicut, Kerala and the same has not been submitted elsewhere previously for the award of any other degree or diploma.

Calicut University **Jasna V.C**

Acknowledgement

I am indeed fortunate to have been working with a great number of people whose contribution in assorted ways to the research and the making of the thesis deserve special mention. It is only because of them I have reached my dream successfully. Hence it is a pleasure to convey my gratitude to them all in my humble acknowledgment.

*All the admirations are for **Almighty Allah**, who helped me in difficulties and gave me enough strength and enabled my life's long cherished dream come true...Alhamdulillah*

My research supervisor Dr. M.T Ramesan is a unique personality, sincere, helpful and much dedicated to his work. He is spending his late night for new innovations in this field, implies his family likewise sacrificing and supporting a considerable manner for the advancement of whole science. May almighty favour them and I consider myself extremely lucky to have sir as my guide. His vast experience and limitless knowledge in the field of Rubber Technology enabled me to complete my research work successfully. My heart is full of gratitude to him for the constant encouragement and valuable advice he rendered to me.

With great pleasure I put on record my deep gratitude to Dr. P Raveendran, Head of the Department for providing necessary facilities for the completion of my research work. I am extremely thankful to our former HODs, Dr. K Muraleedharan and Dr. V.M Abdul Mujeeb. With full respect and love I am remembering all the staff members for their hearty support; their sincerity and group strength is appreciable.

I convey my sincere thanks to my teachers in the department of Chemistry, Dr. N. K Renuka, Dr. Gangadevi, Dr.Kannan, Dr. Krishnankutty, Dr. Aravindakshan, Dr. D Bahulayan, Dr. Pradeepan Periyat and Dr. A. Yahya whose pertinent pieces of advice, valuable tips and immense motivation in the field of research has helped me considerably. I am extremely thankful to Dr. Abraham Joseph, for

sharing his expertise and valuable guidance. He motivated us during our M. Sc period and encouraged me to pursue the world of research.

With immense love and respect, I recall Dr. Muhammed Shafi, who is dependably a motivation and image of effortlessness for the understudies. Without knowing the left hand, he had helped me in my scholastic requisites.

There was a strong and mutually supporting polymer group in our lab, without mentioning them I can't step ahead. Being one of them is my greatest luck in the department. My love and prayers are always for you my dears Aparna, Sreejithetan, Jayakrishnan, Shaniba teacher, Subair sir, Jini and my best friend and co-worker, Nihmath; I cannot forget the days we played prank on many people with our looks. She resembled me like a twin sister, thus we confused many and we had real fun in those days. Her support and carers are boundless, no word to pay off my dear. Suhu, she is the youngest one in our group, beyond her childish smile she helped and stimulated me with fruitful discussions during my thesis writing. It is worthless without mentioning my co-worker, Anilkumar sir who helped me for the preparation of sample.

I am so much grateful to my labmates, who supported and loved me as a member of same family, I sincerely thank you my dear friends Rajeena, Soumya, Thasni, Jithin, Jency, Shyam and Shamsi. Many friends are there in our department; I express my heartfelt gratitude to all other research scholars in our department. I am also grateful to the young and energetic M. Phil students.

It is great pleasure to mention many extra ordinary personalities whom I met during this journey. I have no words to express my deep love and gratitude towards Bichuaka and Ayisha mol. They shared food and shelter for me when my elder prince was seven months inside me. Again, God blessed me with a very special couple Ranju and Anil as my neighbours. I take this opportunity to reveal my sincere thanks to their care, love and support in our daily life. Their sincere love towards our children was beyond words, it was always a positive energy to me.

I would like to acknowledge UGC Delhi for my JRF by thankfully remembering Starwin sir. A very special gratitude goes out to STIC Cochin for SEM and DSC analysis, NIT Calicut for SEM analysis and CFSE Manjeri for mechanical studies. I would like to thank Sarathetan, Safna, Jumana, Soufee, Unais and other friends who had helped me in my research work. I am deeply indebted to Dr. Pradyumnan, Department of physics, University of Calicut for facilitating XRD and conductivity studies. I am sincerely thanking Dr. Rosamma Alex, former joint director and Dr. Madhusudanan K.M, scientist, RRI Kottayam for helping me in characterization studies.

My neighbours in Calicut University, Safiya and Anwar mash, Babukaka and Cherimol, Unnietan and family, moreover my house owner who considered me always a little more and I thank them for their love and support.

I take this opportunity to express my gratitude towards my mentors who are the reason for me in this great achievement. Their countless encouragement and support was still my motivation to reach in high. It is my gratitude to mention I.B sir, Habeeb mash, Bapu sir, Alikutty sir and all my teachers in schools and colleges. My profound thanks for S.V sir for his fatherly affection support and still he is looking for my high position. Sir I don't know how I might give u back this much. I would like to appreciate your eagerness about your students.

It was my luck to be a daughter in law of two pure and most loving personalities. Their support is beyond imagination. Being from an undeveloped area, moreover being illiterate they have proved educational qualification is not essential to live, love and direct children in a right path. They are always my luck and models in this world. I salute them for their big mind for looking after my elder one at the early stage of my research. I again thank all the members in my husband's family, their respect and supports were motivated me to this point.

A wordy yardstick will not suffice to write my gratitude towards my parents. Not any daughter or son can do beyond what they had already done for us. Thanking God being their elder one, they are the exact

reason for my achievements, it was my mother's dream to write and qualify JRF to me, and she pushed me by filling full of confidence. But being a coolie and house wife, they had faced a lot to bring their children up to this level without revealing the difficulties. No words can express to thank them, and the endless love they have showed on me. That is why I have no doubt in my role models too. I will be failing in my duty if I do not mention my sincere thanks to my loving brother and sister for their love and support. My sincere thanks to the little brother of my father for giving laptop.

Boundless thanks to Majeedaka, who helped me to find out my perfect partner. Alhamdulillah, God blessed me by a great man, my husband, it was his dream to marry a science student and later it was again his strong determination to getting doctorate for his wife. He shared his will power, immense love, support and positive energy to me. Without these moral support, patience and the sacrifices that he had to make for enabling me to do my research, I would never have been able to fulfil my long-cherished desire. Thank you, my friend and husband, without you my life will not be complete and I am grateful to God for including you when he wrote my life. My love to your gift masters Sidhu and Aju, their smile always cooled my mind and released my all tensions.

Many to list....

Jasna V C

To

My beloved husband

"If I were to order anyone to prostrate to another, I would order a woman to prostrate in front of her husband"

Prophet Muhammad (SAWS)

Contents

	Page No
Chapter 1 Introduction	1-56
Chapter 2 Materials and Methodology	57-68
Chapter 3 Preparation, characterization, cure characteristics, mechanical, transport and electrical properties of Styrene Butadiene Rubber/Zinc Sulphide nanocomposites	69-100
Chapter 4 Chlorinated Styrene Butadiene Rubber/Zinc Sulphide nanocomposites; preparation, characterization, processability, mechanical, electrical and solvent diffusion properties	101-138
Chapter 5 Preparation, characterization, vulcanization, mechanical properties, diffusion study and electrical proprieties of Styrene Butadiene Rubber /Manganous Tungstate nanocomposites	139-168
Chapter 6 Nanocomposites based on Chlorinated Styrene Butadiene Rubber and Manganous Tungstate: curing, mechanical, electrical and solvent transport properties	169-204
Chapter 7 Conclusions and future outlook	205-214
Bibliography	215-231
List of Publication	232-235

Preface

Hybrid nanocomposites are relatively new types of composite materials. The nanoparticles incorporated polymer shows excellent properties, such as enhanced mechanical strength, fire retardancy, thermal stability, solvent and gas barrier properties. The large surface area of nano-fillers with high aspect ratio produces good reinforcement in polymers even at very low filler loading (< 15 %) as compared to conventional fillers, which requiremuch larger quantities of filler (>30%). Major challenges associated with the incorporation of nanoparticles into the polymer matrix include incompatibility between nanoparticles and polymer, agglomerating tendency of fillers and the poor dispersion of nanoparticles. Several strategies have been developed to enhance the uniform dispersion of nanoparticles in the polymer matrix. Most of these methods require an additional step of ultrasonication for the dispersion of nanoparticles in an organic solvent followed by mixing with polymer. The use of such solvents is harmful to our health and environment and therefore their use is limited in industrial applications.

Styrene butadiene rubber (SBR) is one of the most important synthetic elastomers due to its high volume production and low price. The major application of SBR is in the tire industry as well as for the production of footwear, conveyor, belts, hoses, flooring and adhesives. SBR vulcanizates have good abrasion resistance but their tensile strength is very low with poor flame retardancy, oil and ozone resistance. The reinforcement of SBR with polar fillers often leads to poor mechanical properties. This is due to the absence of interfacial

interaction between rubber and filler particles. Functional groups containing SBR or polar rubbers play a vital role in enhancing the interaction between the filler particles and elastomeric matrix. Chlorinated SBR with randomly distributed dichlorocarbene groups was prepared from SBR by the alkaline hydrolysis of chloroform leads to a stereospecific product with superior tensile strength than that of pure SBR. The introduction of chloro groups into the rubber showed excellent oil resistance and flame retardancy.

The mixing of different sizes and shapes of semiconducting metal nanoparticles with elastomers to form composite materials with physical characteristics of both organic and metallic components with a single composition. The metallic portion of the nanocomposite maintains good electrical properties and thermal stability whereas the polymer part can impart good mechanical properties to the elastomeric system. All these nanocomposites are prepared by expecting their vulcanizates with excellent thermal and solvent resistance, and also to get mechanically outstanding products. SBR nanocomposites are showing good solvent resistance towards aromatic and industrial solvents. But there is an extraordinary improvement in all the physical properties due to the presence of chlorine in the macromolecular chain. In this work, a detailed investigation has done on the effect of nano ZnS and $MnWO_4$ as potential fillers for styrene butadiene rubber and chlorinated styrene butadiene rubber.

The thesis divided into seven chapters. **Chapter 1** deals the introduction to polymers, polymer classification, polymer modifications and an overview of polymer composites and nanocomposites. **Chapter 2** deals with the materials, methods and different characterization techniques used in this work. **Chapter 3**

deals with the insertion of ZnS nanoparticles in SBR to study the interaction between ZnS and SBR, solvent imbibing and electrical properties of SBR/ZnS nanocomposites. The effect of ZnS nanoparticles on the structural properties of SBR was investigated by FTIR and UV spectroscopy. Moreover, the structure and morphology of the composites were examined by XRD and SEM. The glass transition temperature and thermal stability were examined by DSC and TGA respectively. The mechanical properties, AC conductivity and dielectric behavior of the nanocomposites were investigated with respect to various frequencies and volume fractions of nanoparticles. The diffusion and sorption behavior of both aromatic and industrial solvents through the cross-linked SBR nanocomposite were studied. **Chapter 4** discusses how metal sulphide nanoparticles affect the thermal stability, flame retardancy, processability, mechanical properties, conductivity and transport properties of sulphur vulcanized chlorinated SBR. The development of a new class of Cl-SBR/ZnS nanocomposites was done through a simple, inexpensive two roll mill mixing technique. The nature of nanoparticles in the Cl-SBR matrix was determined by infrared spectroscopy, UV- visible spectroscopy, X-ray diffraction (XRD), scanning electron microscopy (SEM) and transmission electron microscopy (TEM). The thermal stability, electrical properties, oil and flame resistance of the nanocomposites have been studied with respect to different loading of nanoparticles. Here the effect of the nature of penetrant molecules, loading of nanoparticles, and the temperature on transport solvent through Cl-SBR/ZnS matrix were evaluated.

In **chapter 5** $MnWO_4$ is used as reinforcing filler for the fabrication of styrene butadiene rubber (SBR) composite. $MnWO_4$ was

mixed with SBR in a two-roll mill mixing. The fabricated composites were characterized by FTIR, UV- visible spectroscopy, scanning electron microscopy and X-ray diffraction analysis. Thermal stability and glass transition temperature of the composites were carried out by TGA and DSC respectively. Processability, mechanical and electrical properties were studied with respect to different content of $MnWO_4$ nanoparticles. Also, the transport characteristics of aromatic hydrocarbons and petroleum fuels were studied through the nanocomposites to evaluate the reinforcement of the SBR matrix by the nanoparticles. In **chapter 6** we report a novel elastomer nanocomposite based on chlorinated SBR and $MnWO_4$. A simple open two roll mixing millwas used for the preparation of sample. The main objectives of the present investigation are to analyse the effect of $MnWO_4$ nanoparticles on the curing properties, structural, morphological, thermal, mechanical and electrical properties of the resulting nanocomposite. This study also focused on the effect of manganous tungstate nanofiller on ASTM oils, aromatic and petroleum fuels through sulphur vulcanized chlorinated SBR at different temperatures, thus calculating the overall performance of the nanocomposites. And finally, **chapter 7** contains the summary and future outlook of the present study.

1. INTRODUCTION

For the last decades, polymers became an inevitable part of human day to day life. Simply polymers are the macromolecules formed by the combination of one or more chemical units named as monomers as repeating units through chemical bonds are called as polymers. The word polymer is begun from Greek; here 'poly' signifies 'numerous' and 'mer' signifies 'units' [1,2]. It resembles a chain comprising of many globules punched through a string, the dabs of shaped chain are considered as monomer units and the whole chain resembles a polymer. Monomers are the building blocks of a macromolecular chain of polymers, on varying the monomer units we get a variety of polymers having different applications. The building blocks of a polymer are its monomer; they are the chemical units which forms the polymer string. Depending upon the monomer different types of polymers are formed. For instance, the most widely recognized polymer, PVC made out of 'n' number of vinyl chloride as rehashing monomer unit and the polypropylene contain propene as a monomer. There are numerous common polymers, for example, starch, cellulose and proteins which are exceptionally helpful for individuals. It is extremely hard to discover any items which are utilizing as a part of our everyday existence without having a string of polymer. The most energizing and wonderful case of the polymer are found in our body itself, for instance nails and hair contain keratin and every single cell core contains deoxyribonucleic acid (DNA). Today polymer materials having different applications in multifunctional territories, which begin from exceptionally basic house hold utensils, furniture, automobiles, so

on to space, the airship, aircraft, biomedical and surgical apparatuses [3–5].

We have natural resins and gums in our grasp as regular polymers, which were having novel properties. Before a century, there was a class of natural compounds categorized as colloids in order to differentiate them from crystalline materials. Later researchers investigated and synthesized new polymeric materials and the colloidal concept were thrown out. In 1860 the polymer with somewhat high molecular weight, i.e., polyethylene glycol was synthesized and studies were done to find out its structure. Polystyrene and polyisoprene were synthesized on polymerization of styrene and isoprene in 1839 and 1879 respectively [6–8]. The modern era of polymers is started by the use of rubbers. They are the first artificial product in the field of synthetic plastic industry, in 1832 Barconott synthesized cellulose nitrate as first example [9]. The vulcanization of natural rubber was done in 1839, by two scientists namely Goodyear and Macintosh [10]. In 1846 Schonbein prepared a stable product, nitrocellulose, hence the credit for the discovery of cellulose nitrate goes to him [11]. Hyatt investigated the cellulose derivatives in 1868 and it was known as celluloid which found applications as explosive and synthetic fibers [12].

During the period of 1893-1898 a viscose rayon fibers were discovered [13]. Another important synthetic rubber having better hardness and great heat resistance was introduced by Baekeland (U.S.A) in 1907, which is a purely synthetic rubber formed from phenol formaldehyde resins known as Bakelite; and having usage in

the area of a major industrially important thermosetting polymer [14]. In 1920, Staudinger, the father of macromolecular chemistry introduced macro-molecular hypothesis and which was the first landmark in polymer science. He suggested a long chain formulae for polystyrene, rubber and polyoxy methylene [15]. In 1924 cellulose acetate fibers and in 1926 to 1927 alkyd resins and polyvinyl chloride were also discovered [16]. Polyamide, polyester condensation polymers were synthesized and characterized by Carothers and his analysis was confirmed the macromolecular concept [17–19]. In addition to this neoprene (1931), polyvinyl acetate (1936), polystyrene, Buna S, Buna N (1937), nylon-66 (1938), melamine-formaldehyde resins (1939), butyl rubber (1940) were also considered as great explosion in the field of polymer industries [20–23]. At the time of World War II, a scientist, Flory studied and explained the mechanism for chain-growth reaction polymerization. He stated that the ending of the long chain molecule obeying a normal and satisfied valence structure, which helped to understand chemical method for the analysis of nature of end group [24, 25]. During this period Zeigler and Natta coordination complex polymerization helped to develop high density polyethylene and polypropylene. The discoveries in this area are still going on and the applications in the field of already discovered polymers are again in progress, hence researchers in this field are quite interesting and exciting [26–28].

1.1 Classification of polymers

Macromolecular chain containing polymers are having varying properties like different chemical and physical properties, mechanical

and thermal behaviors, etc. Hence polymers are broadly classified as natural and synthetic polymers [29, 30]. Naturally occurring polymers are natural polymers, they may be usually plant or animal origin. The polymers which are synthesized in a laboratory or industry by man are called synthetic polymers [1].

1.1.1 Natural polymers

These are naturally occurring polymers found in plants or animals; they are inevitable in day to day life. Examples include starch, cellulose, polysaccharides, proteins, nucleic acid, natural rubber etc. Many number of glucose molecules combined to form starch and cellulose. Amino acids on polymerization gives proteins, they are formed by the combination of 20-1000 amino acids. One of the important naturally occurring polymer is rubber, its monomer is 2-methyl 1, 3-butaidiene [31–33]. NR shows the glass transition temperature (Tg) at -70°C and its structure mainly composed of cis-1,4-polyisoprene as monomer units [34, 35]. Upon straining, NR can be crystallized and which offers excellent green strength and tackiness, which imparts vulcanizates having very high resistance to cut growth at severe deformations. They will undergo easily fractured on tearing, and the possibility of molecular scission become high due to the high shear stress and oxygen promoting nature. Hence modification of NR is essential and there are many commercially available examples such as deprotenized NR will inhibit water absorption, hence it is used in electrical appliances. One of the major processing ways for NR is the blending of ordinary and vulcanized NR at the ratio of 80:20 [36–38]. NR on compounding with fillers gives

extraordinary product with high solvent and weather resistant materials [39, 40]. On milling NR and butadiene sulfone, the product obtained will be an isomerized one and this cis-trans isomerization imparts an inhibition towards crystallization. NR on epoxidation has strain induced crystallization behavior and the modified rubber is very much resistant towards different oils, hence they have much importance in industrial field [41, 42].

1.1.2 Synthetic rubber

Synthetic rubbers are the elastomers mainly synthesized from the byproducts obtained from petroleum. Every year there is billion kilograms of rubbers are produced, two third of which are synthetic rubbers. Unlike natural rubbers, synthetic rubbers are used in the field of automotive industry mainly for the production of tires, different types of doors, hoses, manufacturing of belts, floor mats etc. [43, 44]. Nowadays the explosion in the field of motor vehicles and hence the vehicle tire production was started in around 1890s [45]. In 1909 the scientists from Germany prepared first synthetic rubber by polymerizing isoprene units. At the time of World War II, the natural rubber was found in shortage, then it was essential to synthesize artificial rubber in large scale and after the end of war it was again replaced natural rubber [22, 46]. Still the studies on the investigation of synthetic rubber was continued and in 1925 due to the price escalation of natural rubber majority of the companies were in competition for the replacement of synthetic rubber with natural rubber. The studies revealed the first successful synthetic rubber formed was neoprene, which possess high thermal and chemical resistance especially towards

different industrial solvents [47, 48]. Hence, they are mainly used in production of fuel hoses and insulating materials. During World War II, in the rockets nitrocellulose was used as propellants, later it was replaced with a solid fuel in which asphalt is mixed with an oxidizer and aluminium powder. The newly developed solid fuel was comparatively less dangerous to handle and which will burn very slowly than nitrocellulose. But there is a tendency of fuel to expel out of the rocket hence it is essential to find out a substitute for this fuel [49, 50]. In 1950's the researchers found a solution to this, here large missiles having solid fuels based on synthetic rubbers on mixing with ammonium perchlorate and a large ratio of aluminium powder were produced. They can be mold into large blocks without any cracks and any kind of defects that cause non-uniform burning of fuels. Thus finally synthetic solid fuels based on rubber is used in military rockets and also in missiles, hence it was a mild stone in the civilian space effort [51, 52]. After the war, there made some additional rectifications to the production of artificial rubbers. It was a great innovation in the field of rubbers that the synthesis of isoprene, which was gradually, reduced the use of natural rubbers. The main application of synthetic rubbers are in the field of printing in textile industry, for example titanium dioxide can be used with copolymerization and the volatile matter in producing such synthetic rubber for textile use [53, 54]. Moreover, this kind of preparation can be considered to be the pigment preparation based on titanium dioxide. An interesting thing about synthetic rubber that in 1960's some synthetic rubbers were used in production of chewing gum [55]. Synthetic rubbers are again classified in to two general purpose rubbers and special purpose rubbers.

1.1.2.1 General purpose rubbers

They are the hydrocarbon polymers including styrene-butadiene rubber (SBR), butadiene rubber (BR), and polyisoprene rubber etc. The presence of double bonds may cause easy attack of oxygen or even ozone to the unsaturated backbones in these rubbers. And also cause diffusion of solvents through the rubber, or we can say they are more susceptible to swelling by the hydrocarbon fuels. The main application of these elastomers is in the field of automobile industry and in the production of truck tires and some of them is discussed below.

i. Styrene-Butadiene Rubber(SBR)

Styrene-butadiene rubber (SBR) is a copolymer of styrene and butadiene introduced by Goodyear, and he called it as Neolite [56]. On protecting with additives, they possess better abrasion resistance and high aging resistance. It is reported that above 5 million tons of this rubber is produced worldwide in the year 2012. Moreover half of the total car tires are of from varieties of SBR [57]. The properties of SBR may vary on varying styrene/butadiene ratio; on increasing styrene concentration the product becomes harder and less tacky. On mixing styrene and butadiene and polymerizing those through two different methods a) emulsion (E-SBR) and b) solution (S-SBR), in which E-SBR is most commonly used one. The chemical structure of SBR is shown in **figure 1.1**.

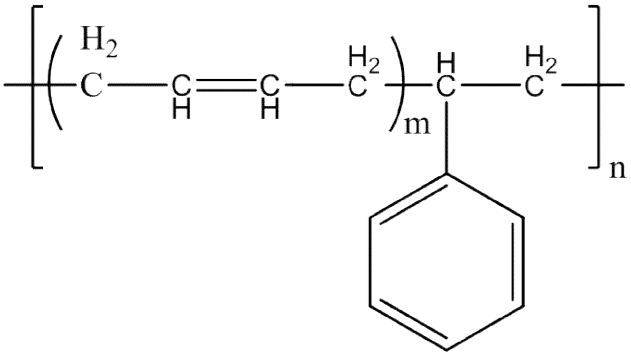

Figure 1.1 Chemical structure of styrene butadiene rubber

a) Emulsion polymerization

Free radicals are the initiators for emulsion polymerization; they are added to the reaction vessels containing monomers and a chain transfer agent like an alkyl mercaptan. Potassium persulfate and hydroperoxides are used as radical initiators by combining with ferrous salts. Soaps are used as emulsifying agents, the molecular weight, and viscosity of the product can be regulated by "capping" the growing organic radicals. The capping agents used are mercaptans for example dodecylthiol. Short stopping is a technique, by which polymerizations are found to result only to ca. 70%, thus one can remove different types of additives from the polymer [58].

b) Solution polymerization

Solution polymerization is carried out by an anionic polymerization, in which the process is initiated by alkyl lithium compounds. The presence of water should be avoided, all the reacting components are dissolved in suitable solvents and hence the process is said to be

homogeneous in nature which provides a control over the reaction [59]. The carbanion is generated by adding alkyl lithium into one of the monomers, which is then added to another monomer and the process is continued. On comparing with E-SBR, S-SBR is much favored due to its high water and rolling resistance, it again offers pleasing safety and its fuel economy is also very high [60].

The main applications of SBR in competition with natural rubber are as follows. E-SBR is widely used in pneumatic tires even though S-SBR is growing in popularity. It is also used in the production of shoe heels and soles, gaskets, and another interesting use is in the preparation of chewing gum. Instead of PVA, it is used as a sealing and binding agent behind renders, but high cost is its drawback. It possesses better durability, lower shrinkage and enhanced flexibility, as well as being resistant to emulsification in damp conditions. It is also used in cutting boards, as a binding agent in electrodes of lithium ion battery.

ii. Polyisoprene rubber (IR)

It is prepared by two methods namely anionic and Zeigler-Natta polymerization. Upon anionic polymerization, the product formed has 95% cis- microstructure, but on the second method it has about 98% stereo regularity. On comparing with NR, the green strength of IR is very less and it tacks more. The elongation at break and modulus of IR is comparatively lower than that of NR [61].

iii. Polybutadiene rubber (BR)

BR can be prepared as that of IR, i.e., either anionically or by Zeigler-Natta polymerization. It is also available in cold emulsion form. On anionic method, the prepared BR contains about 90% 1, 4 structure (an equal mixture of cis and trans forms) and 10% 1, 2 structure (vinyl). The anionic polymerization is done in hydrocarbon solvents, on adding a little amine or ether as a co-solvent the vinyl content can be increased. On the other hand, BR formed by emulsion polymerization mainly possesses trans microstructure, which does not crystallize. But the Zeigler Natta product contains cis as the major product and which can be crystallized [62]. Among rubbers, the lowest glass transition temperature is of low-vinyl BR and is found at -100^0C. While the high vinyl BR's reaches the Tg value at 0°C. Low vinyl BR on blending with SBR, NR and IR used for the manufacturing of tire treads having excellent abrasion resistance [63].

1.1.2.2 Special Purpose rubbers

General purpose rubbers have many limitations due to their low swelling and age resistance, hence special purpose rubbers have to prepare for meeting our needs.

i. Polychloroprene rubber (CR)

Chloroprene rubber is prepared by the emulsion polymerization of 2-chlorobutadiene and having a Tg of about -40°C. Due to the presence of an electron withdrawing group oxygen and ozone cannot attack the double bond and also the chlorine atom imparts polarity to the rubber,

which makes it solvent resistant. On comparing with general purpose elastomers, this is having very high weather and thermal resistance, flame retardancy and can easily combine with polar substrates especially with metals. They will not permeate air and water vapour through it. The CR microstructure mainly consist of trans-1, 4 and homopolymer grades, which can crystallize simply standing or by straining, in spite of its low stereo regularity as compared to NR. The crystallization can also be induced due to the presence of C-Cl dipoles which will enhance inter-chain interaction between the polymers. This rubber is mainly used for the production of wire, cables, hoses and many other mechanical goods [64].

ii. Acrylonitrile Butadiene Rubber (NBR)

NBR is formed by the emulsion polymerization of acrylonitrile and butadiene, which is named as nitrile rubber. The Tg of NBR is around 35°C. In this copolymer, the acrylonitrile part varies from 18-50%. NBR is also coming under polar rubber, in which acrylonitrile monomer imparts polarity to the system; hence they are resistant towards fuel and oil. On increasing the acrylonitrile concentration, the Tg of resulting polymer gets up and there is a reduction in resilience, swelling behavior, lowers gas permeability, an enhancement in thermal stability and hence strength of the rubber also increased [65]. Even though in NBR there is still some kind of oxygen and ozone attack occurs due to the presence of double bonds present in the butadiene portion. On blending with PVC the ageing behavior NBR can be improved. The main applications of this rubber are in sealing fuels and oils [66].

iii. Hydrogenated nitrile rubber (HNBR)

Ageing, fuel and heat resistance of nitrile rubber can be enhanced on hydrogenation, which is due to the removal of double bonds present in the rubber. It is used for oil field applications, in which hydrocarbons comes in contact with these materials, hence it is required even at elevated temperatures [67].

iv. Butyl rubber (IIR)

Isobutylene and a small amount of isoprene units undergo copolymerization to form butyl rubber. It is less permeable to gases and possesses excellent ageing due to the highly saturated structure. It is widely used in inner tubes and inner liners. Its brominated and chlorinated forms having very high cure characteristics also have many applications than general purpose rubbers [68].

v. Ethylene Propylene rubber (EPR or EPDM)

These are the low-density copolymers prepared by Zeigler-Natta and metallocene polymerization. The non-conjugated diene termonomer, like 1, 4 hexadiene, ethylidene norbornene, or dicyclopentadiene etc. are added for introducing unsaturated curates. There are only a very small number of double bonds present in EPDM (Ethylene- Propylene Diene Monomer) hence this method is used for getting more unsaturation. Commercially, 50/50 to 75/25 ratios of ethylene and propylene are used for the fabrication of EPDM. They have good heat and weather resistance. The partial crystallization of these rubbers

imparts high green strength to the rubber. It is mainly used in roofing, seals, gaskets and hose [69].

vi. Silicon rubber

Silicon rubbers have flexible siloxane backbones like carbon present in elastomers. The Tg of silicon rubbers is very low, for example, the Tg of polydimethylsiloxane is -123°C and they are very stable towards temperature. In addition, they possess good biocompatibility and hence they are used in implants and prostheses [70].

vii. Polysulphide rubber

Rubbers containing sulphur as the substantial proportion in their backbone are called polysulphide rubber. It can be prepared by the reaction between dichloroethane and sodium tetrasulphide having about 80% of sulphur to the total weight. Hence these rubbers are protected from many solvents like ketones and esters. These are used as permanent putties of fuel tank sealants, gaskets and fuel hose liners [71].

viii. Chlorosulphonated polyethylene (CSM)

Polyethylene on chlorosulphonation yields a very stable elastomer. They have very good weather ability and excellent flame retardancy. On increasing chlorine content, the oil resistance of the material increases while it is noted that low temperature flexibility and heat ageing resistance are enhanced by decreasing the chlorine content [72].

ix. Chlorinated polyethylene (CM)

Simple chlorination of polyethylene produces a new class of rubbers and are cheaper compared to chlorosulphonated polyethylene rubbers and its vulcanizates have lower compression set. The effect of chlorine content reflects in its resistance towards oils and fuels, but they have poorer heat resistance [73].

x. Ethylene-methyl acrylate rubber (AEM)

It is a terpolymer of ethylene, methyl acrylate and small amount of carboxylic monomer. The curatives used are amines and peroxides. These are resistant towards aliphatic solvents but are very poorly resist strong acids and some other hydrolyzing agents. They are used in power steering hose, transmission seals and spark plug boots [74].

xi. Acrylic rubber (ACM)

It is the copolymers of the acrylate monomer with a cure site monomer, like 2 chloroethyl vinyl ether. On comparing with ethyl acrylate, the Tg and oil resistance of butyl acrylate is found to be less. The oil resistance can be improved by copolymerization with acrylonitrile. ACM possess good thermal resistance, but they are less resistance towards alkali and acids. Applications are gaskets O-rings, transmission and seals oil hose production [75].

xii. Fluorocarbon rubbers

The most inert and very expensive fluorocarbon rubbers are produced by emulsion polymerization. It is made by the copolymerization of

fluorinated ethylene and propylene. Acids, alkalies or aromatic hydrocarbons cannot attack this rubber, while acetates and ketones can attack this rubber easily. Aircraft applications for these rubbers such as gaskets, O rings and seals.

xiii. Urethane rubber

Two types of urethane rubbers are available, i.e., polyester and polyether type. The polyether type has good hydrolytic stability, while the mechanical properties are poor. The vulcanization of urethane rubbers has to be done either with sulphur or using peroxide, and vulcanizates formed have excellent weather, abrasion resistance and refuse to swell in contact with oils. Applications include in gaskets, industrial rolls, shoe soles, castor wheels and conveyor belts [76].

xiv. Epichlorohydrin rubber

The polyepichlorohydrin are formed by the copolymerization of ethylene oxide and they have lower Tg. These rubbers are highly resistant towards solvents like aliphatic or aromatic hydrocarbons, also possess excellent building tack. It is very important to notice their resistance to ozone and decreased gas permeation and it resists heat up to 150°C. The main area of applications are packing, jackets, hoses, belting, cable and wire [77].

1.2 Modification of rubber

A rubber in its born form itself offers many useful properties, but in order to improve the mechanical and thermal properties of rubber, its modification is essential; which opens a wide area in the field of

research. The rubber modifications can be done either by chemical or by physical means or by the combination of these two. And is presented in **figure 1.2**.

1.2.1 Physical modification

The physical methods for the modification of rubber include incorporation of additives, which may not chemically react with the rubber; Oil extension, polymer blending, master batching, prevulcanization etc. There are very lower number of chemical reaction will take place between rubber and additives, which means the modification is only result of a physical combination of these [57].

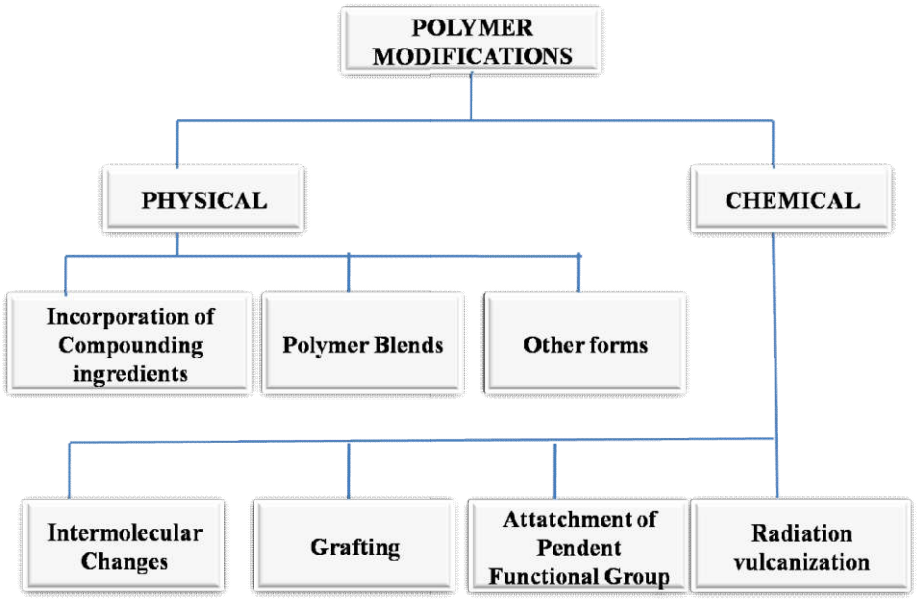

Figure 1.2 Scheme of modifications of rubber

1.2.2 Chemical modification of rubber

Chemical modification of rubber is an important study, in which the presence of double bond is the reason for their reactivity. The elastomers having unsaturation are of technological important because they are susceptible to various chemical reactions [78]. Thus, the chemically modified product is of extraordinary physical and chemical properties. The chemical modifications are of different types and they can be listed in the following manner

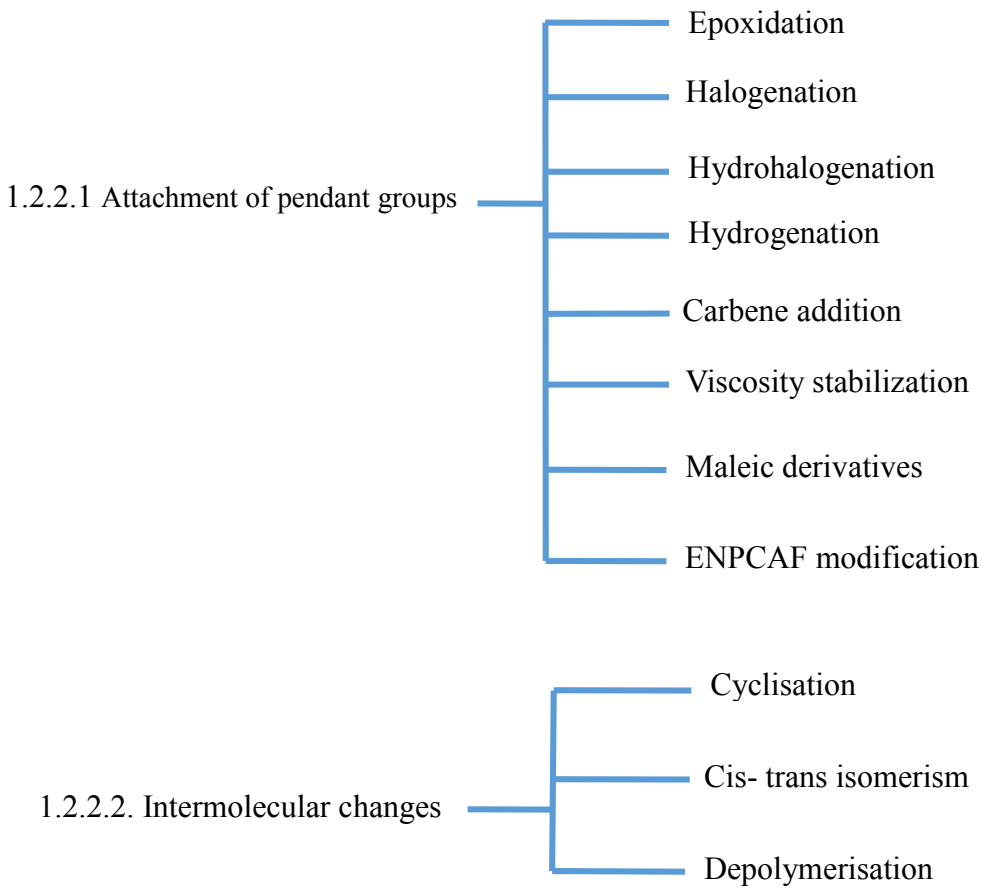

1.2.2.3 Grafting

1.2.2.4 Radiation vulcanization

1.2.2.1. Attachment of pendant groups

a) Halogenation

The unsaturation in the elastomers provides great interest and applications in chemical reactions which results products with excellent properties. The polymer reactions explaining the halogenations contribute a wide area to the young researchers. Halogenations may further because some complex reactions like addition, substitution, polymer degradations, sometimes cyclisation and cross-linking etc. Among the halogenated rubbers, brominated rubber possesses good adhesive properties and their cure rates are faster than its chlorinated forms. But on chlorinating the rubber one can improve the adhesion and cure characteristics of rubber. It is found that the flame, weather, chemical and oil resistance of the natural rubber is increases on chlorination. In order to resist corrosion of paints and pigments the chlorinated rubber is used as a protective coating, here it is applied by brush or even by spraying. Hence the main application of such paint is focused for resisting environmental attack come about in wood, steel, walls, and even in the paints of road traffic signals. One of the interesting advantages of chlorination of natural rubber is which lowers the frictional resistance and tackiness of surgical and household NR groves. Chlorinated styrene butadiene is with polyurethane adhesives are used in footwear industry [79, 80]. Chlorination can be done via different methods such as plasma

chlorination, acidified hypochlorite solution, chloramine solution, trichloroisocyanuric acid solution etc.

b) Hydrogenation

The scientist named Berthalot studied about the hydrogenation of natural rubber first [81]. Hydrogenation of synthetic rubber provides improved physical properties and they are more stable compared to unsaturated polymer matrix [82]. The elasticity of rubber is maintained even after hydrogenation having a relatively high molecular weight. Hydrogenation can be done by two ways, catalytic and non-catalytic methods. Catalytic method may be homogeneous or heterogeneous, and diimide and hydroboration are the examples of non-catalytic hydrogenation. A fully saturated NR is produced in a reaction, in which a 2% solution of rubber in cyclohexane is hydrogenated using nickel-Kiesleguhr as catalyst under 30-60 atm pressure and 200-220°C for 12h [83]. The fully hydrogenated rubber is prepared using a two component Nickel – Cobalt system with tri isobutyl aluminium. Singha et al reported the properties and applications of hydrogenated diene rubbers [84]. Upon hydrogenation the rubber become colourless and sometimes transparent [85]. They become a plastic type waxy solid material on stretching them they form threads. Hence hydrogenated rubbers are mainly used in cable industry and are mainly used in insulating materials. Completely saturated rubber is chemically inert. Hence the vulcanisation of fully hydrogenated rubber is very difficult, and partially saturated elastomers are still possessing vulcanizing behavior. They are used in many applications such as adhesives and rubber to metal bonding.

c) Hydrohalogenation

Hydrohalogenation of rubber can be done by using hydrogen chloride, bromide, iodide or fluoride in order to get rubber hydrochloride, hydro bromide, hydro iodide or hydro fluoride respectively. Of these the cheapest and the most feasible one is the addition of hydrogen chloride. On the other hand, the addition product of hydro bromide is not stable. While there is only a limited attention for hydrogen iodide addition and it is very difficult to prepare hydro fluoride product because of its toxic nature. On hydrohalogenation the chemical reactivity of rubber become declined which is due to the absence of double bonds this is what we expected on this modification. Bunn and Garner established the structure of rubber hydrochloride and also confirmed the addition of hydrogen chloride to polyisoprene is occurring purely according to Markonikoff's rule. Weber extended a great way to the hydrohalogenation of rubber by passing hydrogen chloride through natural rubber dissolved in chloroform [86]. The elasticity of rubber becomes very low on hydrohalogenation, which shows highly crystalline nature of the material and at room temperature they are very resistant to dilute acids or bases. Harries and Hinrichsen et a1 [87–89] reported the hydrogen bromide addition of NR; and all the reaction mechanisms are same as that of HCl addition, but the product is unstable. Hydrogen fluoride addition is reported by Tom [90]. There occur some side reactions such as cyclisation reactions, which can be avoided by selecting suitable solvent and appropriate temperature for the reaction; thus, formed product yields about 65-79% addition. The product formed will have high solvent resistance, and

they are less permeable to hydrocarbons. While the hydrogen fluoride addition is not encouraged due to its toxic nature and high cost.

d) Epoxidation

Epoxidation of NR and many other elastomers are of much interest in recent years. This study was investigated primarily by Pdummerer and Burkard [91], and then it was reported by Rouse et a1 [92]. Peracids react with trialkyl ethylenic double bonds present in NR and which forms epoxide groups. There is another problem related to epoxidation reaction, during this reaction, ring opening will occur as a side reaction; hence epoxidation reaction is of little interest. Malaysian Rubber Producers Research Association was developed this type of epoxidized rubber under controlled condition, which was a landmark in this area. The secondary ring opening in epoxidation can be controlled by applying required acid concentration and temperature. The 50, 25, and 10 mol % epoxidized rubbers can be prepared and are named as ENR-50, ENR-25, and ENR-10 respectively. Gelling and Morrison reported that epoxidized NR on sulphur vulcanization imparts poor ageing resistance as compared to vulcanized pure NR [93]. Due to improved wet resistance and rolling resistance in tire treads Epoxidation of NR is of great interest. They possess many applications such as a product having a better resistance to hydrocarbon oils, solvent resistance, adhesion and better resistance toward gas permeation.

e) Carbene addition

Carbenes (>C :) readily react with NR in presence of a phase transfer catalyst called quarternary ammonium salt. The later compounds will favour the aqueous reagents in contact with polymer containing organic phase. Cis-poly isoprene in aromatic solvent with dichlorocarbene prepared from ethyltrichloro acetate with sodium methylate gives a white power. Here the double bonds are modified as gem dichlorocyclopropane rings. Polyisoprene react with dibromocarbene produced insitu from bromoform give 70-75% saturation of polymer double bonds.

f) Viscosity stabilization

During the primary processing and subsequent storage under ambient conditions natural rubber becomes hard or highly viscous; which is the storage hardening and may increase by lower relative humidity. This is happened via the cross-linking reaction of carbonyl groups which are present in the main chain of rubber and the amino acid groups present in the non- rubber part [94]. Storage hardening may cause some complications like extra energy consumption. By the incorporation of chemicals like hydroxylamine hydrochloride, hydroxylamine neutral sulphate or semicarbazide this storage hardening can be eliminated. The above chemicals block the carbonyl groups present in the main chain and stabilize the viscosity of rubber.

g) ENPCAF modification

NR modified with ethyl N-pheny1carbamoyl azoformate (ENPCAF) is having only a scientific interest as in the case of hydrogenation. Upon

this modification we get an idea about the effect of polar pendant groups on the physical properties of NR. Knight and Pepper investigated the practical use of ENPCAF addition to NR [95], Barnard studied its use by means of chemically modified rubber [96]. This modification can be done in latex stage or mill mixing of rubber and the modifier at 110°C. Here the vulcanization of rubber can be done using sulphur system. The above reaction results in the formation of hydro ester pendent groups. On this modification the glass transition temperature (Tg) of the polymer increases. On comparing to pure rubber, the modified rubber possesses high damping. The solvent resistance and gas permeability of modified rubber also enhances. But it is difficult to bring in practical due to the high cost.

h) Maleic derivatives

The reaction between diene and maleic anhydride was interesting and it was first prompted by Diels Alder reactions; which is the reaction between simple conjugated dienes and activated unsaturated compounds, here we know the polymer unsaturation in all the diene polymers were not conjugated. The reaction between NR and maleic anhydride was studied by Bacon and Farmer, there the reaction was accelerated by benzoyl peroxide [97]. Infrared studies have indicated that on the reaction of polyisoprene with maleic anhydride the unsaturation or the change in cis-trans ratio will not affected. Pinazzi *et al*. showed that these reaction can be accelerated by using many catalysts like azodiisobutyronitrile or peroxides [98]. This proves the reaction follows a free radical mechanism involving a peroxide group instead of a specific reaction mechanism. The extent of addition

(expressed as the number of maleic anhydride units added per 100 polyisoprene units) is found to be less than 25. By the addition of amines like diethylamine the tendency of the product to gel has been solved. Over the years there was an interesting reaction of vulcanized maleated polyisoprenes due to their superior solvent resistance, flex cracking resistance and ageing resistance as compared to pure NR vulcanizates. Maleated rubber has not become commercially significant because of the great availability of polymers like plasticized PVC, ethylene vinyl acetate copolymers and the polyurethane rubbers etc. [99].

1.2.2.2 Intramolecular changes

a) Isomerization

Cis-trans isomerisation of unsaturated macromolecule like 1, 4-polyisoprene was investigated in 1950's. In 1957 Goulb investigated the conversion of cis-1,4-polybutadiene in to its trans isomer having an increase in crystallinity [100]. The isomerisation agents used are such as selenium, sulphur dioxide and butadiene sulphone. Isomerisation of rubbers can be done by thermal, photolytic, irradiative and catalytic methods. NR in thin film or sheets or crumbs can be isomerised on heating with SO_2 at a temperature of above 100°C. The stereo regularity and tensile strength of NR is reduced on isomerisation. In all methods there we get an equilibrium cis content of about 45%.

b) Cyclization

The cyclization of NR was the first chemical modification done by Bedford and Wilkinson [101] and NR on treatment with H_2SO_4 became

hard and brittle. It is also found the product formed after cyclization is less elastic too. It can be also done by using acidic catalysts such as p-toluene sulphonic acid and by Lewis acids like, $SnCl_4$, $TiCl_4$, BF_3 and $FeCl_3$. It can be done solid, solution or latex stage and it was seen that the product formed is have enhanced softening point, density and refractive index than NR. A very simple way of preparation of cyclised NR is by mixing 100 parts of NR with 8 parts of p-toluene sulphonic acid at 140°C. Cyclised rubber may find applications in adhesives, bonding agents, paints, shoe soles, hard mouldings, industrial rollers etc. and as a reinforcing resin.

c) Depolymerisation

In the market majority of the polymers available in their oligomeric forms; in which synthetic rubbers are found in liquid or semi liquid forms. In 1990 itself the liquid silicones and liquid butadiene rubbers have found wide acceptance amounting to 35,000 tonnes and 20,000 tonnes in a year respectively. By controlling the extent of polymerization, at the time of preparation from its monomers one can easily prepare synthetic rubber oligomers. NR has unique property in its production due to its high molecular weight as it obtained from the plant as such. Hence, it is important to depolymerise it in order to get lower molecular weight oligomers. But, the mechanical properties of liquid NR vulcanizates are lower than that of to its higher molecular weight counterparts. To get a highly cross-linked network on vulcanization the molecular weight of a liquid or sufficiently fluid rubber will not suffice. Due to the presence of loose chains and chain ends they cannot replace satisfactorily to the solid rubber. Progress in

this end demands a chemical breakthrough. Above that, the liquid rubbers are currently more expensive as compared to their solid form. On oxidative scission under controlled conditions will help the formation of liquid or depolymerised NR. They find application as plasticisers, a binder in the manufacture of grinding wheels and bowling balls, a cement for brush bristles, in corrosion-resistant paints, a sealant for pipe works and in the manufacture of printing rollers and battery boxes [102].

1.2.2.3 Grafting

Grafting of polymer can be done by two ways

a) Chemical grafting by using peroxides

b) Radiation grafting by gamma irradiation

Radiation grafting has some advantages on chemical grafting: such as time saving, controlled product quality there the reaction is done in a gamma chamber which regulates the overall grafting process. Moreover, it is a clean process where one can avoid the contamination of product with chemicals. On the other hand, the chemical grafting of NR was done by mixing with maleic anhydride. Where the modification of rubber was done by mixing 5% of maleic anhydride and 0.5% benzoyl peroxide with the rubber in a Brabender torque rheometer at100°C and 50 rpm speed for 10 minutes. Upon FTIR spectroscopy and titration, the reaction between maleic anhydride and elastomers were confirmed. Graft polymers of NR can be prepared by the polymerization of vinyl monomers in latex or in the solution forms.

For grafting NR the commonly used monomers are methyl methacrylate, styrene and acrylonitrile [103]. The most important and popular grafted NR is of polymethyl methacrylate; it has been commercialized in Malaysia with a trade name Heveaplus MG since mid-1950's. Blackly one of the great scientist recently reviewed the about the development of grafting at the period of 1950-1990 [104]. After that there occurs a considerable competency to get characteristics of thermoplastic elastomers for these grafted polymers by controlling polymerization conditions [105]. Using AIBN as an initiator, NR latex was grafted by styrene methylmethaccrylate and its efficiency is studied by using vinyl acetate which is reported by Lehrle *et al.* [106]. Using t-butyl hydro peroxide/TEPA redox system, Fukushima *et al.* compared the grafting of styrene on to NR obtained from extremely deprotenized latex and ammonia concentrated latex [107]. But the results show better towards latex concentrated with ammonia. The modulus of the rubber can be varied in accordance with the percentage of methylmethaccrylate grafted to it. It is called as Heveaplus MG, and the main application of this is in adhesives. They have many automotive applications like light shield, soft fronds, rear ends, rubbing strips and bumpers when Heaveaplus MG49 is blended with NR. There is another use as a compatibilizer in rubber-plastic blends [108]. It is seen that the styrene grafted NR is used in micro cellular soleings. Hoursten *et al.* [109] studied the modification of NR latex into the NR having an interpenetrating networks. Under controlled conditions, NR latex can seed the emulsion polymerization of an extremely hydrophobic monomer namely vinyl neo-deaconates [110].

1.2.2.4 Radiation vulcanization

It is a new method of vulcanization of rubber, typically reaction of latex and gamma rays in the presence of normal butyl acrylate as sensitizer. In order to decrease radiation, rate the sensitizer is used here. The main advantages of radiation vulcanization over sulphur vulcanization are the absence of n-nitrosamines, low cytotoxicity and protein allergy. This radiation vulcanized latex can be used for the commercial production of gloves, condoms, catheters etc. In India, radiation vulcanization plant with a capacity of 3 tonnes/day installed in Rubber Board is the only facility available for the production of vulcanized latex.

1.3 Composites

Human civilization has a great history of modifications done for the construction of novel materials. Years ago, to improve the strength and performance of materials and to attain humankind's technological needs, the utilization of cheap and easily accessing materials are very common. Nowadays also there is a continuous use of cost-effective fillers are inevitable for the construction of variety of products. Composites are the joined results of at least two parts having diverse properties, consolidate to frame altogether different material having predominant properties than that of individual ones. A polymer itself has not much thermal stability, green strength, and flame or weather resistance. Hence additives are added to improve these properties of polymers. Composites can be made by incorporating fibres, metals and mineral fillers into elastomers and plastics [111]. The idea of filler, its

fixation, shape estimate and even their interfacial communication amongst polymer and matrix will influence the nature of composites. Composite materials are formed by combining two or more materials having characteristic interface in between them. Composites contain two distinct phases, one continuous and another discontinuous phase. The continuous phase is the matrix, and the stronger and stiffer discontinuous phase is called reinforcement. Every constituent protects singular character, since they won't absolutely union or disintegrate in each other. The composites are valuable in planning fabricator, for assembling types of gear and purchasers can meet their requests in various zones with fulfilment. Depending on the nature of fillers, especially on considering the size of fillers they are classified into micro and nanocomposites. If the filler size is above 100nm the composite is said to be micro and if it is below 100nm which comes under nanocomposites. In the development of nanotechnology nanocomposites are having most critical position.

1.4 Nanocomposites

Class of composites with one of the phase in nanometer range are called nanocomposites. Because of the additional common properties and applications in many fields, nanocomposites are considered as another option to micro composites. Due to the difficulty in controlling elemental stoichiometry and composition, preparation of nanocomposites is still a challenging one. In 1991 the discovery of carbon nanotubes and its applications in fabrication was milestone in nanotechnology. Comparing conventional composites, the reinforcing nanoparticles possess high surface area to volume ratio [112]. The

reinforcing fillers may be particles, sheets or fibres. The most studied nanofillers in the area of polymer matrix are nano-clays. Research in material science reveals the amount of filler in the polymer nanocomposites are very less, hence the processability of neat rubber is retained. They show improved product with good thermal stability, electrical conductivity, flame retardancy, chemical resistance, mechanical strength, surface appearance etc. These whole improvements in properties are accomplished even by a low substance of nanoparticles. Polymer nanocomposites are also used in making thin film capacitors of integrated circuits and also in batteries as solid polymer electrolytes. All these promise a wide area for research field. On adding filler, the barrier properties of composites also increased [113]. Nano fillers offers haze characteristics and transparency to the film. They are used in timing belt cover, fuel hose in automobile, engine cover and oil reservoir tank too. Nanocomposites are also used in sensors, tire cords for radial wires, in automotive industry as interior and exterior body parts, food grade drinking containers, an electric component, artificial bio-implants etc.

1.5 Polymer Composites

For the last few years, composite materials replaced many other materials such as metals, wood, polymers, metal alloys and ceramics. Based on the filler, composites can be classified into fibre reinforced composites, particle reinforced composites and structural composites. Nanocomposites are also classified on the basis of matrix used; they are ceramic–matrix composites, metal–matrix composites and polymer–matrix composites.

Polymer–matrix composites are prepared on mixing polymers and inorganic reinforcing fillers like reinforcing fibres like carbon, glass, etc. or with particulate solids like carbon black, talc, calcium carbonate, mica, etc. Thus, formed composites have synergistically derived properties of both matrix and inorganic filler components. They exhibit excellent mechanical and thermal properties by maintaining the processabilty. Conventional polymer composites required a higher concentration of filler loadings sometimes it is ≥ 20 wt% [114]. By using nanofillers, traditional composites can be replaced with more effective materials known as nanocomposites having a considerable attraction in technological developments.

1. Ceramic matrix nanocomposites
2. Metal Matrix Nanocomposites
3. Polymer matrix nanocomposites

1.5.1 Ceramic Matrix Nanocomposites

Nanocomposites of ceramic matrix with having one phase at nano meter range comes under a new generation emerging material in engineering and have an industrially wide area of applications. Mechanical and electrical properties of nanoceramic composites are excellent due to its microstructure. Ceramic matrix nanocomposites can be prepared by different methods, spray pyrolysis, conventional powder method, precipitation and colloidal methods and chemical methods like sol-gel method. Examples for ceramic matrix

nanocomposites are Al_2O_3/SiC, SiO_2/Ni, Al_2O_3/SiO_2 and Al_2O_3/TiO_2 [115].

1.5.2 Metal matrix nanocomposites

Metal matrix reinforced with nanoparticles are come under these metal matrix nanocomposites. They have different and much improved chemical, physical and mechanical properties than that of matrix materials. The nanoparticles can improve damping characteristics, wear resistance and mechanical properties. Nowadays researchers are investigated more about this metal matrix nanocomposite because on embedding with nanoparticle, wide range of useful applications are satisfied. The interaction of nanoparticles will impart an improvement in mechanical properties due to the restriction of nanoparticles to the dislocation movements. The common techniques used for the processing of metal matrix nanocomposites can be processed by spray pyrolysis, rapid solidification, liquid metal infiltration, vapour techniques and also chemical methods like sol-gel and colloidal methods. Examples for metal matrix nanocomposites are Al/CNT, Fe-Cr/Al_2O_3, Fe/MgO, Ni/Al_2O_3 and Mg/CNT [116].

1.5.3 Polymer matrix nanocomposites

Polymer matrix with nanoparticles as reinforcing materials comes under this category. The fillers can be nanotubes or fibres (one-dimensional), the clay having a layered structure (two-dimensional) or spherical particles (three-dimensional). With a very small concentration of nano fillers, the polymer nanocomposites attain outstanding properties like strength and elastic stiffness; this offers

both academic and industrial applications for this. Polymer nanocomposites possess many applications as wear resistance, barrier resistance, optical properties, flame retardancy, magnetic and electrical properties. The interaction between polymer matrix and fillers are weak intermolecular force, but sometimes it may be a chemical bond. If there is a chemical bonding between the matrix filler, there is a remarkable improvement in the mechanical properties of the nanocomposite material, which means there occurs an unexpected or exotic change in properties. Hectorite, montmorillonite and saponite are commonly used clay minerals which provide high strength to the composites.

Polymer nanocomposites have excellent properties like lightweight, easy processing, high durability, low cost, corrosion resistance, and ductility. Polymer matrix nanocomposites have decreased thermal, electrical and mechanical properties in comparison with metal and ceramic matrix nanocomposites. Also, they have very low heat resistance, gas barrier properties and fire performance. Polymers have very low coordination number are made of using lightweight atoms like carbon and hydrogen in its backbone hence they are less dense compared to metals and ceramics. Therefore they are used for the production of automobile, electronics, defense and aerospace materials though they are the structural and construction materials used for lightweight applications [117]. Investigations revealed that even a nanoscale range of fillers can change the materials into a new world. Nanoparticles having high surface area and surface energy with anisotropic geometry when combines with polymer matrix

reduces the interparticle distance in one side and enhance the interaction between polymer and nanoparticles. Polymer nanocomposites having extremely useful properties with outstanding applications are brought forward in the space of traditionally filled polymer composites.

1.5.3.1 Properties of polymer matrix nanocomposites

The properties of nanocomposites depend on the properties of both matrix and fillers, and also which may vary according to orientations and types of filler, extent of adhesion at the interface of matrix, method of nanocomposite fabrication, effectiveness in mixing of both phases, nanoparticle characteristics like size and shape of fillers used, volume fraction of nanoparticles and the morphology of entire system [118]. For obtaining nanocomposites with outstanding properties, the nanoparticles must disperse or distribute in the matrix properly, because there is a chance of agglomeration of nanoparticles which cause deterioration of nanocomposites. The aggregates on nanocomposite will limits the enhancement in properties, hence for obtaining best properties, homogeneous dispersion of nanoparticles on the matrix is essential [119]. Nature of interface between the nanoparticle and the matrix also affect the enhancement of properties.

The most widely recognized element of polymer matrix nanocomposites is the presence of phase border amongst network and filler material and the advancement of interface layer between the two. The properties, content and microstructure at the interface vary over the interface region and are unique in relation to both matrix and filler.

If the interface region possesses a better bond between matrix and filler material the general properties of the nanocomposite will be much significant. A large portion of the interphase properties rely upon the bound surface and hence the nanocomposite properties can be tailored by improving the interfacial bond between the nanofiller and polymer lattice. The collaboration between the interconnecting stages relies upon the proportion of surface energy of filler and framework. Nanosized particles have high surface area and the aggregate surface area of a nanoparticle decides the degree of interface phenomenon adding to the properties of nanocomposites. The thickness of the interphase area relies upon many factors, for example, adaptability, vitality of adsorption, and the degree of polymer chain entrapment. The interface structure decides the pressure or load exchange from framework to filler [120]. The host polymer needs better interaction with the nanofiller material surface either physically or chemically keeping in mind to achieve better polymer properties. Great attachment at the interface enhances interlaminar shear quality, erosion protection, weariness, dielectric properties, thermal dependability, and fire retardancy at low filler-volume portion [121]. The degree to which the host polymer properties modify additionally relies upon the viewpoint proportion, shape and introduction of nanoparticles. High perspective proportion nanoparticles have high surface territory contrasted with low angle proportion nanoparticles and high viewpoint proportion assumes a critical part in improving the properties of nanocomposites. Asymmetric nanoparticles, for example, layered silicates or carbon nanotubes upgrade polymer properties (tensile strength, shear modulus, viscosity) as it were, then symmetrical nanoparticles with circular

shape and so forth. Sheet-like nanoparticles improves polymer properties, for example, mechanical properties and gas permeability in comparison with highly symmetric and elongated rode like nanoparticles. The morphology of the composite portrays the structural property relationship of polymer nanoplatelets kind of nanocomposites. The better distribution of nanomaterial is difficult to accomplish, particularly in non-polar polymer, however, uniform distribution of nanoplatelets guarantee the quality improvement of composites [122]. On account of nanocomposites containing layered reinforcements, according to the processing techniques, nature of the filler (layered silicate, polymer matrix and organic cation), the interaction between polymer matrix and layered nanomaterial and their dispersion techniques, the microstructure of nanocomposites can be classified as, intercalated, exfoliated and phase aggregated [123]. At the point when the polymer can't be intercalated between the silicate layers, an aggregated composite is framed; whose properties are nearly the same as that of conventional micro composites. In intercalated nanocomposites, the polymer chains intercalate into the silicate layers in a crystallographically regular manner, without considering clay to polymer proportion.

1.5.3.2 Types of Polymer Matrix Nanocomposites

The major component of nanocomposites of polymer matrix is the polymer itself. For example there are nanocomposites of thermosets, thermoplastics and elastomers like NBR, XNBR and SBR [124]. The decision in choosing polymer matrix for getting ready polymer matrix nanocomposites for a particular application is for the most part guided

by their biocompatibility, optical, mechanical, attractive, electrical, fictionalization and chemical stability. Generally thermoset matrix nanocomposites are most regular nanocomposites and are utilized as a part of numerous applications, yet thermoplastic-based nanocomposites have pulled in a great part of the research intrigue both in the industry and the scholarly community. The properties of polymers, for the most part, depend upon the polymer structure, which again based on the chemical composition, processing techniques and surface morphology. The contrast amongst thermoplastic and thermosets polymer is that they react all together diversely to the heat and this is essentially because of the distinction in their atomic structure.

a) Thermoplastics

Upon heating, thermoplastics become soften and then to liquid on further heating. As there is no cross-linking take place, the curing of thermoplastics occurs completely reversible manner. They liquefy on heating and solidify on cooling. This property enables thermoplastics to be remoulded and reused without influencing the properties [125].

b) Thermosets

Thermosets include polymer that cross-interface together amid curing procedure and frame an irreversible chemical bond. Instead of softening or melting, they breakdown on heating continuously. Thermosets have enhanced mechanical properties, high chemical and temperature resistant properties. On comparing with thermoplastics, thermosets are rigid and brittle [126].

c) Nanocomposites based on SBR, NBR and XNBR.

Researchers were attracted on working elastomeric nanocomposites filled with various nanofillers due to very good mechanical, electrical, dynamic mechanical, thermal, ageing and fire retardancy of the nanocomposites. Nanoparticles considered for the arrangement of elastomeric nanocomposites filled with nano silica, layered silicates, extended graphite, carbon nanotubes and so forth. There are little reports on the utilization of layered silicates as reinforcing fillers in rubber industry, however, there are enormous works detailing the improvement in thermal stability, mechanical properties, barrier properties, fire retardancy and so on. The montmorillonite (MMT)is the most widely utilized and contemplated layered silicate is [127].

Various methods and techniques were used for the preparation of rubber clay composites, for example, solution blending, melt intercalation mixing, co coagulating elastomeric matrix and by mill mixing. Wu *et al.* 128] produced SBR, NBR, and XNBR and NR/clay nanocomposites by a co coagulating procedure reported a new idea of 'isolated' elastomeric/clay nanocomposites as against the intercalated and exfoliated structures. The impact of NBR reinforced with organo modified montmorillonite was synthesized by melt intercalation method by Kim *et al.* [129]. NBR reinforced with unmodified clay composites were synthesised by Kader *et al.* [130] by a latex mixing strategy. Das *et al.* [131] contemplated nanocomposites of carboxylated nitrile elastomer reinforced with organomodified clay under different blending conditions. At higher temperature the change in properties were much higher than that the initial one. They

introduced a mechanism for the greater interaction of layered silicate distribution with carboxylated nitrile rubber(XNBR) [132]. A similar group investigated the use of XNBR in the production of superior elastomers by melt mixing. Fritzsche *et al.* [133] took a shot at XNBR, containing 10 wt% of layered silicate and researched the properties utilizing dynamic-mechanical studies and dielectric properties. By latex coagulation and melt intercalation strategies Salehi and Kashani studied the SBR/clay composites, but it was found that the better scattering and better properties were acquired for the clay composite prepared by first method [134]. Also, SBR reinforced with organomodified MMT composite produced by the latex technique have better properties on comparing to the composite prepared by the compounding technique. Again, SBR clay composites were prepared by mixing SBR latex with clay and coagulating the mixture by Zhang *et al.* [135]. NR reinforced with silane modified kaolin composites had excellent thermal stability, mechanical properties and gas barrier properties. Studies on the tensile properties of unmodified kaolinite and octadecyl amine modified kaolinite and NR composites were synthesized by latex compounding technique revealed that the uniform dispersion of silicate layers is the important parameter in upgrading the physical properties of the prepared composites [136]. Acrylic acid and poly acrylic acid modified kaolin reinforced NR and SBR composites were synthesized by Zoromba *et al.* [137]. NR composite were also synthesized by Yahaya *et al.* using tea seed oil modified kaoiln [138]. Nitrile rubber with excellent mechanical properties such as tensile strength, ageing resistance, abrasion resistance, and so on when mixed with a flexible filler like MWCNT resulting outstanding properties. For

the preparation of MWCNT/ elastomers composites, Perez *et al.* proposed an effective technique known as melt mixing technique [139]. NBR/MWCNT composites prepared by this method demonstrated enhanced properties, for example, they have better solvent resistance, upgraded glass transition temperature, enhanced storage and loss modulus because of the higher interaction between the nitrile group of the polymer chain and the functional groups incorporated in MWCNT surface. The morphological and electrical properties of the prepared NBR/MWCNT composite were again studied Verge *et al.* by melt mixing strategy [140]. The grafting of polymer chain onto the CNT was done very easily by the free radicals produced on the surface of NBR on heating and shear mixing. For the first time, by using a two roll mixing mill Chen and Song [141] prepared SBR/MWCNT composites and an enhancement in the mechanical properties like elasticity, tear resistance, Shore hardness and abrasion resistance of the composites were observed. Powder SBR/clay composites by spray drying of the suspension of CNT in SBR latex was synthesised by Zhou *et al.* [142]. Predominant mechanical and electrical properties of graphene have cleared the path for the preparation of polymer composites in advanced area. Zhan *et al.* produced NR graphene composites by ultrasonically helped latex compounding and an insitu reduction of graphene oxide [143]. The influence of functionalized graphene sheets (FGSs) on the better mechanical properties and strain-induced crystallization of NR was studied by Ozbas *et al*. [144]. NBR/nanographite composites synthesized by latex compounding method and mechanical mixing by Wang *et al*. [145].

1.5.3.3 Processing techniques for fabrication of polymer nanocomposites

Fabrication of polymer matrix nanocomposites can be done either by a chemical or mechanical process. Uniform and homogeneous distribution of nanoparticles in the polymer lattice is one of the significant issues experienced in the fabrication of polymer nanocomposite. There is a possibility of nanofillers to agglomerate and form micron sized clustors of filler, which confine the scattering of nanoparticles in the polymer matrix in this manner the properties of nanocomposites get deteriorating. Scientists have made many endeavours to scatter nanofillers consistently and homogeneously in the polymer network by chemical methods, very complicated polymerization reactions or modification of filler materials [146]. Generally, polymer nanocomposites are manufactured by the accompanying four techniques.

1. Intercalation method
2. Melt intercalation method
3. In situ polymerization
4. Sol gel method
5. Direct mixing of polymer and nanofillers

1. Intercalation method

Intercalation strategy largely includes the scattering of nanoplatelets sorts of nanomaterials into the polymer matrix. It is notable that

incorporation of clays (nanomaterial) into polymer networks enhances the mass properties, for example, shrinkage, stiffness, and flame retardancy. Intercalation is a best down approach and requires modification of nanoplatelets for the homogeneous scattering of plate-like nanofillers in the polymer matrix. Intercalated morphology happens when polymer chains diffuse into the display dividing of layered structure [147]. The nanoplatelets can be homogeneously scattered by the accompanying two procedures.

a) Chemical technique

This procedure includes the in-situ polymerization strategy in which nanoparticles are scattered in monomer and afterward polymerization occurs. In this strategy, nanoplatelets are scattered into polymer took after by extra polymerization process. The nanoplatelets are swollen in monomer solution and the polymer development happens between the intercalated sheets by polymerization technique.

b) Mechanical technique

In this strategy, a direct intercalation of polymer with nanoplatelets happens by solution mixing. The polymer is dissolve into a solvent and nanoplatelets sheets are swollen in such solvent and these two solutions are combined, the polymer chains in the formed solution intercalate into the nanoplatelets layers and which displace solvent.

2. Melt intercalation method

Melt intercalation is a promising technique broadly utilized in industry. This technique includes mixing the nanofillers into the polymer matrix

at melting temperature. In this strategy, the annealing of the mixture of polymer and nanofillers are done either by stastically or under shear. This strategy is perfect for current mechanical procedures, for example, injection and extrusion molding and it permits the utilization of polymers, which are not appropriate for in situ polymerization or solution intercalation. Melt blending is also a similar technique, it includes the melting of polymer powder or pellets to produce a viscous solution and nanofillers are incorporated into polymer by high shear rate accompanied with high temperature diffusion. By compression molding the final form of constituents can be fabricated by injection molding or compression molding or fibre production strategy.

3. In situ polymerization method

In situ polymerization includes the swelling of the nanofillers in monomer solution since the lower monomer solution has lower molecular weight, which can very easily seep within the layers inducing swelling. The subsequent mixture is polymerized either utilizing radiation, initiator diffusion, heat or by an organic initiator. The monomer is then polymerized between interlayers accordingly framing either intercalated or exfoliated nanocomposites. There is a similar method named in situ template synthesis, in this strategy, the clay layers are produced in polymer chain itself. Here the matrix and clay layers are simultaneously dissolved in aqueous in the presence of the gel, is refluxed at high temperature. The polymer chains are caught inside the clay layers and nucleation and growth of mud layers happen on the polymer chains at this high temperature. The main drawback of

this procedure is that high temperature causes disintegration of the polymer.

4. Sol- gel method

It is a base up approach and it depends on a contrary principle than all the previous strategies. The term sol-gel is related to two relations steps, sol and gel. A colloidal suspension of solid nanoparticles in monomer solution is called sol, and a 3D interconnecting system framed between stages called gel. In this technique, nanoparticles are scattered in the monomer solution, framing a colloidal suspension of nanoparticles (sol), they result interconnecting system between phases (gel) by polymerization took after by the hydrolysis methodology. The polymer works as a nucleating agent and advances the development of layered crystals. As the crystals develop, the polymer is seeped amongst layers and therefore nanocomposite is produced.

5. Direct mixing of polymer and nanofillers

Direct mixing of a polymer network and nanofillers is a top down approach of nanocomposite manufacture and it depends on the breakdown the agglomerated nanofillers at the mixing process. This strategy is reasonable for manufacturing polymer network nanocomposites and it includes two general methods for mixing the polymer and nanofillers. One way is the mixing of polymer, in the absence of solvents, with nanofillers over the glass transition temperature of the polymer, generally called melt compounding technique. The other way includes mixing of polymer and nanofillers

in solution utilizing solvents are called solvent method/solution mixing.

Melt Compounding

This technique includes addition of nanofibres expansion to the polymer over the glass transition temperature. In this sort of strategy, a hydrodynamics force is incited in the polymer which liquefies by viscous drag, and this hydrodynamics force is utilized to breakdown the nanofiller clusters and in this way advances homogeneous and uniform nanofiller scattering in the polymer lattice.

Solvent Method

In this technique, nanoparticles are scattered in the particular solvent and polymer is disintegrated or dissolved in a co-solvent. The subsequent nanocomposites are sustained from solvent through a solvent evaporation or by the solvent coagulation technique. In this technique, the shear stresses instigated in the polymer framework are brought contrasted down with that in melt compounding. The nanofillers are pre-scattered in the solvent by sonication keeping in mind the end goal to breakdown the nanofiller aggregates. The polymer nanocomposites created by one of the above strategies are at long last handled by regular processing techniques like calendaring, injection moulding, compression moulding, casting, rotational moulding, blow moulding, thermoforming, extrusion moulding and so on.

Mill mixing

This strategy depends on the incorporation of filler with the other reagents into the polymer matrix in an open two roll mill. The sample obtained after mixing is then vulcanized based on its cure time, pressure and temperature keeping in mind the end goal to get the required composite.

1.6 Nanoparticles

A nanoparticle is a fundamental component in the fabrication of a nanostructure having dimensions between 1 to 100 nm. Nanoparticles are generally the final products of a series of chemical, physical and biological processes. Metallic nanoparticles have different chemical and physical properties than their bulk counterparts (e.g., lower melting temperatures, specific properties, high surface area, mechanical strength etc.). These properties are very attractive for various industrial applications. A nanomaterial (dimension <100 nm) can take many forms such as particle, wire, tubes, rod and sphere. Nanoparticle products generally include silicon dioxide, metal oxides, quantum dots, some layered structures and dendrimers. In recent years, the development of new nanoparticles has been growing rapidly. The categories of nanoparticles are as below: articles, pole and circle. Nanoparticle items by and large incorporate metal oxides, quantum specks, silicon dioxide, dendrimers, and some layered structures. Lately, the improvement of new nanoparticles has been developing quickly. The classifications of nanoparticles are as beneath

Fullerenes

Fullerenes are an unadulterated type of carbon atoms as a tube, hollow sphere, ellipsoid, and also in different shapes. Fullerenes are comparative in structure to graphite, which is made out of a sheet of connected hexagonal rings, yet they contain pentagonal (or in some cases heptagonal) rings that keep the sheet from being planar. Spherical fullerenes are named as buckyballs. Carbon nanotubes are circular in nature. Fullerenes are like graphite in structure, which is made out of a hexagonal ring that shapes a three-dimensional structure. Fullerenes were first synthesized by laser removal of graphite focus in helium gas. In any case, laser vaporization is likewise utilized as a part of fullerene synthesis. Alternate methods utilized as a part of fullerene synthesis are done by the thermal disintegration of hydrocarbon and thermal plasma pyrolysis [148].

Carbon Nanotubes (CNTs)

Carbon nanotubes are long, thin cylinders of carbon, and were first found by Lijima and Ichihashiin 1991 in Japan utilizing an arc discharge strategy [149]. These are extensive macromolecules having one of a kind size, shape and have striking physical and mechanical properties. CNTs are a unique type of fullerenes, comprising of concentric layers of graphite (multi-walled CNTs) isolated by Van der Wall forces. Even though, CNTs made out of a solitary layer (Single-walled CNTs, or SWCNTs) were additionally found. CNTs are comparable in structure to C60 (buckyballs), yet they are stretched to frame a tubular structure. A solitary walled CNT has a dimension of

0.6–5 nm, though a multi-walled CNT has an internal measurement of 1.5–15 nm and an external diameter across of 2.5– 50 nm. CNTs can be created in different aspect ratios, and their lengths additionally fluctuate, contingent upon the preparing procedure. Nanotubes have an extensive variety of electronic, warm, and basic properties that change contingent upon the various types of the nanotube (characterized by its breadth, length, and chirality, or turn). CNTs are a decent case of genuine nanotechnology, since they are under 100 nanometer in distance across and can be more slender than 5 nanometers [150].

Nanowires

Nanowires are greatly thin wires having a diameter across on the range of few nanometers or less. There are two procedures that are commonly part used to produce nanowires: suspension and deposition. The nanowire is made out of either conducting or semiconducting nanoparticles with a diameter across between 1 to 100 nanometer and high aspect ratios. These wires are likewise named as "quantum wires" since quantum effect turns out to be more prevailing at the nanoscale [151]. Different kinds of nanowires are being manufactured including metallic, semiconductor and protecting nanowires.

Quantum Dots

Quantum dots are modest semiconductor nanostructure that binds the movement of electrons in the conduction band, holes in valence band or excitations of bound sets of conduction band electrons and valence band holes in each of the three spatial directions. They have a diameter of 2-10 nanometer (10-50 particles) having novel electronic, optical,

catalytic and magnetic properties. Analysts have discovered their applications in numerous territories, for example, sun-powered cells, transistors and LEDs [152].

Carbon Black

Carbon black is the purest form of elemental carbon exists in the form of colloidal particles that are synthesized by incomplete combustion or by thermal decomposition of petroleum derivatives like fossil fuels. It is generally utilized as a part of rubbers, tires and numerous plastic items and also in printing ink. Usually, anthropogenic burning of petroleum derivative creates different types of particles, including some ultra-fine particles that perfectly match with nanoparticle definitions, and in this way alluded to as carbon black, having particle size in the range of 10-300 nm [153].

Dendrimers

Dendrimers are a group of three-dimensional nanoscale macromolecules having a star-like structure with highly branched design. Dendrimers have three primary segments: an inner core, branches and surface gathering at the outside surface. Dendrimers of various shapes and sizes can be created by shifting these three parts. Their structure significantly impacts their chemical and physical properties. Dendrimers are a perfect candidates for applications in science, designing and material science [154].

Nanoclays

Nanoclays are actually the nanoparticles obtained from layered mineral silicates, have turned into a class of inorganic and organic hybrid

materials. Depending upon the chemical constituents and morphology of particles, nanoclays are classified into various classes, for example, bentonite, montmorillonite, hectorite, halloysite, and kaolinite. They come under hybrid inorganic and organic nonmaterials with potential applications in polymer nanocomposites, as gas absorbents, rheological modifiers and carrier bags for drug delivery. Layered silicate is a nonexclusive term alluding to synthesized layered silicates (laponite, montmorillonite and hectorite) and also natural clays. Montmorillonite is the most widely recognized nanoclay utilized as a part of numerous materials applications. The plate-like montmorillonite comprises of a one-nanometer-thick aluminum silicate layer surface changed with cations having dimensions estimated in 100 nanometers.

Nanocrystals

Crystalline particles having atleast one dimension in nanometers are called nanocrystals. Relying upon the methods in their formation the behavior of nanocrystals can be varied. They have been utilized as a part of the fabricate of channels that refine raw petroleum into diesel fuel. Nanocrystals can likewise be layered and applied to flexible substrates to create solar panels. They can be consolidated into electronic devices like light emitting diodes (LEDs). They are additionally discovering application in other areas like sensors, catalysts and solar cells.

Metallic Nanoparticles

The term metal nanoparticle is utilized to depict nanosized metals with dimensions (length, width or thickness) within the range of 1-100

nanometers. A nanoparticle is an essential segment of a nanostructured material. Generally, the measure of a nanoparticle is of 1– 100 nm. Metallic nanoparticles display diverse chemical and physical properties than their mass partners and some of these properties may demonstrate appealing in mechanical applications. Nanoparticles have some extraordinary highlights, for example, high surface energy, high surface area-volume proportion, quantum confinement, short-range order, and so on. The commercially accessible metallic nanoparticles are Au, Ag, Pt, ZnO and other metal oxides such as copper oxide (CuO), TiO_2, SiO_2, aluminum oxide (alumina) (Al_2O_3), and some iron oxides (Fe_2O_3 and Fe_3O_4). Metal sulphides like CuS, nickel, iron sulphides etc.

Nowadays polymers find application in flexible electronics, which are used in flexible displays, electronic solar cell arrays, conformal antenna arrays, flexible batteries, RFID tags, electronic circuit etc. In heart patients, sometimes there is a need for incorporation of electronic monitoring devices into the human body. Therefore, the electronics should frame of the object inside it to combine every complex movement of these objects satisfying the requirement for stretchability. In biomedical applications, the need of flexibility in stretching is important, then only they can undergo reversible deformation. A great scientist, Rogers and his group introduced a completely integrated stretchable electronics. They prepared a highly stretchable and simply foldable silicon integrated circuit on a wavy silicon ribbon, in a polymer matrix called polydimethylsiloxane (PDMS) and they introduced excellent devices like electronic eye sensor, implanted

medical devices, smart gloves and very useful ergonomic biomedical sensors for wearing [155]. Commonly used carrier substrate is viscoelastic or elastic polymer like silicos or polyurethanes. Nowadays it is very easy to utilize stretchable electronic products everywhere. One of the very interesting application is even in human body, which can control brain waves into heart activity, in which rigid flat batteries might fail. This is a great opening to polymer chemists, and many works are done inorder to modify rubbers as semiconducting or sometimes conducting [156]. From these inspirations, in the present work, an attempt is done using metallic nanoparticles in order to check whether there is any change in dielectric behavior of styrene butadiene rubber. For that we have selected two nanofillers, ZnS and $MnWO_4$ nanoparticles.

The $MnWO_4$ has as wolframite structure with intriguing electrical properties, appealing antiferromagnetic, sensing properties and superb photoluminescent [157, 158]. Additionally, the individual constituent of $MnWO_4$ is MnO and WO_3 which plays a noteworthy part in different electrochemical applications particularly for electrodes in super capacitor applications. The studies revealed that the thermal and electrical properties of nanocomposites were increased upon filler concentration [159]. Manganous tungstate ($MnWO_4$) is an imperative metal oxide with astounding properties, for example, photo catalytic activity, thermal resistance, optical fibers, photograph sensors, multi-ferroic materials and humidity sensor and so forth. Because of particular structure and properties, $MnWO_4$ demonstrates its critical part in the manufacture of different electronic gadgets. Saranya et al.

Synthesized polyaniline/$MnWO_4$ nanocomposites, and they found the prepared composites are thermally very stable and also possessed excellent electrochemical properties [160].

Metal sulphides, especially ZnS nanoparticles are used as great photo catalyst because of quick production of pairs of the electron-hole by the photo excitation and exceedingly negative reduction potentials of energized electrons; as conduction band position of ZnS in an aqueous solution, which will be higher than that of different semiconductors, for example, TiO_2 and ZnO [161]. Since a bigger proportion of surface to volume of a catalyst would encourage a superior synergist movement; the size controlled combination of ZnS nanostructures to deliver a bigger proportion of surface to volume is of extraordinary significance [162]. The improved surface to volume proportion causes an increment of surface states, which change the movement of electrons Synthesis, characterization of ZnS nanoparticles by precipitation technique utilizing different capping and holes, influencing the chemical reaction procedure. The size quantization expands the band gap of photo catalysts to upgrade the redox potential of conduction band electrons and of valence band holes [163]. As it is one of the first semiconductors investigated, which also shows remarkable applications in the field of science and technology as electroluminescence, biosensors, field emitters, electro catalyst etc. On comparing with bulk ZnS, the nano ZnS have fantastic chemical and physical properties, for example, improved surface to volume proportion, surface to volume impact and the quantum size effect,

chemical activity, higher optical absorption, catalysis, the low melting point and high thermal stability [164].

1.7 Scope and objectives of the present work

SBR finds broad application in tire treads, camelback, cycle tires, drive and transport lines, hoses, vibration mountings, safeguards, microcellular soles and other hard elastic items.SBR has more thermal resistance and lower gas penetrability in comparison with NR. Even though, it has poor gum quality and they easily susceptible to thermo-oxidative degradation. Numerous attempts have been done to increase the green strength of SBR by the chemical modification. It is the cohesiveness in stretched uncured elastic compound is of awesome significance particularly in tyre processing. For instance, in the development of radial tires uncured stocks might be subjected to twisting of up to three times of its initial dimension in the framing step. Carboxylation of emulsion SBR by copolymerization with carboxylic acids (acrylic and methacrylic) brings about items that have enhanced green strength. Carboxylation of SBR leads to better adhesion into fabrics and henceforth utilized as a part of backing carpet. Styrene-vinyl pyridine-butadiene terpolymer lattices have been produced primarily for application as rubber to-textile cohesive specifically as tire line cements. Copolymerization of styrene and butadiene with tertiary amine containing monomers followed by reaction with dihalides to frame few labile (shear and temperature sensitive) cross-links, likewise result in SRR with upgraded green strength. Protection from thermo oxidative disintegration is an imperative criterion to be fulfilled for elastomeric products utilized as a part of open air

applications. It is notable that the degradation of elastomer is mainly depends on the interaction with molecular oxygen. These reactions cause deactivation of double bonds. The properties of SBR can be improved by the reinforcement with nanofillers. The extensive use of these matrixes in industrial applications requires further improvement in these composites. The product with much solvent resistance is shown in the presence of polar functional groups. Thus, the elastomers can be modified by the dichlorocarbene addition, which can produce good enhancement in mechanical properties. Modified forms of SBR play a vital role in enhancing interaction between the filler particles and the elastomeric matrix. Chemically modified SBR with randomly distributed dichlorocarbene groups within the backbone of polymer reduces the degree of unsaturation in SBR. The introduction of chloro groups into the rubber showed an elevation of the glass transition temperature. The dichlorocarbene reaction using the alkaline hydrolysis of chloroform is stereospecific and hence the resultant chlorinated SBR (Cl-SBR) shows superior tensile strength compared to the pure SBR. Moreover, the oil resistance and flame retardancy of styrene butadiene rubber were drastically enhanced by the dichlorocarbene reaction. On reinforcing with nanoparticles, the mechanical, thermal and electrical properties can be improved in an inexpensive manner.

The main objectives of this work include

- Preparation and characterization of ZnS and $MnWO_4$ nanoparticles.

- Fabrication of SBR/ZnS, SBR/ $MnWO_4$ nanocomposites by a two-roll mill mixing technique.
- Preparation of Cl-SBR and its nanocomposites with ZnS and $MnWO_4$ nanoparticles.
- To characterize the nanocomposite using different spectral studies like FTIR and UV-visible, XRD, SEM, TEM, TG and DSC.
- To study the processability of SBR and Cl-SBR with ZnS and $MnWO_4$ nanoparticles using sulphur vulcanization techniques.
- To study the different mechanical properties such as tensile strength, tear resistance, hardness and abrasion resistance of ZnS and $MnWO_4$ filled SBR and Cl-SBR.
- To study the effect of ZnS and $MnWO_4$ nanoparticles on various electrical properties such as AC conductivity, dielectric constant and dielectric loss tangent of SBR and Cl-SBR nanocomposites.
- To study the diffusion and transport behavior in aromatic and industrial solvents at different temperatures.
- To study the oil resistance of Cl-SBR nanocomposites in ASTM 1, 2 and 3 oils.

2.1 MATERIALS

SBR (Synaprene 1502) was procured from Synthetics and Chemicals Ltd., India. Cetyltrimethylammonium bromide (CTAB), zinc sulphate and sodium sulphide for the preparation of ZnS nanoparticles, were purchased from HiMedia chemicals. Manganous chloride, sodium tungstate, sodium hydroxide chloroform, isopropyl alcohol and the solvents like benzene, toluene and xylene for diffusion studies were purchased from Merck India. The solvents like petrol (mol. wt. 100), kerosene (mol. wt. 170) and diesel (mol. wt. 230) were of reagent grade procured from Bharat Petroleum Corporation Limited, India. Rubber ingredients such as stearic acid, zinc oxide (ZnO), cyclohexylbenzathiazole (CBS), 2, 2, 4-trimethyl-1, 2-dihydroquinoline (TDQ), processing oil and sulphur were obtained from local chemical suppliers. Details of solvents used for diffusion studies are given in **table 2.1**

Table 2.1 Characteristic properties of Solvents used

Solvents used	Characteristic properties	
Benzene	Molecular weight ($gmol^{-1}$)	78.11
	Density (gcm^{-3})	0.874
	Boiling point (°C)	80
	Solubility parameter ($cal\ cm^{-3})^{1/2}$	9.2
	Molar volume	89.17
Toluene	Molecular weight ($gmol^{-1}$)	92.14
	Density (gcm^{-3})	0.867
	Boiling point (°C)	109
	Solubility parameter ($cal\ cm^{-3})^{1/2}$	8.9
	Molar volume	105.90
	Molecular weight ($gmol^{-1}$)	106.17
	Density (gcm^{-3})	0.860

Xylene	Boiling point (°C)	138
	Solubility parameter (cal cm^{-3})$^{1/2}$	8.8
	Molar volume	123.45
Petrol	Molecular weight ($gmol^{-1}$)	80-100
	Density (gcm^{-3})	0.710-0.737
	Boiling point (°C)	70-150
Kerosene	Molecular weight ($gmol^{-1}$)	150-170
	Density (gcm^{-3})	0.810-1.817
	Boiling point (°C)	140-230
Diesel	Molecular weight ($gmol^{-1}$)	170-330
	Density (gcm^{-3})	0.82-0.95
	Boiling point (°C)	240-350

For analysing oil resistance of the samples, ASTM 1, 2 and 3 oils (IRM 901, IRM 902 and IRM 903) which were having commercial grade used as such, and their properties are given in **table 2.2**.

Table 2.2 Characteristics of oils

Property	ASTM 1	ASTM 2	ASTM 3	ASTM methods
Aniline point (°C)	124±1	93±3	70±1	D 611
Viscosity – gravity constant	0.790-0.805	0.860-0.870	0.875-0.885	D 2140
Refractive index	1.4848	1.5105	1.5026	D 1747
Aromatics (C_A %)	3	12	14	D 2140

2.2 METHODOLOGY

2.2.1 Preparation of ZnS nanoparticles

ZnS nanoparticles were prepared using a hydrothermal method [165]. An equimolar ratio of $ZnSO_4.5H_2O$ and $Na_2S.7H_2O$ powder was

dissolved separately in de-ionized water. The sodium sulphide solution was then added drop by drop to the $ZnSO_4$ solution with constant stirring. The white precipitate formed was charged into the Teflon-lined stainless-steel autoclave and maintained at a temperature of 220 °C for 12 h., then cooled down to room temperature. De-ionized water, then alcohol was used to remove the impurities in the precipitate. The washing procedure was repeated several times to remove impurities from samples. After washing the precipitate, it was dried at 60°C in a vacuum oven for 12 h.

2.2.2 Preparation of $MnWO_4$ nanoparticles

$MnWO_4$ nanoparticles were prepared by the chemical co-precipitation technique [166]. Equimolar ratios of manganous chloride and sodium tungstate were dissolved in distilled water separately. Then cetyltrimethylammonium bromide in aqueous solution was added to the manganous chloride solution with constant stirring. Sodium tungstate solution was added drop wise to the above mixture with continuous stirring. The precipitated product was washed with water several times and dried. The dried powder was then calcined at 800°C for 5 h.

2.2.3 Chemical modification of SBR

Chlorinated SBR with 15% chlorine content was prepared from SBR by the in situ reaction of chloroform with aqueous caustic soda using phase transfer catalysis (CTAB), as reported earlier [167]. Briefly, after dissolving SBR in toluene, CTAB was added in to the solution with constant stirring. The chloroform was added drop wise followed

by an aqueous NaOH solution. By coagulating it with isopropyl alcohol, the chlorinated SBR was separated from the solution and dried. The scheme and molecular weight of SBR and Cl-SBR are given in **figure 2.1** and **table 2.3** respectively.

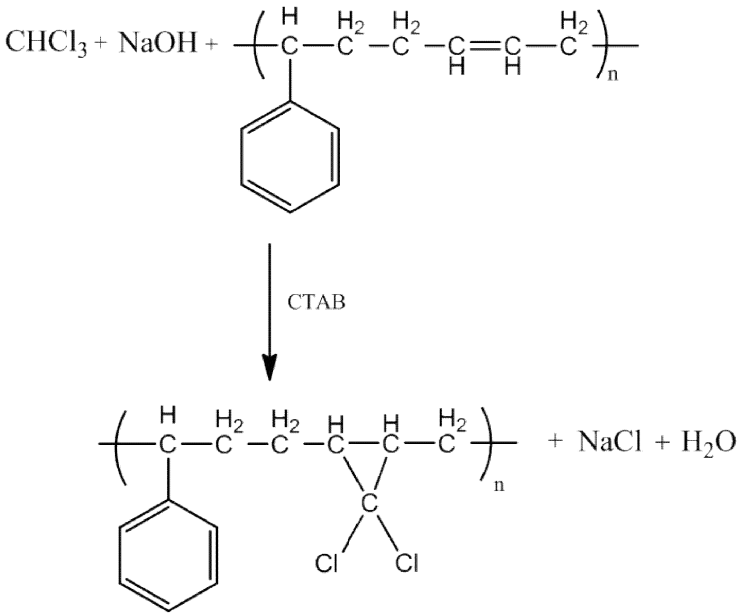

Figure 2.1 Chlorination of SBR

Table 2.3 Molecular weight of SBR and 15% Chlorinated SBR

Materials	M_n (Daltons)	M_w (Daltons)	M_z (Daltons)	Polydispersity
SBR	125,550	399,501	996,024	2.8633
Cl-SBR (15% Cl)	158,879	518,712	1,134,567	3.0987

2.2.4 Sample preparation

2.2.4.1 Preparation of SBR/ZnS, Cl-SBR/ZnS, SBR/$MnWO_4$ and Cl-SBR/$MnWO_4$ nanocomposites

Chlorinated SBR/ZnS, Cl-SBR/ZnS, SBR/$MnWO_4$ and Cl-SBR/$MnWO_4$ nanocomposites were prepared at room temperature in a two-roll mill mixing technique using the sulphur vulcanization procedure. Compounding of the individual matrix with different loadings of ZnS/$MnWO_4$ nanoparticles (0, 3, 5, 7, 10, and 15 parts per hundred parts rubber (phr)) was carried out in an open two roll mixing mill. The rotors operated at a speed ratio of 1:1.4. The vulcanization ingredients were added to the rubber before the addition of nanoparticles. Finally, the sulphur was added. The mixing was done at 28°C as pert he ASTM D-15-627 (1994) method, with special attention to ensure the uniform distribution of filler particles. The sample codes used for this study are SZ_0 for SBR with no filler loading, SZ_3, SZ_5, SZ_7, SZ_{10} and SZ_{15} are composites with 3, 5, 10 and 15 phr of ZnS nanoparticles, SM_0 is SBR with no filler loading SM_3, SM_5, SM_7, SM_{10} and SM_{15} are polymer composite with 3, 5, 10 and 15 phr of $MnWO_4$ nanoparticles, CSZ_0 for Cl-SBR without ZnS, CSZ_3, CSZ_5, CSZ_7, CSZ_{10}, and CSZ_{15} and CSM_0 is Cl-SBR with no filler loading CSM_3, CSM_5, CSM_7, CSM_{10} and CSM_{15} are polymer composite with 3, 5, 10 and 15 phr of $MnWO_4$ nanoparticles. The basic sulphur vulcanization formulations of SBR and Cl-SBR nanocomposites with different content of ZnS and $MnWO_4$ nanoparticles are given in **table 2.4**.

Table 2.4 Mixing formulation in sample preparation

Ingredients	Amount (phr)
Rubber (SBR/Cl-SBR)	100
ZnO	5
Stearic acid	2
TDQ	1
Processing oil	$1/20^{th}$ of filler
Filler (ZnS/ $MnWO_4$)	0, 3, 5, 7, 10 and 15
CBS	1.2
TMTD	0.8
Sulphur	2.2

2.3 CHARACTERIZATION TECHNIQUES

2.3.1 FT-IR spectroscopy

The IR spectra of the samples were recorded with a JASCO NO: 4100 Spectrophotometer. Absorption bands in the spectrum result from energy change arising as a consequence of molecular vibrations of the bond stretching and bending type. The IR region covers 4000 to 400 cm^{-1}. IR spectrum gave information about the structure of the compound. For taking IR spectrum, the samples were dissolved in chloroform and the solution was put to the surface of KBr pellet and dried.

2.3.2 UV-Visible spectroscopy

The UV-Vis absorption spectra of samples with different loadings of fillers were carried out by a Perkin Elmer Lambda 650 spectrophotometer. The sample was dissolved in chloroform and the solution was used for the analysis.

2.3.3 X-ray diffractometry (XRD)

The X-ray diffraction studies (XRD) of the composite materials were recorded on Bruker AXS D X-ray diffractometer using CuKα radiation (k=1.5406 Å) with an accelerating voltage of 30 KV. The diffractograms were recorded in the range of 2θ=10 to 80° at a speed rate of 2°/min. XRD is a rapid analytical technique used for phase identification of a crystalline material and can provide information on unit cell dimension. The interaction of the incident rays with the sample produces constructive interference and a diffracted ray when conditions satisfy Bragg's Law. These diffracted X-rays are then detected, processed and counted. The Bragg's diffraction angle (**2θ**), along with interplanar spacing (**d**), and the relative intensity of the peaks were calculated using Bragg's **equation 2.1**,

$$n\lambda = 2\mathrm{d}\sin\theta \qquad \textbf{(Eq: 2.1)}$$

Where, `**θ**' is one half of the angle read from diffractogram. Scherer's equation was

Used to estimate the particle size & the **equation 2.2** is,

$$\mathrm{D} = 0.9\,\lambda/\beta\cos\theta \qquad \textbf{(Eq: 2.2)}$$

Where; **D** - Average particle size

λ - Wavelength of radiation of the X-ray beam

β - Width of the peak at half of the maximum intensity (in radian)

θ - Half of the diffraction angle 2θ

2.3.4 Scanning Electron Microscopy (SEM)

By using Hitachi S-3000 H scanning electron microscope (SEM), the surface morphology of the nanocomposites was studied. Area ranging from approximately 1cm to 5 microns in width was imaged in a scanning mode using conventional SEM technique.

2.3.5 Transmission Electron Microscopy (TEM)

The structure of composites was analysed by a transmission electron microscope (TEM). Ultra- thin sections of the specimens for the TEM were prepared by cutting the rubber samples with a Reichert Ultracut E ultramicrotome at about 100°C and the images were collected from a TEM Libra 200 model.

2.3.6Thermal analysis

2.3.6.1 Differential scanning calorimetry (DSC)

DSC was done by Mettler Toledo DSC 22e at a heating rate of 10°C /min (atmosphere N_2; flow 40 ml/min). For the DSC analysis 5 mg of the material was heated from -80°C to room temperature under nitrogen atmosphere with a programmed heating rate of 10°C/min.

2.3.6.2 Thermogravimetric analysis (TGA)

Thermal decomposition behavior of the nanocomposite was studied using Perkin Elmer thermo gravimetric analyser from room temperature to 600°C at a heating rate of 10°Cmin^{-1} in nitrogen atmosphere.

2.3.7 Flame retardancy

The flame retardancy of the composite was carried out by a Stanton Red croft FTA flammability tester, under mixed nitrogen–oxygen atmosphere. The minimum concentration of the oxygen in the oxygen–nitrogen gas mixture environment just sufficient to sustain the flame for 30s was taken as the limiting oxygen index (LOI): and which is calculated using the **equation 2.3**

$$LOI = \frac{\text{Volume of oxygen}}{\text{Volume of oxygen+Volume of nitrogen}} \times 100 \qquad \textbf{(Eq: 2.3)}$$

2.3.8 Cure Characteristics

Vulcanization properties were studied using a Monsanto Rheometer R-100 at 150^{o}C according to ASTM D 2084-01. The rubbery materials were moulded in the respective optimum cure times in an electrically heated hydraulic press at a pressure of 40 MPa.

2.3.9 Mechanical properties

2.3.9.1 Tensile and Tear Strength

Tensile and tear strength of sulphur vulcanized SBR and Cl-SBR nanocomposites were measured using Zwick Universal Testing Machine (UTM) with a load cell of 10 kN capacity as per ASTM D 412-16 and ASTM D 624-00 respectively. The measurements were done at a cross-head speed of 500 mm/min at room temperature. Average of at least of five sample measurements represents each data point.

2.3.9.2 Hardness (Shore A)

By using Shore A type durometer, the hardness of the samples was measured according to ASTM D 2240- 95. The samples having a thickness of 6 mm were used for the harness measurement.

2.3.9.3 Resilience

The resilience of rubber is the ratio of the energy which returned back to its original position to that of the energy which is applied to deformation of the rubbers by indentation due to a single impact. Using a Dunlop Tripsometer, the rebound resilience rubber composites were measured as per ASTM D 1054-02.

2.3.9.4 Abrasion Resistance

The abrasion resistance of Cl-SBR and Cl-SBR/ZnS nanocomposites was carried out in a DIN abrader according to the DIN EN ISO 5470-01 method.

2.3.9.5 Compression Set

Compression set values was determined using the constant strain method, by keeping the compound at 70°C for 22 h, according to ASTM D 395-16 method B.

2.3.9.6 Heat Build-up

Hat build-up occurs in a rubber material when it subjected to a variety of compressive stresses in a controlled environment. The heat build-up

of Cl-SBR and Cl-SBR/ZnS nanocomposites was determined by a Goodrich flexometer according to ASTM D 623-07.

2.3.10 Electrical properties

2.3.10.1 AC-conductivity and dielectric properties

The dielectric constant of the elastomeric materials was analysed by automatic Hewlett Packard LCR meter (HP: 4284A) in the frequency range 10^2 to 10^6 Hz. Thin film of the samples was used to find out the dielectric constant. The capacitance 'C', loss tangent 'tanδ' and resistance 'R' were obtained. Dielectric constant or relative permittivity were calculated using the **equation 2.4**,

$$\varepsilon_r = C.\frac{d}{\varepsilon_0}.A \qquad \textbf{(Eq:2.4)}$$

Where; d- thickness of the sample, C- capacitance, A- area of cross section of the sample and ε_0- relative permittivity of air.

AC conductivity can be calculated using the **equation 2.5**,

$$\sigma_{AC} = \omega.tan\delta.\varepsilon_0.\varepsilon_r (\text{S cm}^{-1}) \qquad \textbf{(Eq: 2.5)}$$

Where; 'ω' is the angular frequency.

2.3.11 Oil resistance

Oil resistance of the samples were done using ASTM D-471 method; the vulcanized samples were immersed in ASTM 1, 2 and 3 oils at two different temperatures; 27 and 100°C respectively. The samples were taken out after 72 h and in order to remove oils on the surface, samples

were immediately dipped in acetone and wiped off using filter paper to remove excess oil from the surface. The oil uptake was assessed gravimetrically.

2.3.12 Sorption experiments

The diffusion and transport mechanism of elastomeric nanocomposites were done using circular samples which were punched out from the vulcanized samples using sharp edged steel die. Initially, the thickness of the sample was measured using a screw gauge and the weighed samples were immersed in about 20-25 ml of various solvents like benzene, toluene, xylene, petrol, kerosene and diesel taken in the diffusion flask. The solvent uptake was taken at regular interval of time and again immersed in the corresponding solvents. The weighing process of rubber vulcanizates was continued until an equilibrium stage was obtained. The solvent uptake measurements were repeated at various temperatures also.

3.1 Introduction

Over the last few years nanoparticles have fascinated the academic and industrial community. Nanocomposites, especially polymers as the matrix like elastomers lead to improved mechanical properties, flame retardancy, air and liquid barrier properties coupled with dimensional and thermal stability. Since they have the potential to replace engineering materials, find use as excellent substitute in construction and automotive sectors. Among the broad variety of nanoparticles available for the development of elastomeric nanocomposites, nanoparticles having specific functional group are desirable due to their novel properties, which further widen their applications [168–170].

Even though, elastomers are good insulators, flexible dielectric composite materials with a high dielectric constant and low dielectric loss tangent are of immense interest at present. Their uses include application as charge storage capacitors, electrostriction artificial muscles and as a material for controlled drug delivery. Metal oxides or metal sulphides nanoparticles are unique dielectric materials, having excellent thermal stability and therefore number of studies have been carried out to make the polymers thermally stable and conductive, by introducing metal nanoparticles [171, 172]. Flame retardancy, thermal stability and electrical properties such as the AC conductivity and dielectric properties of a polymeric system depend on the nature and amount of metal nanoparticles [173, 174]. The increase in AC conductivity of such nanocomposites stems from the formation of a continuous network of nanoparticles in the polymer matrix. These

conductive nanocomposite materials are being widely applied in the area of electrostatic discharge dissipation, electro-magnetic interference shielding and other electronic applications [175–177].

Among the widely used synthetic elastomers, styrene butadiene rubber (SBR) deserves a prominent place due to excellent abrasion resistance; thermal and aging stability. SBR is a major and unavoidable component of tyres, cables and insulating materials [178–180]. However, unfilled SBR has poor tensile strength, flame retardancy and oil resistance. The poor tensile strength is due to the absence of strain induced crystallisation and the highly amorphous nature of SBR. The mechanical properties can be improved by the reinforcement of SBR with filler particles, and the novel is by the incorporation of nanoparticles [181–183].

Polymer composites are widely used in the construction and automobile industries. In the automobile industry they serve as oil seals and gaskets. In order to have satisfactory performance, the oil seals should be thermally very stable [184]. During service if they subjected to excess temperature, the material may undergo thermal degradtion and may become soft. Also the contact of these materials with industrail solvents/fuels results in leakage problems and failure in sealing. The study of sorption, diffusion, and permeation in elastomeric nanocomposite provides valuable information about the interaction of the components, the mobility of the chain, and the distribution of organic solvent molecules in polymeric compounds. This study is essential to the successful use of the elastomeric composites in a wide range of applications. The transport properties of nanocomposites

strongly depends on the nature of the polymer, the nature of the penetrant, crosslink density, nature of cross-links, temperature and the polarity of the matrix [185]. Several works were carried out on the effect of nano-clay on the diffusion and sorption processes [186–188]. However, the studies on the transport of inorganic nanofillers with elastomers are few.

The main purpose of the work is to explore on the insertion of ZnS nanoparticles in SBR to study the interaction between ZnS and SBR and the diffusion and transport properties of SBR/ZnS. The effect of ZnS nanoparticles on the structural properties of SBR was investigated by FTIR and UV spectroscopy. Moreover, the structure and morphology of the composites were examined by XRD and SEM whereas the glass transition temperature and thermo gravimetric analysis were examined by DSC and TGA. The effect of loading of ZnS nanoparticles on the rheometer processing characteristics such as cure time and torque values of SBR were studied. The mechanical properties of sulphur vulcanized SBR nanocomposites namely tensile strength, modulus, elongation at break, tear resistance, hardness, abrasion loss, heat build-up and compression set were determined according to the filler loading. The AC conductivity and dielectric properties of the nanocomposites were investigated with respect to various frequencies and volume fractions of nanoparticles. The diffusion and sorption behavior of both aromatic and industrial solvents through the cross-linked SBR nanocomposite were studied.

3.2 Results and Discussion

3.2.1 FT-IR spectroscopy

Figure 3.1 shows the FT-IR spectra of SBR, ZnS nanoparticles and SBR/ZnS nanocomposites. The characteristic absorption band of SBR is observed at 2910 cm^{-1}, which arise from the CH stretching of phenyl ring. The band centered around 1470 cm^{-1} from the C=C modes in the phenyl ring. The absorption at 703 cm^{-1} is due to the out-of-plane aromatic ring. The *trans* –CH= mode of butadiene part appeared at 989 cm^{-1}[189]. FT-IR spectrum of ZnS shows an absorption band centered at 3483 cm^{-1}, which is attributed to the O-H stretching vibrations and the HO-H bending vibration (from atmospheric absorbed water) at 1622 cm^{-1}. The main characteristic band of metal sulphide is observed as a broad and strong peak at 615 cm^{-1}, which is the typical absorption of ZnS. The SBR/ZnS composite shows the characteristic absorption band of SBR with the typical stretching of metal sulphide. The typical ZnS vibration of composite appears at 609 cm^{-1}, indicating the interaction of nanoparticles with the SBR matrix. Moreover, the stretching vibration of *trans* –CH= group (989 cm^{-1}) in the composite shifts to a lower wave number region (976 cm^{-1}).Hence, it can be inferred that the absorption frequencies of nanocomposite are strongly influenced by the insertion of nanoparticles into the elastomeric matrix [190].

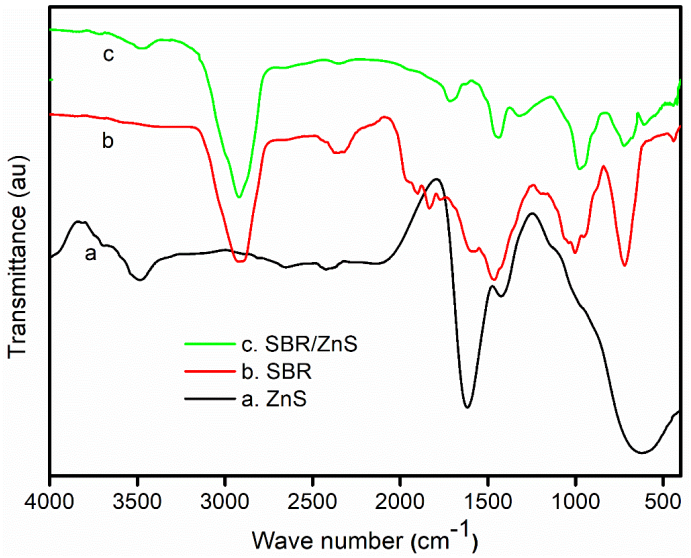

Figure 3.1 FTIR spectra of SBR and ZnS filled SBR

3.2.2 UV-Vis Spectra

Figure 3.2 shows the optical properties of SBR and SBR with different contents of ZnS nanoparticles. SBR shows a sharp and prominent peak at 297 nm due to the π-π* transition of the polymer.

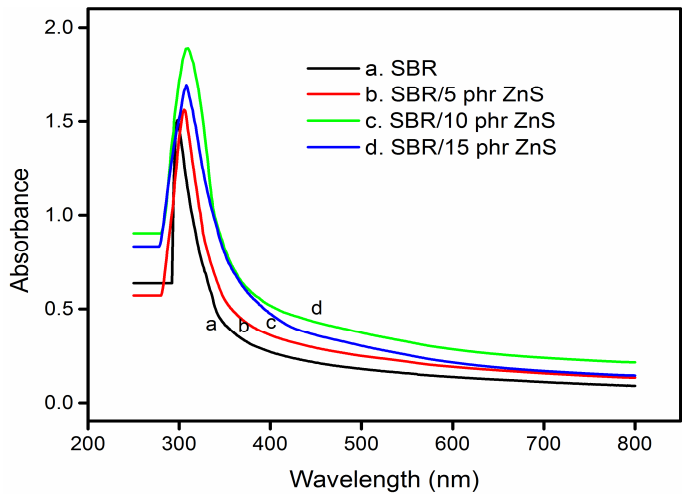

Figure 3.2 UV spectra of SBR and SBR/ ZnS nanocomposites

From the UV spectrum of nanocomposite, it can be seen that the characteristic peak of SBR is slightly shifted into a higher wavelength region and the intensity of the absorption peaks of all the composites are higher than that of pure SBR. For example, the sample with 10 phr loading shows a higher UV absorption peak at 309 nm. This suggests that the nanoparticles are uniformly dispersed into the elastomeric matrix which, in turn, increases the interfacial adhesion between the nanoparticles and the SBR chain. It can also be seen from the figure that the absorption edge of nanocomposite is higher than SBR in the entire range of UV absorbance from 200 to 800 nm. The intensity and broadness of the nanocomposite is found to be increasing with the addition of nanoparticles up to 10 phr loading. This means that the interfacial adhesion maximum at this loading. The lower absorption edge of the composite beyond 10 phr loading is due to the clustering of nanoparticles in the elastomers and this leads to the poor interaction in the polymer matrix.

3.2.3 X-ray diffraction analysis (XRD)

XRD was used to probe the structure of SBR/ZnS nanocomposites and is displayed in **figure 3.3**. The XRD of ZnS (**Figure 3.3 (e)**) shows that the 2θ values at 28.79, 48.23 and 56.97° are the corresponding crystal plane of (111), (220), and (311) respectively of the cubic phase of ZnS matching with JCPDF 80-0020. The XRD peaks are broadened due to nano crystalline nature of the synthesised ZnS. No additional peaks are detected for impurities in the sample confirming the phase purity of the synthesised ZnS nanoparticles. The average crystallite size of the powder has been estimated automatically from corresponding XRD

data using Scherer formula, $D=0.94\lambda/\beta\cos\theta$ and the average crystallite size is 2.9 nm. SBR shows a broad peak at $2\theta=20.17°$ indicating its amorphous nature. It is evident from the figure that the amorphous peak is slightly shifted along with a decrease in the broadness of the peak than that of the corresponding position in pure SBR. For example, the diffraction of 15 phr composite is slightly shifted to a lower diffraction angle from $2\theta=20.17°$ to 18.76°. The decrease in amorphous nature of SBR with the shift in diffraction angle is assigned to the strong interfacial interaction between the nanoparticles and the elastomeric chain. In order to obtain more structural information, the average crystallite size of ZnS nanoparticles in the composite is calculated from corresponding XRD data and the average size is 16.4 nm [191].

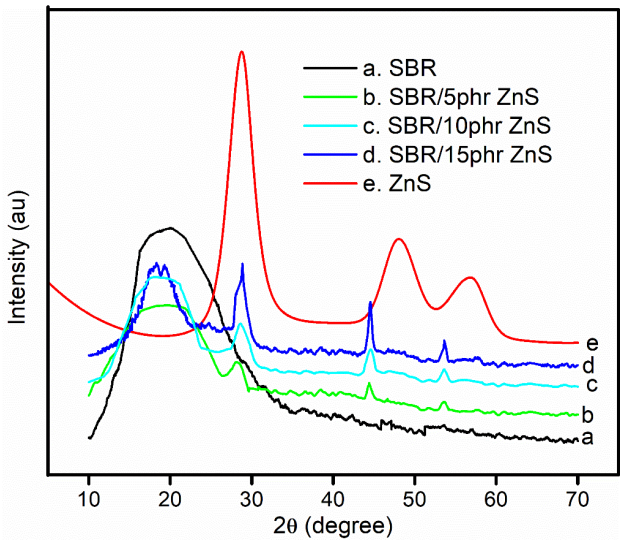

Figure 3.3 XRD pattern of ZnS, SBR and different contents of ZnS filled SBR

3.2.4 Scanning Electron Microscopy (SEM)

The morphological studies of SBR nanocomposite with different contents of ZnS nanoparticles are analysed by SEM and given in **figure 3.4**. The SEM image of SBR (**Figure 3.4 (a)**) presents a smooth and homogeneous structure. However, the inclusion of nanoparticles into the SBR matrix changes the surface morphology of the elastomers composite [192, 193]. From **figure 3.4 (b)**, it is clear that the sample with 10 phr of the ZnS particles containing SBR shows a uniform structure with several nanoparticles which are uniformly distributed. The change in the structural morphology of the composite is attributed to the strong interfacial interaction of the SBR phase with the nanoparticles. At 15 phr loading of the nanoparticles (**figure 3.4 (c)**), the surface morphology of the elastomeric composite changes drastically and shows some agglomeration of nanoparticles in the matrix.

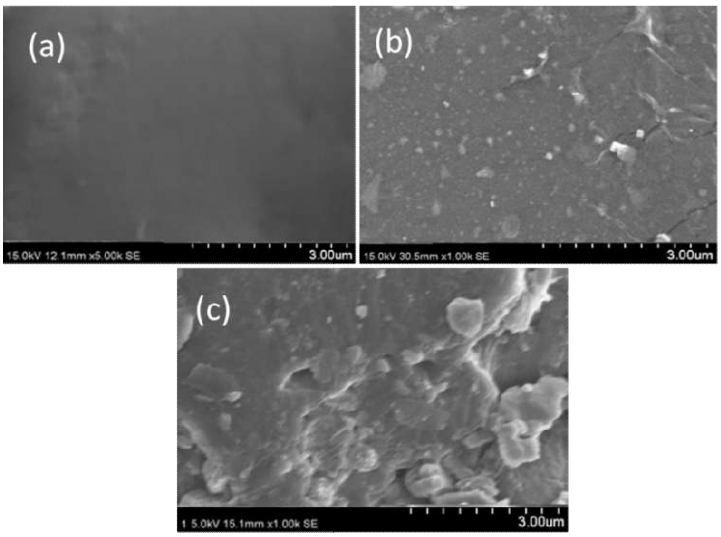

Figure 3.4 SEM pictures of **(a)** SBR, (**b)** SBR with 10 phr and (**c)** SBR with 15 phr ZnS nanoparticles

3.2.5 Thermal properties

3.2.5.1 Differential scanning calorimetry (DSC)

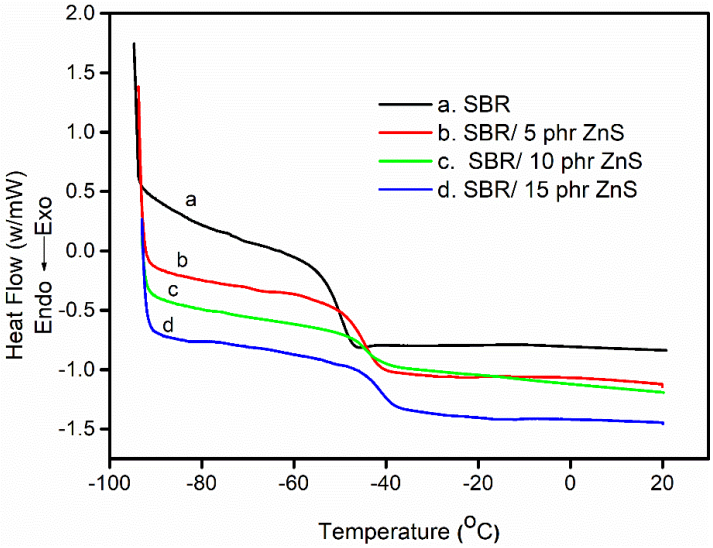

Figure 3.5 DSC thermograms of SBR and SBR/ ZnS nanocomposites

The DSC profile of SBR and SBR/ZnSnanocomposite with 5, 10 and 15 phr of ZnS nanoparticles is given in **figure 3.5**. It can be seen that the glass transition temperature (T_g) of SBR appears at -56°C. However, the T_g values of nanocomposite with 5, 10 and 15 phr loading of ZnS nanoparticles are observed at -54.2°C, -51.3°C, and -49.1°C, respectively. Generally, the T_g of elastomeric composite depends on the mobility of the chain, polarity of polymer and filler particles, i.e., the Tg values varies in accordance with free volume and the interaction between filler particles and the macromolecular chain. The high T_g values of nanocomposites, while increasing the loading of nanoparticles, are due to the interfacial interaction between nanoparticles and the macromolecular chain of SBR. In addition to

this, the inter-particle distance is short at higher loading, which increases the immobile polymer chain and thereby leads to higher T_g values [194].

3.2.5.2 Thermogravimetric analysis (TGA)

The thermal stability of neat SBR and the different contents of ZnS nanoparticles filled SBR at a heating rate of 10°C min^{-1} is shown in **figure 3.6**. From the figure it can be seen that all samples show single step degradation. The onset degradation of SBR is at 401°C which ends around 491°C. The improved thermal stability of SBR/ ZnS nanocomposites is clear from the initial and final temperature of the thermograms. The higher thermal stability of nanocomposites with the increase in concentration of nanoparticle is due to the increased interfacial adhesion between the ZnS nanoparticles and the elastomeric chain. The nanoparticles with a large surface area can strongly reinforce the SBR matrix, producing a protective layer on the surface of SBR and thereby acquire excellent thermal stability. The char residue remaining at 600°C is 9.61% for the neat SBR. However, the composites with 5, 10 and 15 phr of nano-ZnS filled SBR show the residue of 14.62, 18.68 and 22.94% respectively at 600°C.The char layer act as a protective coating on the surface of nanocomposite, which prevents further burning.The higher char residue is an indication of the better thermal and flame resistance of the polymer matrix [195,196]. This broadens the utility of these materials in various applications.

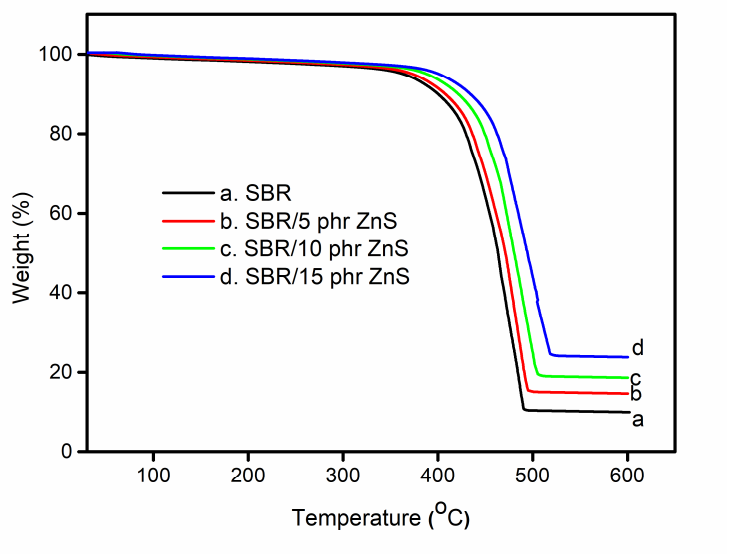

Figure 3.6 TGA curves of SBR and SBR/ZnS nanocomposites

3.2.6 Cure characteristics

The effect of loadings of ZnS nanoparticles on the rheometer processing characteristics such as cure time and torque values of sulphur vulcanized SBR is presented in **table 3.1**. The scorch time and optimum cure time values decrease with the loading of ZnS nanoparticles in SBR. This shows that the rate of SBR curing increases with the addition of nanoparticles. This is advantages because it can enhance the production rate of elastomer products developed using these materials. As shown in **table 3.1**, the addition of nanoparticles significantly increases the minimum and maximum torque values. The increase in rheometric torque indicates a better polymer-filler interaction. Here the metal sulphide act as co-activators during the chemical vulcanization process, creating better linkages between the molecular chains of rubber by sulfur, which ultimately led to the increase in cross-linking. The composite with 10 phr samples shows

the maximum torque value and beyond 10 phr loading, the torque value is found to decrease. At higher loading, greater stress develops in the elastomeric matrix which leads to poor cross-links between the polymer and ZnS nanoparticles [189].

Table 3.1 Processing characteristics of SBR and SBR/ZnS nanocomposites

Sample code	Cure time, t_{90} (min)	Scorch time, t_2 (min)	Maximum torque (dNm)	Minimum torque (dNm)
SZ_0	15.7	4.8	29	6.9
SZ_3	15.3	4.6	32	7.5
SZ_5	14.6	4.3	35	7.9
SZ_7	14.1	4.1	37	8.0
SZ_{10}	12.8	3.8	40	8.2
SZ_{15}	12.3	3.6	38	8.1

3.2.7 Mechanical properties

The mechanical properties of SBR nanocomposites namely tensile strength, modulus, elongation at break, tear resistance, hardness, abrasion loss, heat build-up and compression set were determined for all nanofiller loadings. The tensile strength, modulus (at 200% elongation) and tear resistance values are greater than pure SBR (**Table 3.2**). The variation incomposite tensile properties is more pronounced at 10 phr loading. This means primarily that the nanoZnS filleracts as a reinforcing filler in SBR and secondarily there is homogeneous dispersion of nanoparticles in the polymer matrix [197]. The slight decrease in tensile strength, modulus and tear strength observed at higher loadings (15 phr), may be due to the agglomeration

of ZnS nanoparticles. This fact is supported by the SEM analyses discussed earlier in this work. The elongation at break (EB)given in **table 3.2** shows that the EB decreases with the loading of nanoparticles in all cases and it is well known that a decrease in EB is indicative of higher reinforcement by nanoparticles [185].

Table 3.2 Mechanical properties of SBR and SBR/ ZnS nanocomposites

Properties	Loading of ZnS nanoparticles (phr)					
	0	**3**	**5**	**7**	**10**	**15**
Tensile strength (MPa)	2.13	3.87	4.65	5.94	7.19	6.63
Elongation at break (%)	425	419	407	390	381	363
Modulus (300%)	1.94	2.94	4.21	5.19	6.99	5.88
Tear strength (kN/m)	18	23	26	29	32	30
Hardness (Shore A)	33	34	35	36	38	40
Heat build-up (^{o}C)	10	10.5	11.9	12.8	14.3	15.8
Compression set (%)	19.8	19.2	18.32	17.44	16.9	16.3
Abrasion loss (mm^3)	66.8	66.6	66.3	66.0	65.5	65.2

Durometer hardness is one of the most commonly used hardness tests for elastomeric materials; it assesses the material resistance to indentation and is widely employed in the elastomer industry. The hardness of the nanocomposite vulcanizates at different filler loadings is shown in **table 3.2**. A progressive increase in the hardness of composite can be seen with the increase in ZnS nanoparticle content, which is again due to the better interaction between SBR matrix and the nanofiller. Abrasion resistance is the material ability to resist the rubbing, scraping or erosion that tends to progressively remove material from its surface. The abrasion resistances of SBR vulcanizates

with various loadings of nanoparticles are also given in the same table. The abrasion resistance of the composite increased with an increase in the nanoparticles up to 10 phr loading. The voids or cracks at the growing tip of flaw are arrested by the nano-sized and crystalline ZnS particles which increases the abrasion resistance. The decrease in abrasion resistance beyond 10 phr loading of ZnS can be attributed to the poor interfacial interaction between SBR and the nanoparticles resulting from agglomeration of ZnS. The compression set measurement is used to measure the ability of elastomeric materials to maintain elastic properties even after prolonged compressive stress. **Table 3.2** shows the compression set values of the SBR vulcanizates with different loadings of ZnS nanoparticles. Pure SBR has higher compression set values than nanocomposites and on increasing filler loading the compression set values decreases. A lower compression set is the key property for the rubber industry in sealing applications. Heat build-up is another important property of elastomers, arising from the internal friction in the compounds. From **table 3.2**, it is clear that the heat build-up of the elastomeric composite enhances with the amount of ZnS nanoparticles and thisis mainly due to the higher internal friction resulting from more extensive cross-linking and improved thermal conductivity of the nanocomposites. The magnitude of the increase in heat build-up is higher at 15 phr ZnS loading. The reinforcing effect and higher thermal conductivity of metal sulphide filled compounds is responsible for the high heat build-up value.

3.2.8 Electrical properties

3.2.8.1 AC conductivity

The AC conductivity of various concentrations of nano-ZnS filled SBR and unfilled SBR at different frequencies at room temperature is given in **figure 3.7**. The SBR shows minimum electrical conductivity than that of the metal sulphides nanoparticles filled SBR. Owing to the highly amorphous nature of SBR (confirmed from XRD analysis), the macromolecular chains are randomly oriented in the SBR matrix. Therefore, the linkages through grain boundaries are poor, leading to the lower electrical conductivity of the elastomers. The AC conductivity increases continuously with an increase in frequencies for all the samples. This is due to the rapid transport of hopping charge carriers within the polymer matrix and its composites. From the figure, it can be seen that the AC conductivity of the composite greatly increases with the addition of nanoparticles; the composite with 10 phr filler shows the maximum AC conductivity. This indicates the strong interfacial interactions between the ZnS nanofiller particles and the SBR matrix. The interfacial interaction changes the molecular orientation of SBR from a randomly oriented conformation to a well-defined compact structure. It may also be noted that the bulk conductivity of nanocomposites depends on the loading of fillers, filler-rubber adhesion and uniform dispersion of nanoparticles within the polymer matrix [198]. However, at a higher concentration of nanoparticles (15 phr) the interfacial adhesion between the polymer and filler decreases due to the high aggregating tendency of nanoparticles. This breaks the formation of effective conducting chains

of ZnS nanoparticles and therefore the conductivity is lower at a higher concentration of nanoparticles.

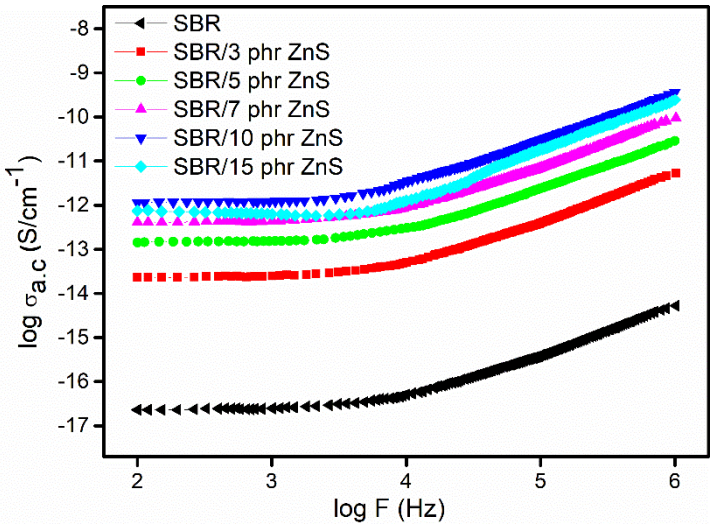

Figure 3.7 AC conductivity of SBR and SBR/ZnS nanocomposites

3.2.8.2 Dielectric constant

Figure 3.8 shows the variation of dielectric constant with the frequency of SBR and different loading of ZnS nanoparticles containing SBR. The dielectric constant of the polymeric material is directly related to the polarizability of the materials and the interfacial interactions. Also, the presence of aromatic ring, zinc, nitrogen, and sulphur is considered as highly polarisable by the application of an electric field. The dielectric constant of all the composites continuously decreases with an increase in frequency. This is attributed to the tendency of dipoles to orient themselves in the direction of the applied field. The dielectric constant of all the nanocomposites is higher than that of SBR in the entire range of frequencies. In the present study, the

higher dielectric constant of the composite is due to the enhanced interfacial interaction between the nanoparticles and the presence of aromatic ring in SBR [199]. The dielectric property of the composite is found to be increasing with the loading of nanoparticles up to 10 phr. When the concentration of nanoparticles reaches to 15 phr, the dielectric constant is found to be decreasing. The poor dielectric constant of nanocomposite at higher loading is due to the generation of more and more clusters in the elastomeric matrix (as evident from the UV study).

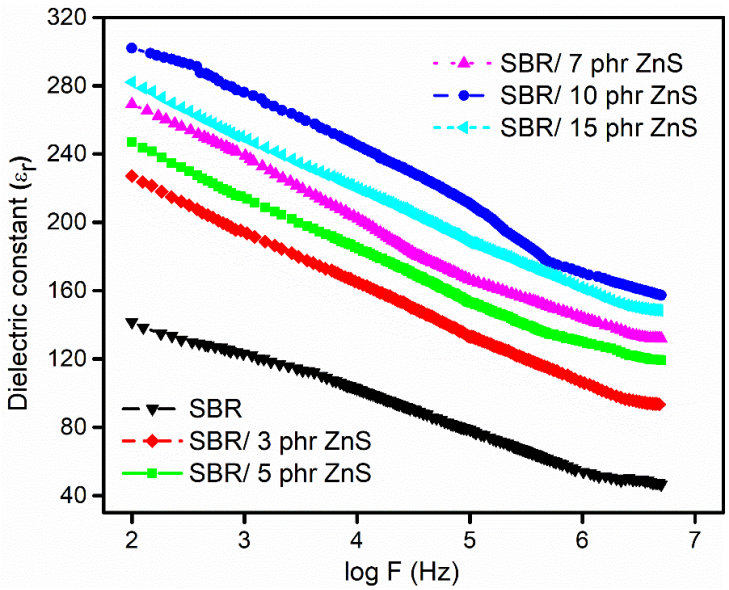

Figure 3.8 Dielectric constant of SBR and SBR/ZnS nanocomposites

3.2.8.3 Dielectric loss (tan δ)

Dielectric loss tangent (tan δ) is the ratio of the electrical energy dissipated in a material to the total power in a circuit. **Figure 3.9** shows the variation of the dielectric loss tangent (tan δ) as a function of frequency ranging from 100-10^6 Hz of SBR and SBR-ZnS nanocomposites at room temperature.It is observed that the tan δ of the composite with different contents of nanofiller is higher than that of pure SBR. It is evident that dielectric loss of all the samples decreases steadily with the frequency and reaches a constant tan δ value at 10^4 Hz. This is due to the time lag associated with the orientation of dipoles within the polymer matrix. The tan δ values of SBR/ZnS nanocomposite is greater than that of the pure SBR. The nanoparticles present in the macromolecular chain of SBR increases the interactions between the components, leading to field distortions and thus an increase in dielectric loss. It is interesting to note that a higher dielectric loss is observed for 10 phr of ZnS, which might be due to the large surface area, surface domain polarisation and the effective electrical network formation [177]. The dielectric loss of the 15 phr loading is lower than that of 10 phr loaded composite. This is due to the formation of clusters or discrete aggregates in the SBR matrix, which prevents charge carriers from migrating through the elastomeric system.

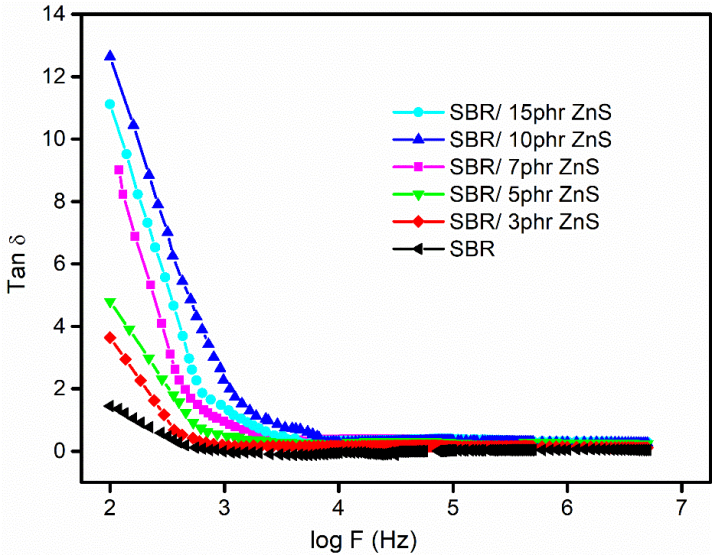

Figure 3.9 Dielectric loss tangent of SBR and SBR/ZnS nanocomposites

3.2.9 Analysis of swelling data of aromatic and industrial solvents

3.2.9.1 Mol % uptake

The mole % uptake of aromatic solvents through SBR/ZnS nanocomposite is studied at room temperature and the mole% uptake of solvent (Q_t) was calculated from the **equation 3.1**.

$$Q_t(mol\%) = \frac{mass\,of\,solvent\,sorbed/molecular\,weight\,of\,penetrant}{initial\ weight\ of\ polymer/polymer\ nanocomposit} \times 100 \quad \textbf{(Eq: 3.1)}$$

The mol % uptake (Q_t %) was plotted against the square root of time ($\sqrt{t}$) in order to get diffusion curves with special reference to the effect of filler loading, effect of solvent and the effect of temperature.

Effect of filler loading

The mole % uptakes of benzene and petrol through the SBR with different loading of ZnS nanoparticles are given in **figures 3.10** and **3.11** respectively. It is clear from the figures that the mole uptake progresses first; then it reaches equilibrium and finally becomes constant. It can be seen that, on increasing the ZnS concentrations, the equilibrium sorption decreases and the minimum solvent uptake is observed for the nanocomposite with 10 phr of ZnS. This indicates a better polymer-filler interaction, which inturn leads to the decreased flexibility of the polymer chain and the nanocomposite becomes less permeable [200]. On adding filler to the matrix, the free volume inside the matrix decreased, which restricts the free movement of solvent inside the matrix. Thus, upon reinforcement with the filler, the solvent resistance also increases. A better distribution of nanoparticles in the matrix causes an increased surface area of the reinforcing phase, which is the reason for the higher solvent resistance of 10 phr of the composite. However, it is found that, upon further addition of ZnS nanoparticles (above 10 phr); the mole uptake again increases due to the decreased filler-matrix interaction, which leads to the agglomeration of nanoparticles in the SBR matrix. Sorption experiments are found in a similar trend in other two aromatic (toluene and xylene) and industrial (kerosene and diesel) solvents.

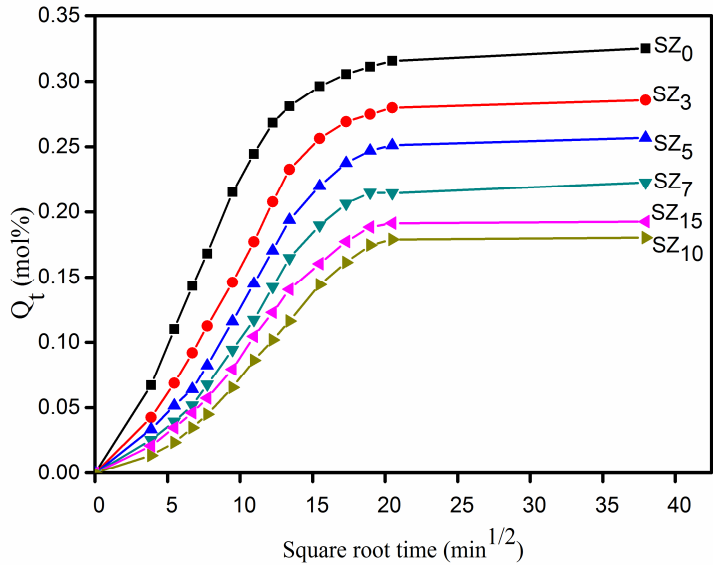

Figure 3.10 mol % uptake of SBR and SBR/ZnS nanocomposites in benzene

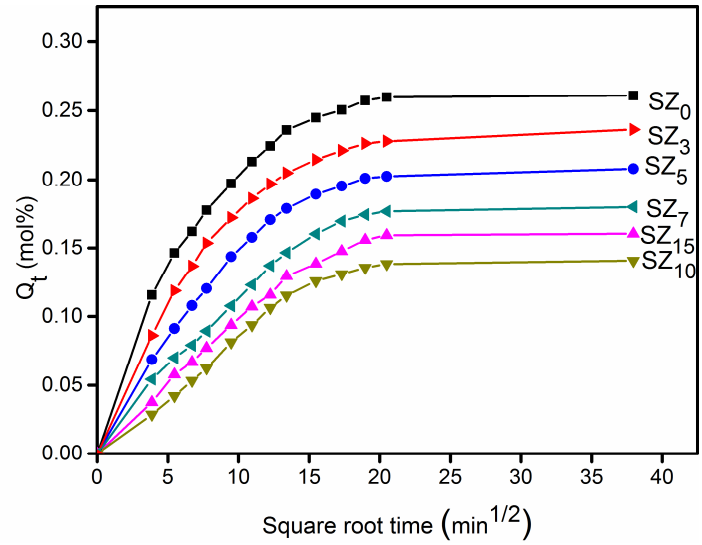

Figure 3.11 mol % uptake of SBR and SBR/ZnS nanocomposites in petrol

Effect of penetrant size

The nature of the solvent also affects the mole uptake of the nanocomposite. The transport properties of SBR/ ZnS nanocomposites with 10 phr of ZnS nanoparticles in homologous series of both aromatic and industrial solvents are shown in **figure 3.12** and **3.13** respectively. From the figure, it is evident that on increasing solvent density/penetrant size benzene showed highest mol uptake and xylene showed the lowest and the decreasing order is benzene > toluene > xylene. In the case of industrial solvents, the order is petrol > kerosene > diesel.

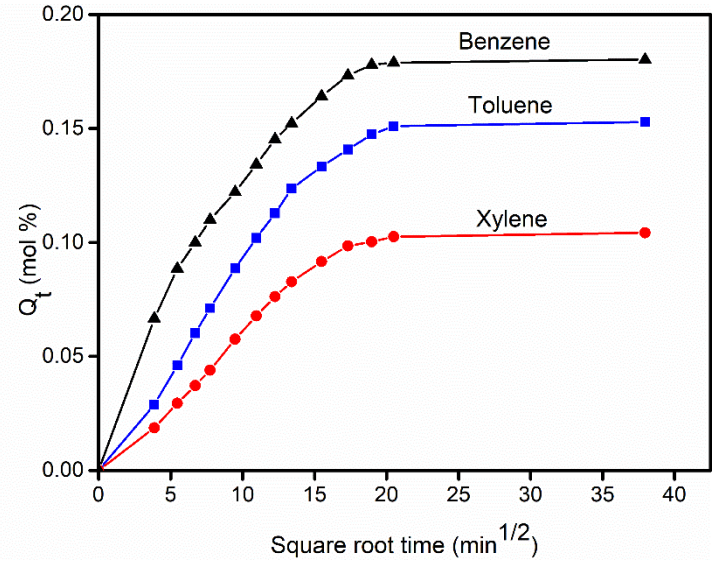

Figure 3.12 Solvent uptake of SBR with 10 phr of ZnS in aromatic solvents

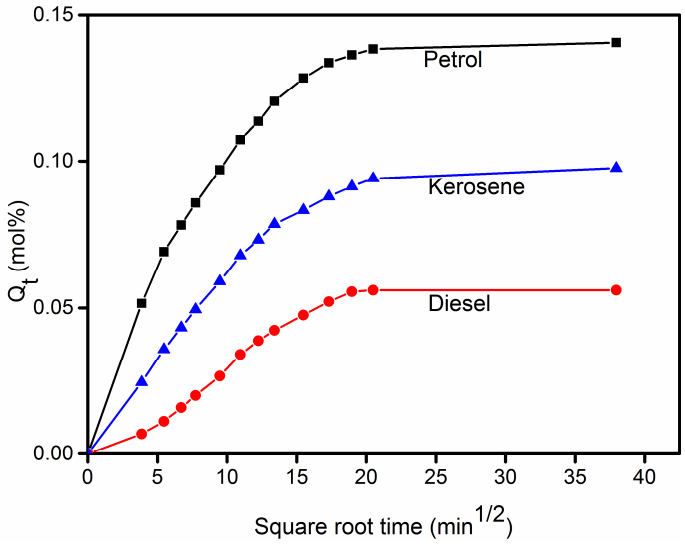

Figure 3.13 Solvent uptake of SBR with 10 phr of ZnS in petroleum fuels

The decrease in solvent uptake on increasing molar volume is reported by many researches. On increasing the molar volume, it needs more space and the exchange become very difficult. It is well established from free volume theory that the increased molar volume will impart restriction on the solvent to enter into the polymer matrix and high activation energy is needed for large molecules to penetrate [201].

Temperature dependence on sorption and diffusion of solvents

The effect of temperature on transport properties of the composite is analysed at different temperatures such as 50 and 70°C for aromatic solvents and 40 and 50°C for industrial solvents. **Figure 3.14** depicts the effect of temperature on the solvent uptake for SBR/ZnS nanocomposite in benzene and **figure 3.15** in petrol at different temperatures. It can be seen that the solvent uptake of 10 phr nanocomposite is found to be increasing with the temperature. This is

mainly due to the increased segmental mobility; as a result, the free volume inside the matrix increases. This again causes the kinetic energy inside the polymer chain to rise [202]. A similar trend is observed for all the samples in all solvents.

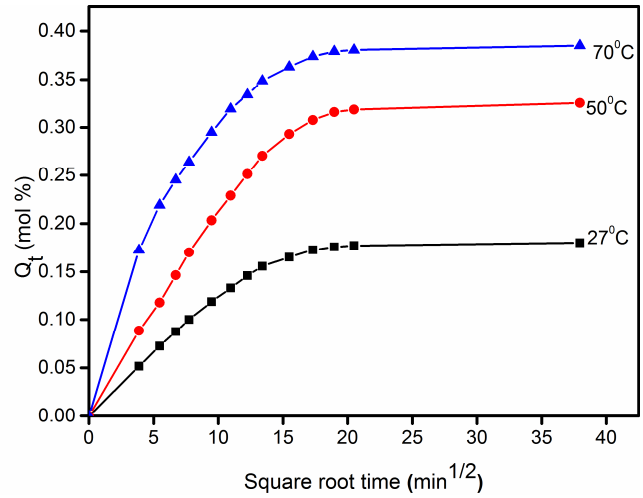

Figure 3.14 The Q_t (mol %) of SBR and SBR/10 phr of ZnS in benzene at 27, 50 and 70 °C

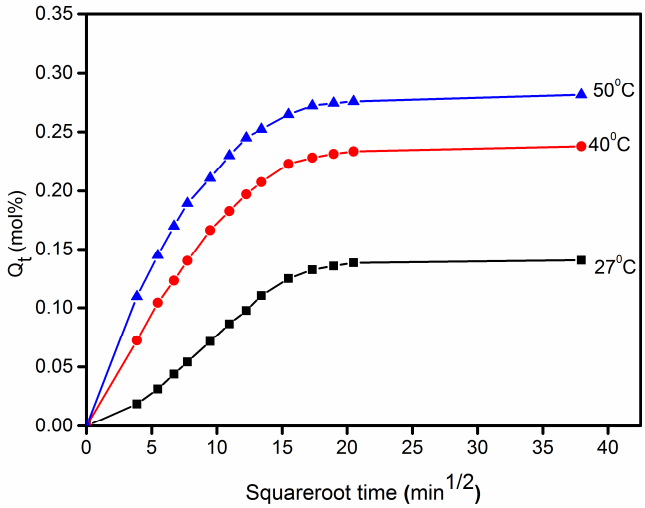

Figure 3.15 The Q_t (mol %) of SBR and SBR/10 phr of ZnS in petrol at 27, 40 and 50°C

3.2.9.2 Diffusion (D), sorption (S) and permeation (P) coefficients

The diffusion coefficient (D) is a kinetic parameter, on the basis of segmental mobility which controls diffusion rate. It is calculated using the **equation 3.2**

$$D = \pi\left(\frac{h\theta}{4Q_\infty}\right)^2 \qquad \textbf{(Eq: 3.2)}$$

where h is the thickness of the sample, θ is the slope of the initial linear region of the plot of Q_t versus the square root time and Q_∞ is the equilibrium mol uptake. **Table 3.3** and **3.4** clearly demonstrate that the investigations are done for all samples in all three aromatic and industrial solvents. The D values decrease with an increase in concentration of the ZnS nanoparticles up to 10 phr loading. The lowest value of the diffusion coefficient is observed for 10 phr of ZnS containing composite. This is due to the strong interfacial adhesion between the elastomer and nanoparticles. The D value increases upon further addition of filler to the matrix beyond 10 phr. This is because of the agglomeration of nanoparticles cause a decreased interfacial interaction and non-uniform distribution of ZnS filler particles in the polymer matrix. In the case of petroleum fuels, upon increase of penetrant size, diffusivity decreases, petrol shows a higher D value and diesel shows the lowest D value. This is explained on the basis of the free volume theory in terms of the effect of solvent on the mole % uptake of solvent [203, 204].

Table 3.3 D, S and P values of SBR/ZnS nanocomposites in aromatic solvents

Samples	Diffusion coefficient D x 10^5 (cm^2/s)			Sorption coefficient S			Permeation coefficient P x 10^5(cm^2/s)		
	Benzene	Toluene	Xylene	Benzene	Toluene	Xylene	Benzene	Toluene	Xylene
SZ_0	1.81	1.67	1.42	1.20	1.16	1.13	2.17	1.93	1.60
SZ_3	1.79	1.61	1.39	1.18	1.14	1.11	2.11	1.83	1.54
SZ_5	1.77	1.55	1.31	1.17	1.12	1.09	2.07	1.74	1.43
SZ_7	1.73	1.52	1.22	1.15	1.09	1.06	1.98	1.65	1.29
SZ_{10}	1.54	1.37	1.09	1.11	1.05	1.01	1.71	1.43	1.10
SZ_{15}	1.67	1.44	1.13	1.13	1.07	1.03	1.88	1.54	1.16

Table 3.4 D, S and P values of SBR/ ZnS nanocomposites in Industrial solvents

Samples	Diffusion coefficient D x 10^5 (cm^2/s)			Sorption coefficient S			Permeation coefficient P x 10^5(cm^2/s)		
	Petrol	Kerosene	Diesel	Petrol	Kerosene	Diesel	Petrol	Kerosene	Diesel
SZ_0	1.51	1.36	1.25	1.21	1.17	1.14	1.81	1.59	1.42
SZ_3	1.38	1.24	1.18	1.19	1.13	1.11	1.64	1.40	1.31
S Z_5	1.34	1.18	1.13	1.11	1.07	1.06	1.48	1.26	1.19
SZ_7	1.19	1.13	1.11	1.09	1.03	1.01	1.29	1.16	1.12
SZ_{10}	1.11	0.94	0.88	1.01	0.92	0.88	1.21	0.86	0.77
SZ_{15}	1.14	1.06	1.03	1.07	0.98	0.95	1.22	1.03	0.97

It can be seen that the sorption, diffusion and permeation coefficients are highest for petrol and lowest for diesel and intermediate for kerosene. It is explained that smaller molecules will diffuse and get accommodated more easily into the polymer matrix, due to steric reasons. The decreased sorption values upon increased nanofiller loading can be explained by the fact that the reinforcing materials create obstacles for the penetrating molecules. The bigger the penetrant molecule, the stronger the resistance and hence less will be the

penetrant uptake. The Permeation coefficient is the combined effect of the diffusion and sorption coefficients. i.e., P=D.S, the measure of the amount of solvent that permeated per unit area of the sample in one second. Hence it shows a trend similar to that of D and S.

3.2.9.3 The transport mechanism

The mechanism of transport can be explained from the **equation 3.3**

$$\log \frac{Q_t}{Q_\infty} = \log k + n \log t \qquad \textbf{(Eq: 3.3)}$$

Where Q_t and Q_∞ are the mol % sorption at time t and at equilibrium respectively, k indicates the interaction between the penetrant and the polymer and *n* represents the mode of transport. On regression analysis of $\log \frac{Q_t}{Q_\infty}$ and log t the values of n and k are obtained for aromatic and industrial solvents and these values are given **table 3.5** and **3.6** respectively. From the table, it is clear that the value of n is found to be non Fickian first and then on increasing filler loading and solvent size it comes above 0.6 and is nearest to 1. This indicates an anomalous mode of transport and is mainly due to the comparable diffusivity and chain relaxation [205]. The increased swelling stress due to reinforcement is also another reason for the anomalous mode of transport. The value of k proves the structural properties and the increased polymer filler interaction. Generally, the value of k decreases when the distribution of the nanoparticles in the matrix increases. Here, the lowest value for k is noted for 10 phr composite. Upon increasing the penetrant's size, the interaction becomes less and therefore the value of k increases.

Table 3.5 n and k values of SBR/ZnS nanocomposites in aromatic solvents

Samples	Benzene		Toluene		Xylene	
	n	$Kx10^2(min^{-1})$	N	$kx10^2(min^{-1})$	n	$Kx10^2(min^{-1})$
SZ_0	0.51	0.24	0.59	0.15	0.69	0.13
SZ_3	0.53	0.19	0.66	0.13	0.77	0.11
SZ_5	0.59	0.17	0.73	0.11	0.81	0.11
SZ_7	0.67	0.14	0.77	0.10	0.84	0.12
SZ_{10}	0.73	0.11	0.83	0.08	0.88	0.07
SZ_{15}	0.69	0.13	0.79	0.09	0.85	0.11

Table 3.6 n and k values of SBR/ZnS nanocomposites in industrial solvents

Samples	Petrol		Kerosene		Diesel	
	n	$Kx10^2(min^{-1})$	N	$kx10^2(min^{-1})$	n	$Kx10^2(min^{-1})$
SZ_0	0.37	0.28	0.49	0.26	0.52	0.22
SZ_3	0.45	0.29	0.56	0.24	0.66	0.21
SZ_5	0.67	0.21	0.62	0.19	0.68	0.17
SZ_7	0.69	0.19	0.66	0.16	0.71	0.14
SZ_{10}	0.77	0.13	0.79	0.12	0.83	0.11
SZ_{15}	0.75	0.15	0.66	0.17	0.72	0.12

3.2.9.4 Activation energy of diffusion (E_D) and permeation (E_P)

The activation energy of sorption can be calculated from the Arrhenius **equation 3.4**

$$X = X_0 \, exp\left(\frac{-E_X}{RT}\right) \qquad \textbf{(Eq: 3.4)}$$

Where X is D or P, and X_0 is D_0 or P_0. E_x is the activation energy from the plots of log D or logP against 1/T. From the slopes of the curves, the Arrhenius parameters for the samples in aromatic and industrial solvents are obtained and are given in **table 3.7** and **3.8**. The activation

energy of diffusion and permeation is found to be increasing with the loading of nanoparticles (**Table 3.7** and **3.8**). The free space in the matrix decreases with increasing filler loading and therefore more energy is needed to obtain free space. Also, on increasing the penetrant's size, the difficulty to enter into the matrix increases and E_P and E_D values increase [206]. Also, the maximum value is for 10 phr composite. A further addition of nanoparticles lowers the activation energy. This is due to the agglomeration of nanoparticles on the surface of the polymer or to the decreased interfacial interaction between the rubber and nanoparticles.

Table 3.7 E_D, and E_P (kJ mol^{-1}) values of SBR-ZnS nanocomposites in aromatic solvents

Samples	Benzene		Toluene		Xylene	
	E_P	E_D	E_P	E_D	E_P	E_D
SZ_0	6.16	4.97	6.39	5.22	6.62	5.43
SZ_3	6.29	5.21	6.51	5.32	6.77	5.51
SZ_5	6.43	5.29	6.62	5.44	6.86	5.57
SZ_7	6.47	5.38	6.64	5.51	6.89	5.62
SZ_{10}	6.54	5.51	6.75	5.67	6.95	5.69
SZ_{15}	6.51	5.44	6.68	5.58	6.90	5.64

Table 3.8 E_D and E_P (kJ mol^{-1}) values of SBR/ZnS nanocomposites in petroleum fuels

Samples	Petrol			Kerosene			Diesel		
	E_D	E_P	ΔH	E_D	E_P	ΔH	E_D	E_P	ΔH
SZ_0	3.59	4.22	0.63	3.97	4.72	0.75	4.62	5.46	0.84
SZ_3	4.49	5.41	0.92	4.54	5.65	1.11	4.63	6.15	1.52
SZ_5	5.92	7.07	1.15	6.18	7.44	1.26	7.08	8.89	1.81
SZ_7	6.08	7.29	1.21	6.32	7.69	1.37	7.19	9.09	1.9
SZ_{10}	6.29	7.54	1.25	6.49	8.36	1.87	7.59	9.64	2.05
SZ_{15}	6.16	7.39	1.23	6.39	7.88	1.49	7.29	9.23	1.94

3.2.9.5 Thermodynamic parameters

Thermodynamic parameters such as ΔH_s and ΔS_s can be obtained from Van't Hoff's **equation 3.5**

$$logK_s = \frac{\Delta S_s}{2.303R} - \frac{\Delta H_s}{2.303RT} \qquad \textbf{(Eq: 3.5)}$$

Where K_s is the equilibrium sorption constant, which is the ratio of the number of moles of solvent sorbed at equilibrium to the mass of the polymer sample. On regression analysis of log Ks against 1/T, the values of ΔH and ΔS are obtained. The thermodynamic properties of SBR and SBR/ZnS composites in aromatic (benzene, toluene and xylene) solvents are given in **table 3.9** while **table 3.10** depicts the thermodynamic parameters of SBR/ZnS in industrial solvents.

Table 3.9 ΔH, ΔS and ΔG (kJ/mol) of SBR- ZnS nanocomposites in aromatic solvents

Samples	ΔH			ΔS			-ΔG		
	Benzene	Toluene	Xylene	Benzene	Toluene	Xylene	Benzene	Toluene	Xylene
SZ_0	0.871	0.884	0.896	0.071	0.058	0.052	20.43	16.51	14.70
SZ_3	0.877	0.889	0.902	0.068	0.054	0.044	19.52	15.31	12.29
SZ_5	0.882	0.894	0.907	0.065	0.051	0.042	18.61	14.41	11.69
SZ_7	0.889	0.899	0.914	0.061	0.048	0.038	17.41	13.50	10.48
SZ_{10}	0.899	0.912	0.921	0.055	0.041	0.031	15.60	11.39	8.37
SZ_{15}	0.891	0.903	0.917	0.059	0.044	0.034	16.81	12.29	9.28

The positive ΔH value proves the sorption is endothermic. Sorption will occur only by the creation of free space inside the matrix [207].

The reduced entropy on adding filler is due to the decreased interfacial interaction, and is lower in benzene at 10 phr. The value of ΔG also increases upon reinforcement. Among the nanocomposites, 10 phr composite shows the minimum spontaneous sorption which indicates a better interaction between the nanoparticles and the SBR matrix.

Table 3.10 ΔH, ΔS and ΔG (kJ/mol) values of SBR/ZnS nanocomposites in petroleum fuels

Samples	ΔH			ΔS			-ΔG		
	Petrol	Kerosene	Diesel	Petrol	Kerosene	Diesel	Petrol	Kerosene	Diesel
SZ_0	0.635	0.758	0.848	0.068	0.048	0.042	19.77	13.64	11.752
SZ3	0.927	1.117	1.527	0.058	0.044	0.039	16.47	12.08	10.173
SZ_5	1.158	1.268	1.817	0.047	0.032	0.029	12.94	8.332	6.883
SZ_7	1.217	1.378	1.979	0.043	0.029	0.022	11.68	7.322	4.621
SZ_{10}	1.258	1.879	2.059	0.029	0.024	0.014	7.44	5.321	2.141
SZ_{15}	1.239	1.497	1.946	0.037	0.026	0.017	9.86	6.303	3.154

3.3 Conclusions

The SBR/ZnS nanocomposites were prepared using a simple and environmentally-friendly two-roll mill mixing technique. The composites were characterized by FT-IR, UV, XRD, SEM, DSC and TGA. The interaction of nanoparticles with SBR was confirmed from the spectroscopic studies through the shift in absorption peaks of the nanocomposite. The XRD showed the ordered arrangement of filler particles in SBR and the amorphous nature of composite decreased with an increase in content of nanoparticles. The SEM images showed a uniform dispersion of the fillers in SBR. The glass transition temperature of the composites increased with the loading of metal sulphide nanoparticles. TGA results showed an increase in thermal stability of nanocomposites upon increasing filler content. The

processability, mechanical properties, electrical properties and solvent penetration studies of the composites were studied with respect to different loading of nano filler. Despite the reduction in scorch safety, the compounded SBR/ZnS samples indicated higher production rate resulting from lowering of optimum cure time. Mechanical properties such as tensile, tear strength, modulus, hardness, abrasion resistance, heat build-up and compression set were in agreement with the reinforcement by ZnS particles. This is advantages because elastomer nanocomposite with improved mechanical properties tends to be high performing and durable in-service life. The AC conductivity of SBR was significantly enhanced by the addition of ZnS nanoparticles. Dielectric properties of composites were greater than pure SBR and the maximum dielectric properties were obtained for 10 phr composite. Diffusion and sorption of aromatic and industrial solvents through SBR/ZnS nanocomposites was studied at different temperatures. The diffusion results were explained in terms of the size of liquid molecules and the diffusion mechanism was found to follow the anomalous in trend. The diffusion and permeation coefficient values decreased with an increase in the molar volume of the solvent. The enhanced dielectric property of the elastomeric nanocomposites can be used in various applications such as electromagnetic shielding, flexible energy storage and other nanoelectronic devices.

4.1 Introduction

Elastomeric materials and composites have served modern society for decades. These materials are used in various industrial applications including transportation, construction, electrical cables, oil seals and packaging materials [208, 209]. However, the poor dispersion of filler particles in the polymeric composites may corrode when exposed to moisture, hazardous solvents, UV radiation etc. This leads to the loss of mechanical properties and reduction in the lifetime of composite materials [210]. The deterioration of the mechanical properties of the conventional polymeric composites can be overcome by incorporating nano-sized particles within the polymer matrix. The deterioration of mechanical properties depends on the size, the aspect ratio, degree of dispersion, and orientation of the nanoparticles in the rubber and the degree of adhesion of nanoparticles to the polymer chains [166, 211, 212]. One of the unique properties of nanocomposites, especially metal nanoparticles filled polymers is the low penetration of solvents and gases. The solvent resistant polymeric films have strong potential applications in various fields. The properties of the solvent resistant membrane depend on the transport in polymers, their molecular properties, nature of penetrates, solubility, and polymer morphology of the interface. Various research works were carried out to verify the importance of nanoparticles in diffusion studies. It is generally found that the incorporation of filler with polymer matrix reduces the diffusion and permeation process of hydrocarbons into polymer matrices [204, 213–215].

Hybrid composites as a way to enhance the properties of composites have received considerable attention from researchers. Metal nanoparticles play an important role in the damping of mechanical vibrations in machine bearings and in vehicle base frames. The use of metal nanoparticles reduces the vulcanization time of the rubber nanocomposites which is due to the easy thermal conductivity through the polymer matrix [216–218]. Among the semiconducting metal nanoparticles, ZnS shows remarkable properties which can be used for various applications such as electroluminescence, field emitters, electro catalysts and biosensors. Several studies have focused on the reinforcement of ZnS nanoparticles with a polymeric matrix. Cheng et al. reported on the preparation of polystyrene/ZnS nanocomposites [219].

The results obtained from the previous chapter, revealed that, the reinforcement of SBR with polar fillers leads to poor mechanical properties due to the poor interaction (polar- nonpolar interaction) between rubber and filler particles. Moreover, SBR vulcanizates have very poor resistance to oil, ozone, and tensile strength, which restrict their use in such fields. Modified forms of SBR and polar rubbers play a vital role in enhancing interaction between the filler particles and the elastomeric matrix. Chemically modified SBR with randomly distributed dichlorocarbene groups within the backbone of polymer reduces the degree of unsaturation in SBR [83, 220]. The introduction of chloro groups into the rubber showed an elevation of the glass transition temperature. The dichlorocarbene reaction using the alkaline hydrolysis of chloroform is stereospecific and hence the resultant

chlorinated SBR (Cl-SBR) shows superior tensile strength compared to the pure SBR. Moreover, the oil resistance and flame retardancy of styrene butadiene rubber were drastically enhanced by the dichlorocarbene reaction [221].

The present study was motivated by a desire to know how metal sulphide nanoparticles affect the processability, mechanical properties, conductivity and transport properties of chlorinated SBR. The nature of nanoparticles in the Cl-SBR matrix was determined by UV- visible, infrared spectroscopy and X-ray diffraction (XRD). The morphology of the composites was studied using scanning electron microscopy (SEM) and transmission electron microscopy (TEM). The thermal stability, flame resistance, cure characteristics, different mechanical and dielectric properties of the nanocomposites have been studied with respect to the different loading of nanoparticles. The oil resistance and the effect of loading of nanoparticles, the nature of penetrant molecules and the effect of temperature on transport solvent through Cl-SBR/ZnS matrix were evaluated.

4.2 Result and Discussions

4.2.1 FTIR spectra

A Fourier transform infrared spectroscopy (FTIR) was employed for examining the interaction of nanoparticles with the functional groups in the elastomer. **Figure 4.1** presents the FTIR spectra of ZnS, chlorinated SBR, and SBR/ ZnS composites.

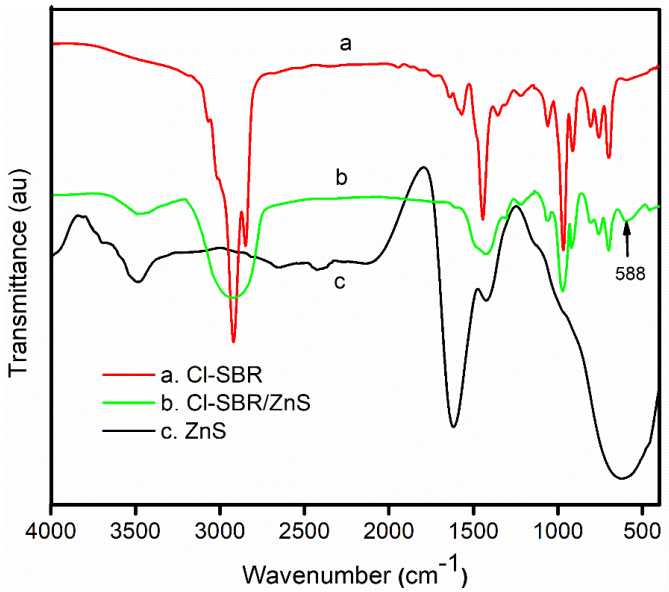

Figure 4.1 FTIR spectra of ZnS, Cl-SBR and ZnS filled Cl-SBR

The IR spectra of ZnS showed a strong absorption peak at 615 cm^{-1}, corresponding to the ZnS particles. The spectra of ZnS also showed two additional peaks at 3487 cm^{-1} and 1619 cm^{-1}, corresponding to the stretching and bending vibration of -OH group on the surface of metal sulphide particles. The spectrum of Cl-SBR showed the C-H stretching at 2930 and 2853 cm^{-1}. Also, the CH_2 in plane deformation and the *trans* C=C stretching of SBR has observed at 1443 and 968 cm^{-1}, respectively. Moreover, the aromatic stretching vibration is appearing at 700 cm^{-1}. The absorption band at 804 cm^{-1} and 1067 cm^{-1} are the corresponding C-Cl stretching and the cyclopropyl ring of chlorinated SBR, respectively. The Cl-SBR/ZnS composite exhibited all the absorption peaks of elastomer with the typical stretching of ZnS particles. The composite showed the typical ZnS absorption at 588 cm^{-1} suggests the insertion of nanoparticles in the polymer.

Moreover, the stretching vibration of C-H groups in SBR (at 2930 and 2853 cm^{-1}) are overlapped and merged to a broad absorption band at 2926 cm^{-1} as a result of ZnS particles insertion. In addition to this, the CH_2 absorption peaks (1443 cm^{-1}) of SBR is slightly shifted to lower frequencies (1419 $cm^{-1)}$. The shift in peaks and the broadness of absorption bands in Cl-SBR/ZnS composite is due to the strong intermolecular interaction between the polymer and nanoparticles, suggesting that the absorption frequencies of nanocomposites are strongly influenced by the insertion of nanoparticles.

4.2.2 UV-Vis spectra Cl-SBR

The UV-Vis spectrum of Cl-SBR and different contents of ZnS/Cl-SBR nanocomposites are shown in **figure 4.2**. The UV spectra of Cl-SBR observed at 287 is due to the π to π^* transition of the polymer [222]. However, the n-π^* transition of Cl-SBR is found to shifting to a higher wavelength region for all the composites. Interestingly, the intensity and broadness of all the composites are significantly higher than that of pure Cl-SBR. This is another evidence for the Insertion of nanoparticles into the elastomeric system. Additionally, the absorption edge of all nanocomposites is higher than Cl-SBR in the entire range of UV absorbance from 200 to 700 nm. Among the nanocomposite, the intensity and broadness of UV peak is the maximum at 7 phr loading. This means that the intermolecular interaction between filler and polymer is the maximum at this loading. The decrease in broadness and intensity of UV peak beyond 7 phr loading is due to the agglomeration of nanoparticles, which prevent the easy passage light energy through the polymer matrix.

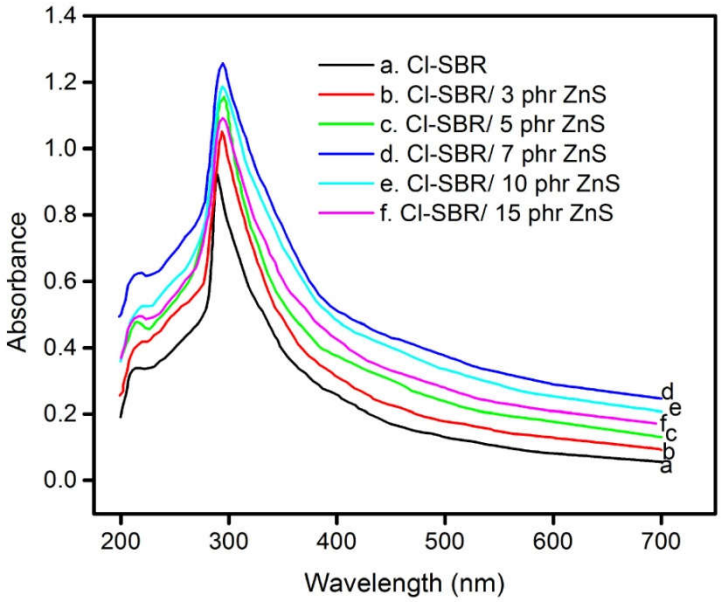

Figure 4.2 UV spectra of Cl-SBR and Cl-SBR/ZnS nanocomposites

4.2.3 X-ray Diffraction Analysis (XRD)

Figure 4.3 (a) presents the XRD pattern of Cl-SBR. Two peaks are recorded. The broad peak at a 2θ=21.2° reflecting the amorphous nature of the SBR segment. The peak obtained at 2θ=29.36°, indicating the semi-crystalline nature of the polymer. **Figure 4.3 (b)** shows the XRD pattern of ZnS, which matches well with the cubic sphalerite structure of ZnS, corresponding to (111), (220) and (311) planes at 29.6°, 48.23° and 56.97°, respectively [223]. From the XRD patterns of nanocomposite (**Figure 4.3 (c)** and **(d)**), one can observe that the diffraction peaks of ZnS in the polymer slightly shift to a lower diffraction angle, indicating the structural changes of composites through the interaction of the polymer with nanoparticles. For example, the weak crystalline peak present in the polymer is slightly

shifted in the composite from 2θ=29.36° to 28.59°. Similarly, the crystalline peaks of ZnS at 2θ=48.23° and 56.97° are shifted to a lower diffraction angle at 2θ=44.78° and 53.82°. Moreover, the amorphous portion of the polymer decreases with the loading of nanoparticles. The shift in diffraction peaks reveals the ordered arrangement of nanoparticles within the elastomeric matrix.

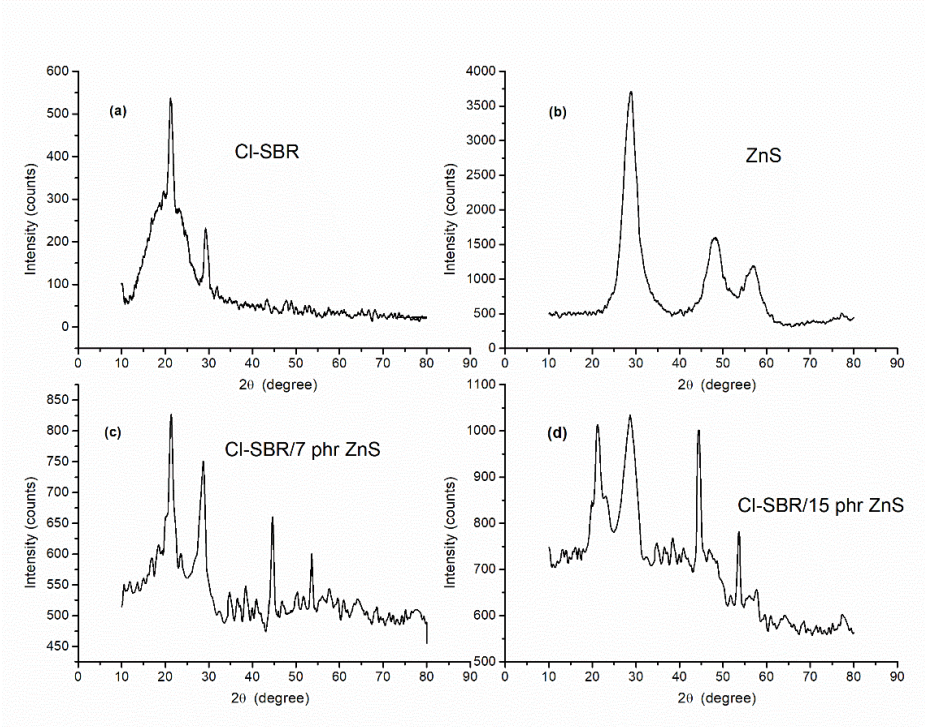

Figure 4.3 XRD pattern of ZnS and Cl-SBR/ZnS nanocomposites

4.2.4 Transmission Electron Microscopy (TEM)

Figure 4.4 shows the TEM images of ZnS, rubber nanocomposite with 7 and 15 wt. % of ZnS particles. The TEM micrograph (**Figure 4.4 (a)**) of the prepared ZnS powder shows several spherical shaped nano-crystals with an average size of 2 to 15 nm. The **figure 4.4 (b)** shows the uniform distribution of metal sulphide particles with various sizes ranging from 30 to 60 nm within the chlorinated SBR matrix. The uniform nature of nanocomposite is due to the strong interfacial adhesion between the chlorinated SBR and ZnS nanoparticles. However, the morphology of the composite (**Figure 4.4 (c)**) is remarkably changed into an elongated structure with the aggregation of nanoparticles indicating the poor interaction between of nanoparticles with the rubber matrix.

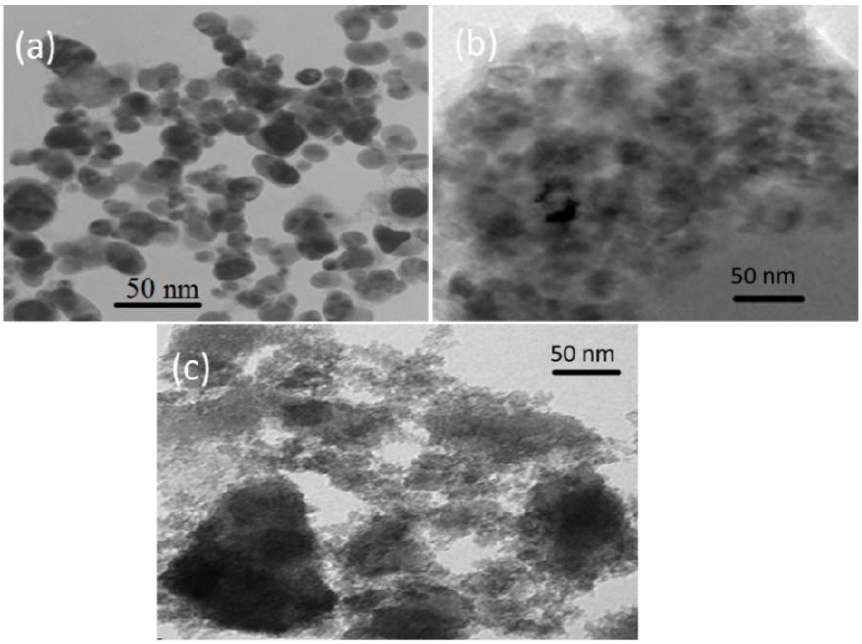

Figure 4.4 TEM images of **(a)** ZnS **(b)** Cl-SBR/7 phr ZnS and **(c)** Cl-SBR/15 phr ZnS

4.2.5 Scanning Electron Microscopy (SEM)

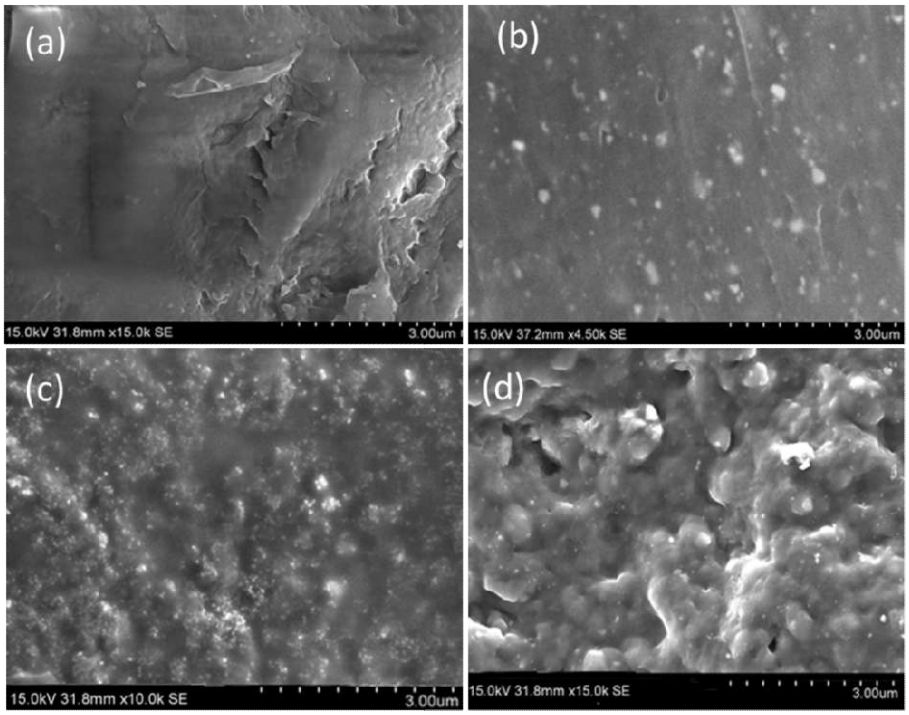

Figure 4.5 SEM images of **a)** Cl-SBR, **b)** Cl- SBR with 5 phr **c)** 7 phr and **d)** 15 phr ZnS

The surface morphology of Cl-SBR with different contents of ZnS nanoparticles is shown in **figure 4.5**. The morphology of Cl-SBR is a porous structure with surface irregularity. However, the surface morphology of chlorinated SBR is totally changed by the addition of nanoparticles. From **figure 4.5 (b)**, it is apparent that the rough surface of Cl-SBR disappeared and the nanoparticles dispersed more uniformly with a much smaller size in the matrix. The uniform dispersion of nanoparticles increased with the loading of nanoparticles up to 7 phr (**Figure 4.5 (c)**). It can be deduced that incorporation of ZnS showed a good dispersion of particles in Cl-SBR matrix with the size ranging

from 60 nm to 90 nm. On the other hand, the dispersion of nanoparticles into the Cl-SBR matrix is poor at higher loading (15 phr) and the domain size of dispersed phase is remarkably increased with some aggregates are shown from **figure 4.5 (d)**. The bad dispersion of nanoparticle in elastomeric matrix is thought to be due to the weak interaction between ZnS and the polar segments of Cl-SBR.

4.2.6 Thermal properties

4.2.6.1 Differential Scanning Calorimetry (DSC)

Figure 4.6 shows DSC measurement of the nanocomposites, from which the effect of ZnS on the glass transition temperature of Cl-SBR is observed. The chlorinated SBR in its pure form depicts thermal transitions at two regions. The first one, at -53°C, corresponds to the glass transition temperature of SBR and the second one at -35.1°C is the chlorinated segment of SBR [221]. The Tg of nanocomposites varies in accordance with polymer chain mobility, the polarity of the polymer matrix, amount of the filler, free volume inside the matrix etc. From the figure, one can see that the addition of the nanoparticles increases the Tg of all the samples. This is attributed primarily to the decrease in inter particle distance within the sample or the decrease in free volume reduces the mobility of the macromolecular chain; hence, Tg increases. The composites with 5, 10 and 15 phr samples showed the Tg at -33.9°C, -31.18°C and -30.9°C, respectively. The increase in Tg with the loading of nanoparticles is due to the interfacial interaction between the polymer and nanoparticles. It is interesting to observe from the figure that the loading of nanoparticles does not affect the

glass transition temperature of the SBR segment. This suggests that the interfacial interaction between the nanoparticles and the polar segments of Cl-SBR is responsible for the higher Tg value of nanocomposites. Also, the compactness of elastomer enhanced with the loading of nanoparticles which reduces the free volume inside the composites and thereby increase the Tg values [224].

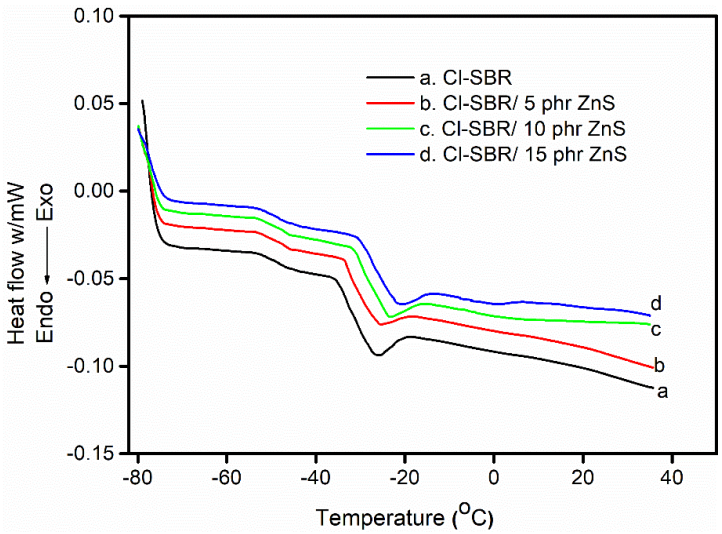

Figure 4.6 DSC thermorgams of Cl-SBR and Cl-SBR/ZnS nanocomposites

4.2.6.2 Thermogravimetric Analysis (TGA)

The thermal behavior of Cl-SBR nanocomposites with various loadings of ZnS was investigated using TGA and the results are presented in **figure 4.7**. It can be seen that all the samples showed two plateaus, suggesting two stages of weight losses. The initial weight loss below 250°C is due to the ingredients of the compound and the removal of HCl from the elastomeric chain. The second thermal degradation from 380°C to 560°C is a continuous weight loss, which

can be attributed to the decomposition of the SBR chain [225]. It is also clear that the initial and final decomposition temperatures of Cl-SBR/ZnS nanocomposites are higher those of the parent polymer, which reveals the high thermal stability of the fabricated composites. The thermal stability usually depends on the crystalline nature of the filler particles and the uniform dispersion of nanoparticles in the polymer matrix. The increased thermal stability with the filler loading is due to the interaction between the nanoparticles and polymer segments. Moreover, the metal sulphide nanoparticles retarded the motion of the elastomeric chains, acting as a protective layer on the surface of the matrix, which prevents the thermal degrading of the polymer and enhanced the thermal stability of the nanocomposites. The final char residue obtained at 600°C for Cl-SBR is only 6.87% whereas the composite with 5, 10 and 15 phr nanocomposite shows the final char residue around 11.26, 17.03 and 21.92%, respectively, at the same temperature.

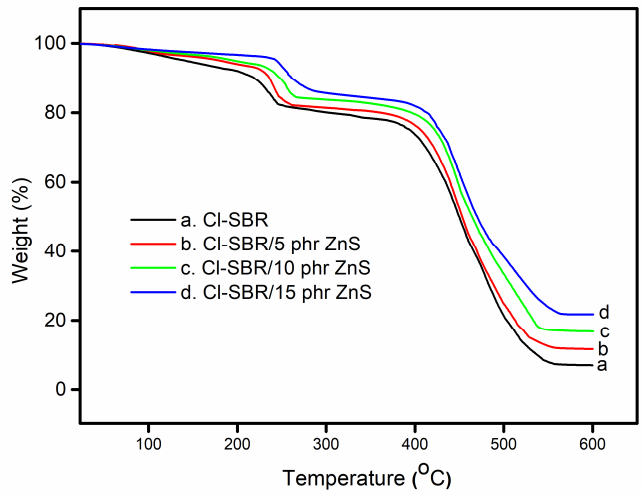

Figure 4.7 TGA curves of Cl-SBR and Cl-SBR/ZnS nanocomposites

The char formed after the thermal decomposition of the polymer matrix is an important factor which significantly improves the flame retardant behavior of the nanocomposite [226]. Here, the increased char residue of the nanocomposite with the increase in the concentration of nanoparticles indicates the enhanced flame resistance of the composite materials. This result will be further substantiated with the help of the LOI values of the composites.

4.2.7 Flame retardancy

Limiting oxygen index (LOI) is one of the major qualitative methods to analyse the flame resistance behavior or fire performance of elastomeric materials. LOI is the minimum content of oxygen required in a nitrogen/oxygen mixture of a self-sustained combustion of any material [227]. The LOI value of Cl-SBR and its nanocomposites with different loadings of ZnS nanoparticles are given in **figure 4.8**. The presence of dichloro groups in Cl-SBR affected the flammability due to the intumescences effect. The chlorine containing heavy gases produced during combustion of Cl-SBR reduced the access of oxygen and consequently suppresses the flame propagation of the polymer matrix. Halogen-containing species usually act in the vapour phase by capturing the radicals to interrupt the oxidative flame chemical processes and thus suppress the combustion of the polymer. It is well known that the fire resistance of polymeric composites depends on the nanofiller distribution and the synergistic interaction between the nanofiller and polymer. In the present study, the increased LOI value with the addition of nanoparticles is due to the strong interfacial interaction between the polar units of Cl-SBR with the ZnS nanoparticles. Also, the metal particles present in the nanoparticles reduces the carbonization of rubber generating more protective char

layer, which resists the transfer of heat and fuel and thereby inhibiting flammability [228].

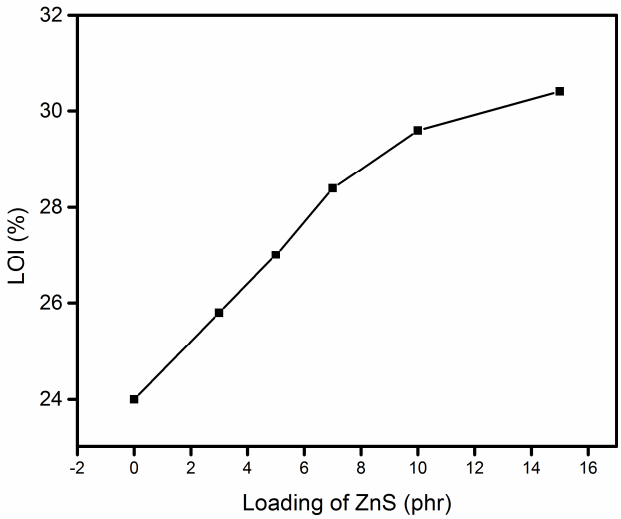

Figure 4.8 Flame resistance of Cl-SBR and Cl-SBR/ZnS nanocomposites

4.2.8 Cure characteristics

The vulcanization properties of rubber composites are expressed in terms of maximum torque (Mh), minimum torque (Ml), scorch time (ts_2) and optimum cure time (t_{90}). The cure properties of composites obtained from the rheometer are given in **table 4.1**. One can see that the maximum and minimum torques of sulphur vulcanized Cl-SBR/ZnS composites is higher than those of pure Cl-SBR vulcanizate, and the magnitude of torque values increases with the filler loading. The minimum torque value provides the viscosity of the polymer system. The maximum torque value provides the reinforcement of filler in the matrix and the cross-link density of the system [166]. From the table, one can see that the maximum and

minimum torque values increase with the loading of the nanoparticle up to 7 phr loading. This indicates a better polymer filler adhesion due to a strong intermolecular interaction among them. The decrease in the rheometric torque of samples at higher loading is attributed to the agglomeration of nanoparticles, which creates a poor adsorption curative for the system. The scorch time and optimum cure time show a decreasing trend with filler loading. This suggests that metal sulfide acts as a co-activator during the vulcanization process, which leads to higher cross-linking in the polymer matrix. Hwang *et al.* [229] have already reported this type of vulcanization behavior in NBR nanocomposites. The metal sulphide nanoparticles are protruded into the interface of NBR and promoting the adsorption of curatives leads to easier and faster formation of cross-links.

Table 4.1 Processing characteristics of Cl-SBR and Cl-SBR/ZnS nanocomposites

Sample code	Cure time, t_{90} (min)	Scorch time, t_2 (min)	Maximum torque (dNm)	Minimum torque (dNm)
CSZ_0	14	4.0	34	9.25
CSZ_3	12.2	3.75	37	10.4
CSZ_5	11.4	3.52	41	11.8
CSZ_7	10.5	3.26	46	12.9
CSZ_{10}	9.6	3.04	45.4	12.3
CSZ_{15}	8.5	2.78	43.7	11.0

4.2.9 Mechanical properties

Various mechanical properties such as tensile strength, modulus, elongation at break, tear resistance, hardness, abrasion loss, resilience and build-up of Cl-SBR with different loading of ZnS nanoparticles are

determined and stated in **table 4.2**. The tensile strength, modulus at 200% and tear resistance of Cl-SBR composites are much greater than the pure Cl-SBR and the magnitude of these properties increases dramatically with the increase of nanoparticle contents up to 7 phr loading.

Table 4.2 Mechanical properties of Cl-SBR and Cl-SBR/ZnS nanocomposites

Properties	Loading of ZnSnanoparticles (phr)					
	0	3	5	7	10	15
Tensile strength (MPa)	7.45	10.79	14.85	19.23	17.69	15.34
Elongation @ break (%)	398	379	362	344	328	302
Modulus (200%)	2.44	3.94	6.21	9.41	9.03	8.09
Tear strength (kN/m)	27.3	31.2	34.8	38.2	37.4	36.1
Hardness (Shore A)	35	36	37	38	39	42
Heat build-up (^{o}C)	12.3	13.2	14.9	16.0	17.3	17.8
Compression set (%)	12.6	13.5	14.8	15.9	15.4	14.8
Abrasion loss (mm^3)	77.0	76.4	76.0	75.6	75.9	76.4
Resilience (%)	36.3	35.6	32.4	30.6	28.7	27.1

The main reason for the reinforcement at this loading is the uniform insertion of nanoparticles into the Cl-SBR matrix. More specifically, the strong intermolecular interaction of the polar segments of Cl-SBR with nanoparticles leads to increased mechanical performance. The reinforcement is also associated with compatibility between Cl-SBR chains and the nanofillers. From the table, one can see that the tensile and tear properties of composites are slightly decreased at a higher loading of fillers (above 7 phr); this is due to the agglomeration of nanoparticles [230]. **Table 4.2** shows the elongation at break (EB) of

the Cl-SBR nanocomposite, and the EB is found to decreases with an increase in the loading of nanoparticles. Shore hardness is a measure of the resistance of a material has to indentation; Shore A values of Cl-SBR nanocomposites are given in **table 4.2**. The hardness of the nanocomposite usually increases with the addition of rigid fillers. Nanocomposites exhibit higher hardness than the unfilled sample. The resistance of rubber to abrasion is measured as the percentage of the loss of weight compared to the original material weight. The abrasion resistance of Cl-SBR/ZnS nanocomposites is given in the same table. Nanocomposites show better abrasion resistance than Cl-SBR vulcanizates. The small particle sized filler has a large surface area and, thus, there is greater interaction between nanoparticles and the polymer matrix. In the present study, the interaction between nanoparticles and polymer is maximum at 7 phr loading and therefore better abrasion resistance is shown. The low abrasion resistance beyond 7 phr loading is due to the self-aggregation of nanoparticles. Rubber rebound resilience is its ability to return to its original position after being bent or compressed; the resilience values of Cl-SBR nanocomposites are also given in the table. Resilience decreases with the addition of nanoparticle; this is a general trend of rubber composite. The compression set measurement is used to measure the ability of elastomeric materials to maintain elastic properties even after prolonged compressive stress. **Table 4.2** shows the compression set values of the Cl-SBR with different loadings of the ZnS nanocomposite. Pure Cl-SBR has higher compression set values than nanocomposites, and upon an increase in filler loading, the compression set values decreases. Heat build-up is an important

property of elastomers; the data is commonly used to estimate the service quality of different compounds for evaluation of material options in end-product applications. From the table, one can see that the heat build-up of the elastomeric composite is enhanced with the number of nanoparticles; this is due primarily to the more extensive cross-linking achieved through better thermal conductivity [231].

4.2.10 Electrical properties

4.2.10.1 AC Conductivity Studies

The AC conductivity of polymers can be altered by the addition of metal nanoparticles due to their intriguing properties arising from their size associated with a large surface area. **Figure 4.9** shows the AC conductivity of Cl-SBR with different loadings of ZnS nanoparticles at various frequencies at room temperature. The conductivity of the polymer/conductive filler composite originates from three mechanisms: (1) the passage of electrons through the conductive system (2) the electron hopping or tunnelling mechanism and (3) the electric field radiation [232]. Among these, the electron tunnelling mechanism is the major factor affecting the conductivity of the polymeric materials. The conductivity pattern shows a frequency independent plateau at a low frequency region and an increasing trend of conductivity at higher frequencies for all the samples.

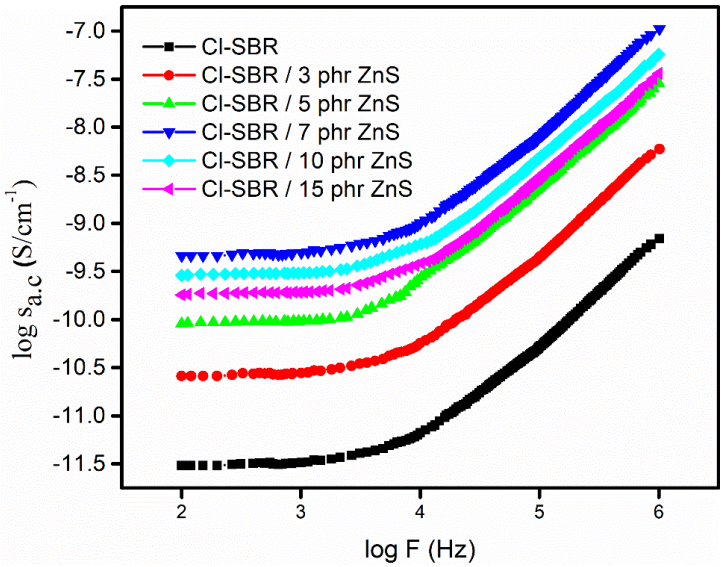

Figure 4.9 AC conductivity of Cl-SBR and Cl-SBR/ ZnS nanocomposites

The AC conductivity of Cl-SBR/ZnS nanocomposite is greater than the pure Cl-SBR and the conductivity increases with the concentration of metal nanoparticles up to 7 phr loading. The poor conductivity of Cl-SBR is due to the randomly oriented macromolecular chains (confirmed from XRD). The increase in conductivity with the ZnS loading can be described to the decreasing distance between the conductive fillers. The tunnelling mechanism is dominant at 7 phr loading due to the strong interaction between the nanoparticles and the polar segments of elastomers. These interactions enhance the uniform compactness of the polymeric structure leading to higher conductivity. The lower conductivity of the nanocomposite at higher concentration of nanoparticles (above 7 phr) is due to the agglomeration of nanoparticles in chlorinated SBR [198].

4.2.10.2 Dielectric Constant

The dielectric properties of polymer composites are determined by its molecular structures. Dielectric constant recorded as a function of frequency, at room temperature, for Cl-SBR/ ZnS nanocomposites is plotted in **figure 4.10**. It can be observed that the dielectric constant of all the composites is greater than the pure chlorinated SBR. This means that the nanocomposites are greatly polarized more than that of Cl-SBR. The enhancement in dielectric constant is ascribed to the interfacial polarization phenomenon developed in the heterogeneous materials that have different conductivity stages. The interfacial polarization of composite usually decreases with increasing the frequencies. The charge carriers developed by the application of electric field are completely oriented in a uniform direction, which results in interfacial polarization and consequently the dielectric constant is high at lower frequencies. However at higher frequencies, the electron exchange among the charge carriers cannot be oriented in the direction of applied field and, therefore, the resultant dielectric constant is always lower, indicating the poor interfacial polarization in polymer composites [233]. The dielectric constant of polymer composites is directly related to the molecular structures, polarizations, and interfacial interactions between the filler particles and polymeric chain. The dielectric constant of 7 phr Cl-SBR/ZnS composite is significantly higher than those of other four composites in the entire range of frequencies. The high dielectric value is due to the formation of uniform clusters. A cluster may be considered as a region where the nanoparticles and the elastomer stick together uniformly or are very

close to each other because of the intermolecular interaction or polar-polar interaction between the filler and the polymer matrix. In the present study, the average polarization associated with the uniform cluster is the maximum in 7 phr loading. The increased interfacial interaction facilitates the orientation of dipoles, thereby leading to an increase in the dielectric values. The decrease in the dielectric constant of the composite beyond 7 phr loading can be explained by the poor interaction of filler and polymer and also with the agglomeration of nanoparticles. It is well known that the segmental mobility of the polymer decreases with the loading of nanoparticles and therefore the dielectric property decreases at higher loading.

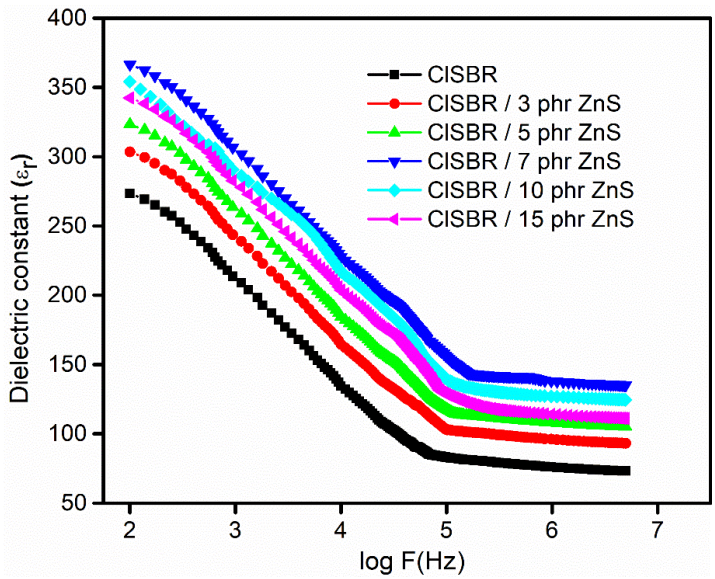

Figure 4.10 Dielectric constant of Cl-SBR and Cl-SBR/ZnS nanocomposites

4.2.10.3 Dielectric Loss Tangent (Tan δ)

Dielectric loss is the amount of energy dissipated through the rotation or movement of molecules by the application of an external electric field. The loss tangent (Tan δ) of Cl-SBR nanocomposites with different loadings of ZnS nanoparticles at room temperature is shown in **figure 4.11**. The dielectric response of composites materials usually depend on the interfacial polarizations, the mobility of the polymer chain and the polarity of the polymer composites.

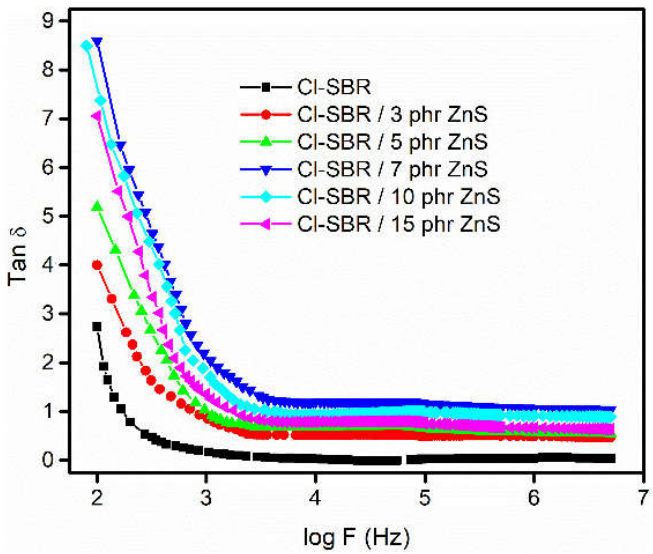

Figure 4.11 Dielectric loss tangent of Cl-SBR and Cl-SBR/ZnS nanocomposite

One can see that the dielectric loss of all the compounds decreases in the frequency range from 10^2 to 10^4 Hz. The decreasing trend of Tan δ at low frequencies is the typical behavior of interfacial polarizations [173]. The Tan δ of all the samples reaches a constant value at 10^5 Hz.

This high frequency behavior is due to the Debye relaxation process through the dipole orientation polarization of the polymer matrix. The Tan δ values of all the nanocomposites are higher than those of the pure Cl-SBR. The dielectric loss of composites increases with an increase of the ZnS loading up to 7 phr. Afterward, the loss factor decreases significantly with the concentration of nano-fillers. At higher loading, nanoparticles agglomerate in the polymer composite, which decreases the interaction between the filler and the polymer, leading to a lower dielectric value.

4.2.11 Oil Resistance

Transport of oil and fuel through elastomers is the major controlling factor in many of the barrier applications in the automobile industry since a variety of spare parts may be exposed to oils, fuels and greases [226]. **Figure 4.12** shows the resistance of the chlorinated SBR and its nanocomposites to ASTM oil. It can be observed that the percentage of oil uptake is significantly decreased after the addition of ZnS nanoparticles to chlorinated SBR. The oil resistance of rubber depends on the electro-negativity of rubbers, crystallinity, crosslink density in the matrix, and polarity of the solvent.

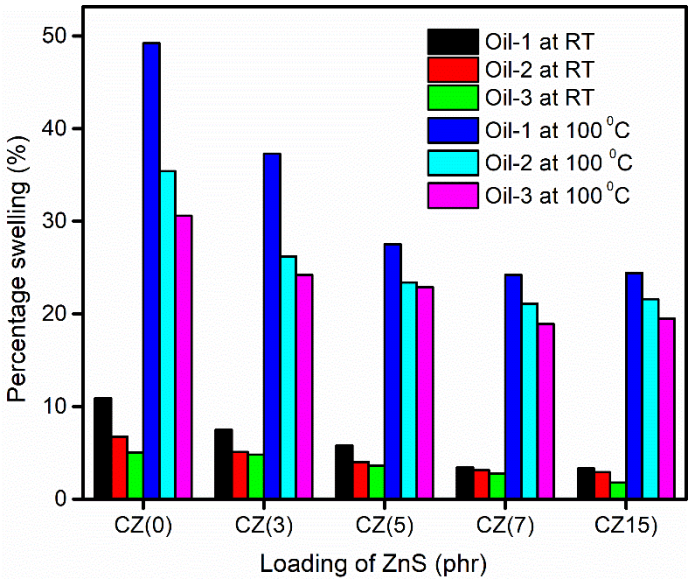

Figure 4.12 Oil resistance of Cl-SBR and Cl-SBR/ZnS nanocomposites at different temperatures

The oil resistance of the composites decreases with the loading of nanoparticles up to 7 phr loading. This can be attributed to the fact that the effective interaction of crystalline ZnS with chlorinated rubber restricts the penetration of oil into the intermolecular spaces and hence decreases the swelling percentage. On increasing the loading of nanoparticles (above 7 phr), the oil resistance is found to be decreasing and this due to the loosely bound filler particles in the polymer matrix. The oil resistance of all the vulcanizates is found to be decreasing with the increases in temperatures, as more solvent could penetrate inside the polymeric matrix.

4.2.12 Diffusion studies

4.2.12.1 Mol % uptake of aromatic and petroleum fuels

The percentage uptake (Q_t %) of different solvents were plotted against the square root of the time. The mol uptake of solvents depends on the filler content, temperature and molecular weight of solvents. And the Q_t % was calculated using the **equation 3.1.**

Effect of ZnS concentration on mol uptake

The influence of ZnS nanoparticles on the mol uptake of benzene and petrol through Cl-SBR/ZnS nanocomposites at room temperature is presented in **figure 4.13** and **4.14** respectively. All the solvents show the same trend and the decrease in diffusion and sorption of the nanocomposites is due to the increased interfacial interaction between the nanoparticles and the macromolecular chain of the polymer. Upon addition of fillers, the local mobility of polymer segments are restricted, thus the flexibility of polymer gets lowered, which leads to the decreased sorption [234]. The better distribution of ZnS nanoparticles in the Cl-SBR matrix enhances the surface area of the reinforcing phase. At lower concentrations of loading, the penetrant molecules can pass through the matrix very easily due to the homogeneous distribution of filler particles. The composite with 7 phr of ZnS showed minimum swelling and the unfilled matrix showed the highest sorption. The solvent uptake of polymer matrix varies with reference to the free volume inside the matrix. By the addition of filler, free volume inside the matrix lowers, which in turn decreases the equilibrium uptake of solvent.

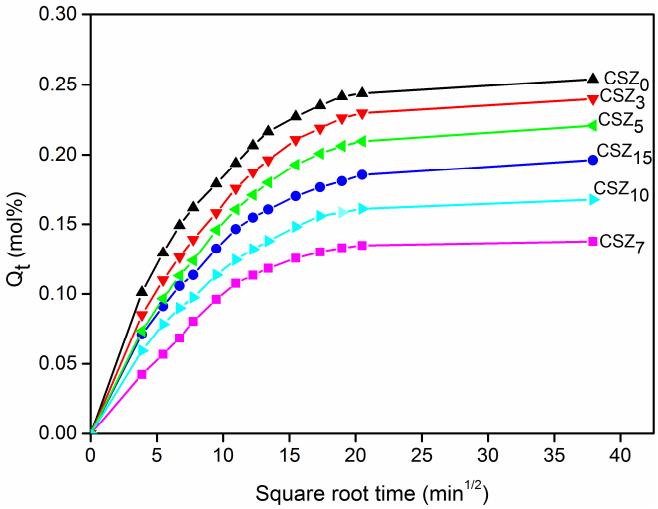

Figure 4.13 Sorption curves of Cl-SBR and Cl-SBR/ZnS nanocomposite in benzene

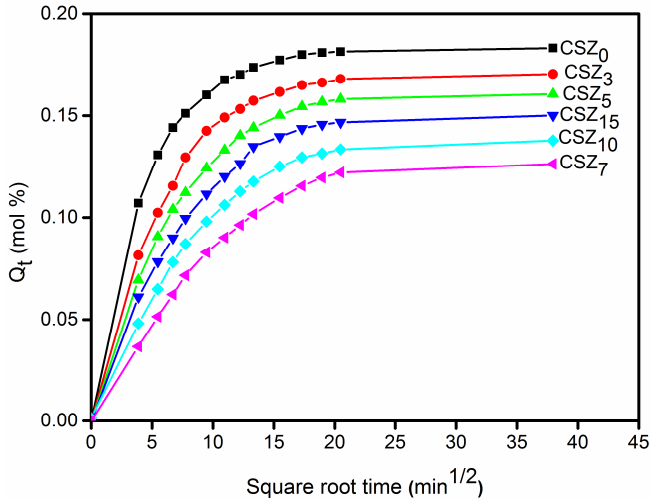

Figure 4.14 Sorption curves of Cl-SBR and Cl-SBR/ZnS nanocomposite in petrol

The Nature of solvent on sorption behavior

The effect of penetrant size was studied using aromatic and industrial solvents like and the results are summarized in **figure 4.15** and **4.16**. In

the case of aromatic solvents, benzene shows the maximum and xylene shows the minimum sorption and the toluene lies in between. Petrol in petroleum fuels shows high sorption and kerosene and diesel shows intermediate and minimum sorption. As penetrant size increases, the diffusivity values decreases, which can be explained on the basis of free volume theory [235]. According to the free volume theory, the rate of diffusion depends on the ease of exchange of polymer segments and their positions with the penetrant molecules. As the molar volume of solvent increases, the exchange of polymer segments becomes difficult. It is well recognized that the solvent uptake decreases with increase in the reinforcement of filler particles in the polymer matrix. The activation energy needed for the sorption of large molecules is very high, which is the reason for the decrease in the solvent uptake.

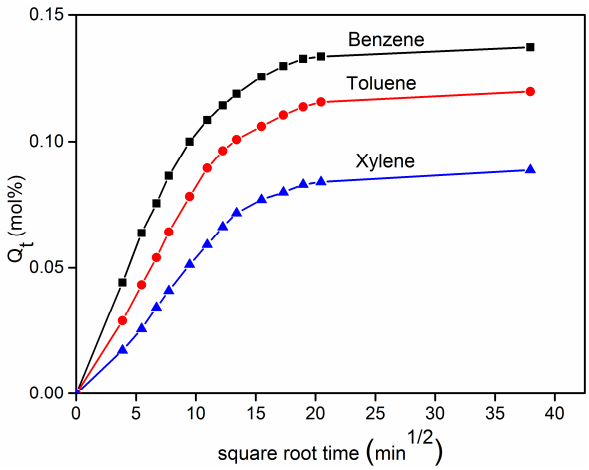

Figure 4.15 Solvent uptake of Cl-SBR with 7phr of ZnS in aromatic solvents

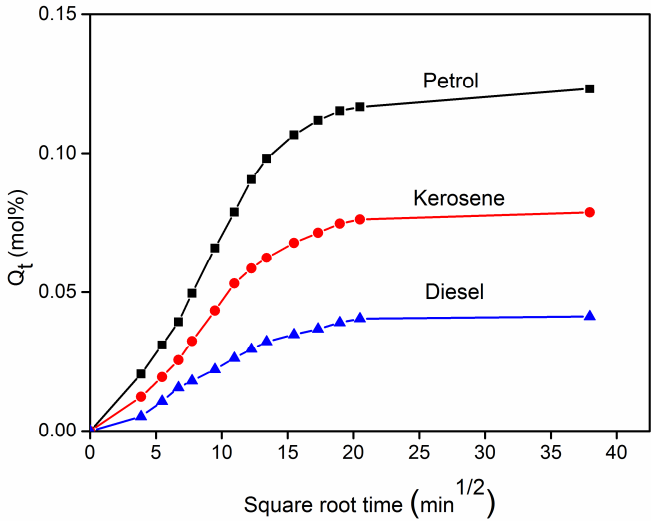

Figure 4.16 Solvent uptake of Cl-SBR / ZnS nanocomposite in industrial solvents

4.2.12.2 Mechanism of sorption

The transport mechanism can be calculated using the **equation 3.3**, the transport is called Fickian, when the value of n=0.5, where the chain relaxation of the polymer chain is higher than that of rate of diffusion of the solvent. If n=1, the mode of transport is called non-Fickian, in which the penetration of the solvent is higher than that of polymer chain relaxation [185]. In this study, the value of n is changing from a Fickian mode anomalous mode of transport in case of petroleum fuels (**Table 4.4)**. The anomalous mode of transport can be due to: (1) the occurrence of a slow and viscous polymer chain relaxation upon reinforcement with the filler and (2) the coupling between Fickian and non-Fickian. From the **table 4.3**, it is found that the value of n is approaching 1, which means the transport mechanism changed anomalous mode to non-Fickian mode [236]. The structural property of

the polymer is obtained from the value of k. It also provides an idea about the interaction between a polymer matrix and penetrant molecules. Nanocomposites have a lower value of k as compared to the pure matrix, indicating the less interaction between the solvent and the penetrant. A composite with 7 phr ZnS showed the lowest k value, which is due to the uniform distribution of nanoparticles in the polymer matrix.

Table 4.3 n and k values of Cl-SBR/ZnS nanocomposites in aromatic solvents

Samples	Benzene		Toluene		Xylene	
	n	$Kx10^2(min^{-1})$	n	$kx10^2(min^{-1})$	n	$Kx10^2(min^{-1})$
CSZ_0	0.54	0.16	0.63	0.12	0.72	0.11
CSZ_3	0.57	0.14	0.69	0.11	0.79	0.09
CSZ_5	0.62	0.12	0.76	0.09	0.83	0.07
CSZ_7	0.79	0.04	0.89	0.05	0.96	0.03
CSZ_{10}	0.73	0.09	0.84	0.07	0.89	0.05
CSZ_{15}	0.71	0.11	0.81	0.08	0.87	0.06

Table 4.4n and k values of Cl-SBR/ZnS nanocomposites in petroleum fuels

Samples	Petrol		Kerosene		Diesel	
	n	$Kx10^2(min^{-1})$	n	$kx10^2(min^{-1})$	n	$Kx10^2(min^{-1})$
CSZ_0	0.42	0.26	0.52	0.23	0.54	0.20
CSZ_3	0.49	0.25	0.58	0.22	0.69	0.19
CSZ_5	0.69	0.20	0.65	0.17	0.72	0.15
CSZ_7	0.79	0.15	0.81	0.11	0.85	0.09
CSZ_{10}	0.78	0.16	0.79	0.15	0.81	0.12
CSZ_{15}	0.77	0.17	0.72	0.14	0.71	0.11

4.2.12.3 Diffusion (D), sorption (S) and permeation (P) coefficients

Table 4.5 and **4.6** summarizes the coefficient of diffusion, sorption, and permeation of Cl-SBR ZnS nanocomposites in aromatic and

industrial solvents. The coefficient of diffusion is a kinetic parameter related to the segmental motion of the polymer matrix, from which the rate of diffusion can be evaluated. According to Fickian law, the coefficient of diffusion can be calculated as the ratio of the diffusing substance per unit area of cross section to the space gradient of the concentration using the **equation 3.2**. The diffusion coefficient decreases with the loading of nanoparticles and the lowest value have obtained for composite with 7 phr of ZnS nanoparticles. The reduction of free volume by the addition of the filler is due to the decrease in free volume within the matrix and a better distribution of nanoparticles in the polymer matrix. It is also seen that the diffusion coefficient values decrease when going from benzene to xylene in the case of aromatic solvents and petrol to diesel in the case of petroleum fuels. Generally, high activation energy is needed for large molecules to create free volume in the polymer matrix [206].

The sorption coefficient S is calculated using **equation 4.1**

$$S = \frac{W_\infty}{W_p} \qquad \textbf{(Eq: 4.1)}$$

Here, W_∞ is the weight of the penetrant at equilibrium absorption and W_p is the polymer's weight. It is also seen from the table that the sorption coefficient decreases upon the addition of ZnS, and the least value of the sorption coefficient is observed for the composite with 7 phr loading. The trend in the sorption coefficient is similar to that of the diffusion coefficient.

Permeation Coefficient (P) is obtained upon the multiplication of the sorption and diffusion coefficient, we have an idea about the penetrant permeated into the unit area of sample per second. **Table 4.5** and **4.6** also reveals that the decrease in diffusion coefficient values in accordance with the filler concentration causes the decrease in the permeation of the solvent into the composite materials. The composite with 7 phr of ZnS shows the minimum, and the sample without filler shows the maximum permeation coefficient. The coefficient of sorption, diffusion, and permeation of all the solvents through nanocomposite with different contents of ZnS show a similar trend as summarized in **table 4.5** and **4.6**.

Table 4.5 D, S and P values of Cl-SBR/ ZnS nanocomposites in aromatic solvents

Samples	Diffusion coefficient D x 10^5 (cm^2/s)			Sorption coefficient S			Permeation coefficient P x 10^5(cm^2/s)		
	Benzene	Toluene	Xylene	Benzene	Toluene	Xylene	Benzene	Toluene	Xylene
CSZ_0	1.72	1.61	1.38	1.18	1.13	1.09	2.03	1.81	1.50
CSZ_3	1.57	1.51	1.32	1.15	1.09	1.06	1.81	1.64	1.39
CSZ_5	1.48	1.39	1.27	1.11	1.06	1.02	1.64	1.47	1.29
CSZ_7	1.15	1.13	1.07	1.04	1.01	0.92	1.19	1.14	0.98
CSZ_{10}	1.37	1.24	1.19	1.09	1.04	0.97	1.49	1.28	1.15
CSZ_{15}	1.39	1.29	1.21	1.11	1.05	0.99	1.54	1.35	1.19

Table 4.6 D, S and P values of Cl-SBR/ZnS nanocomposites in industrial solvents

Samples	Diffusion coefficient D x 10^5 (cm^2/s)			Sorption coefficient S			Permeation coefficient P x 10^5(cm^2/s)		
	Petrol	Kerosene	Diesel	Petrol	Kerosene	Diesel	Petrol	Kerosene	Diesel
CSZ_0	1.47	1.32	1.21	1.17	1.14	1.11	1.71	1.50	1.34
CSZ_3	1.35	1.21	1.15	1.15	1.11	1.08	1.55	1.34	1.24
CS Z_5	1.31	1.15	1.10	1.07	1.04	1.03	1.40	1.19	1.13
CSZ_7	1.09	0.91	0.84	0.98	0.91	0.87	1.06	0.82	0.73
CSZ_{10}	1.17	1.11	0.91	1.03	0.95	0.91	1.21	1.05	0.82
CSZ_{15}	1.19	1.13	1.01	1.06	0.99	0.93	1.26	1.11	0.93

4.2.12.4 Effect of temperature on sorption behavior

The effect of temperature on diffusion studies are done using benzene at 27, 50 and 70°C and petrol 27, 40 and 50°C for the composite with 7 phr of ZnS is shown in **figure 4.17** and **4.18** respectively. The sample CSZ_7 (Cl-SBR/7phr ZnS) has selected to study the effect of temperature on benzene and petrol because it possesses the highest solvent resistance at room temperature. The mol uptake increases as the temperature increases. This is due to: (1) the increase in free volume inside the matrix and (2) the increase in the kinetic energy and segmental motion of the polymer chain [206]. Using the values of D and P in these three temperatures, the activation energy of diffusion and permeation was calculated and summarized in **table 4.7** (aromatic solvents) and **4.8** (petroleum fuels). According to Arrhenius **equation 3.4**

$$X = X_0 \exp\left(\frac{-E_X}{RT}\right) \qquad \textbf{(Eq: 3.4)}$$

Where X is D or P, and X_0 is D_0 or P_0 and E_x is the activation energy of diffusion (E_D) and permeation (E_P). E_D and E_P correspond to the

slope of the straight lines obtained by plotting log P and log D versus 1/T, respectively.

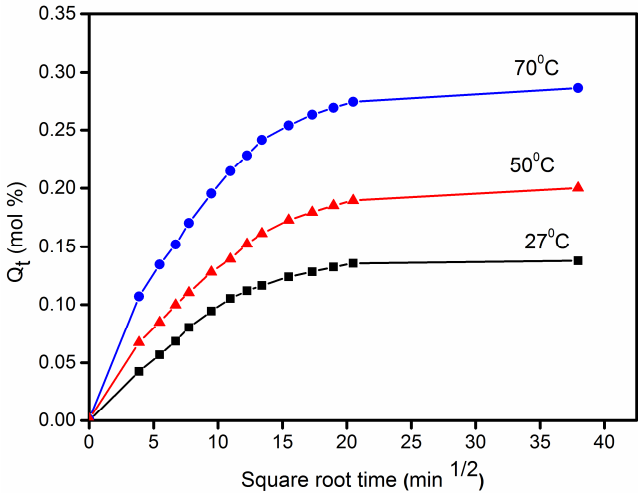

Figure 4.17 The mole uptake of 7 phr Cl-SBR/7 phr ZnS at different temperature in benzene

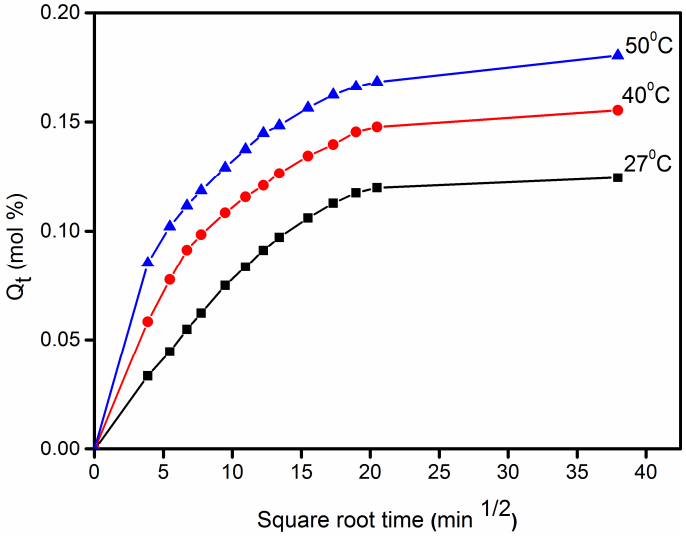

Figure 4.18 The mole uptake of 7 phr Cl-SBR/7 phr ZnS at different temperature in petrol

It is clear from the **table 4.7** and **4.8** that on increasing the filler concentration and penetrant size increase, the activation energy also increases. For larger molecules, more space is needed to penetrate into the polymer matrix. The higher amount of energy is required to create free voids within the matrix and therefore the activation energy of diffusion and permeation increases. In the present study, CSZ_0 (pure matrix) showed the lowest and CSZ_7 (Cl-SBR with 7 phr of ZnS) showed the highest value of E_P and E_D values. The activation energies of diffusion and permeation are low at higher loading of nanoparticles, and this mainly due to the agglomeration of nanoparticles in the polymer.

Table 4.7 E_D, and E_P (kJ mol^{-1}) values of CSBR/ZnS nanocomposites in aromatic solvents

Samples	Benzene		Toluene		Xylene	
	E_P	E_D	E_P	E_P	E_D	E_P
CSZ_0	6.24	5.26	6.42	5.28	6.67	5.46
CSZ_3	6.34	5.29	6.53	5.34	6.79	5.54
CSZ_5	6.48	5.32	6.64	5.47	6.89	5.63
CSZ_7	6.64	5.57	6.79	5.64	6.99	5.72
CSZ_{10}	6.59	5.54	6.76	5.59	6.96	5.68
CSZ_{15}	6.53	5.49	6.69	5.56	6.91	5.65

Table 4.8 E_D and E_P (kJ mol^{-1}) values of Cl-SBR/ZnS nanocomposites in industrial solvents

Samples	Petrol		Kerosene		Diesel	
	E_P	E_D	E_P	E_D	E_P	E_D
CSZ_0	4.83	3.79	5.31	4.23	5.67	4.54
CSZ_3	5.54	4.39	5.69	4.57	6.68	5.39
CSZ_5	7.17	6.01	7.54	6.26	8.89	7.01
CSZ_7	7.79	6.37	8.44	6.52	9.89	7.69
CSZ_{10}	7.62	6.28	8.26	6.48	9.64	7.49
CSZ_{15}	7.47	6.25	7.98	6.37	9.59	7.47

4.2.12.5 Thermodynamic Parameters

The thermodynamic properties such as enthalpy (ΔH_s) and entropy (ΔS_s) of sorption can be calculated from the Van't Hoff's relation [206]

$$\log K_s = \frac{\Delta S_s}{2.303R} - \frac{\Delta H_s}{2.303RT} \qquad \textbf{(Eq: 3.5)}$$

Where K_s is equilibrium sorption constant, which is the ratio of the number of moles of sorbed solvent at equilibrium to the mass of the polymer sample. The values of ΔH_s and ΔS_s are obtained by regression analysis of log Ks against 1/T. From the **table 4.9** and **4.10** it can be seen that all the samples show positive values of ΔH_s, which is a clear indication of endothermic sorption. The entropy changes in all the samples are also positive and are found to be decreasing upon the increase of filler loading. At higher loading, an increase in filler polymer contact occurs and causes a decrease in solvent diffusion.

Table 4.9 ΔH, ΔS and ΔG (kJ/mol) of Cl-SBR/ZnS nanocomposites in aromatic solvents

Samples	ΔH			ΔS			-ΔG		
	Benzene	Toluene	Xylene	Benzene	Toluene	Xylene	Benzene	Toluene	Xylene
CSZ_0	0.874	0.887	0.899	0.067	0.055	0.046	19.23	15.61	12.90
CSZ_3	0.879	0.892	0.907	0.063	0.051	0.041	18.02	14.41	11.39
CSZ_5	0.885	0.897	0.914	0.061	0.047	0.036	17.41	13.20	9.89
CSZ_7	0.899	0.917	0.929	0.052	0.041	0.027	14.70	11.38	7.17
CSZ_{10}	0.894	0.909	0.922	0.057	0.044	0.033	16.20	12.29	8.97
CSZ_{15}	0.892	0.905	0.919	0.059	0.046	0.035	16.80	12.89	9.58

The free energy of sorption (ΔG_s) can be calculated from ΔH_s and ΔS_s values. The sample without the filler showed the minimum free energy

of diffusion and CSZ_7 shows the maximum ΔG_s. It reveals that the diffusion of the matrix without filler is more spontaneous on comparing with its composites, that is, on adding the filler the ΔG_s values become less negative. This is a clear indication of the increase in the tortoisty of sorption through the polymer [237].

Table 4.10 ΔH, ΔS and ΔG (kJ/mol) values of Cl-SBR/ZnS nanocomposites in industrial solvents

Samples	ΔH			ΔS			-ΔG		
	Petrol	Kerosene	Diesel	Petrol	Kerosene	Diesel	Petrol	Kerosene	Diesel
CSZ_0	0.912	0.934	0.973	0.052	0.047	0.037	14.68	13.17	10.127
CSZ3	0.959	1.129	1.568	0.048	0.041	0.035	13.44	11.17	8.932
CSZ_5	1.179	1.298	1.843	0.044	0.034	0.025	12.02	8.902	5.657
CSZ_7	1.277	1.998	2.152	0.027	0.021	0.013	6.828	4.302	1.748
CSZ_{10}	1.262	1.889	2.087	0.036	0.025	0.017	9.538	5.601	3.013
CSZ_{15}	1.259	1.567	1.972	0.039	0.027	0.019	10.44	6.533	3.728

4.3 Conclusions

Cl-SBR/ZnS nanocomposites were prepared by a two-roll mill mixing method with different loading of ZnS nanoparticles and characterized by FTIR, UV, XRD, SEM, TEM, DSC, TGA and LOI analysis. The intermolecular interaction between nanoparticles and Cl-SBR was confirmed from FTIR and UV spectrum by the shift in the absorption peaks of the polymer matrix. The XRD results indicated that the amorphous nature of Cl-SBR was decreased with the addition of nanoparticles. The TEM and SEM images revealed the presence of ZnS nanoparticles which were uniformly distributed in the elastomer at 7 phr loading. The thermal stability and flame retardancy were greatly enhanced with the addition of ZnS nanoparticles. The processability, mechanical, electrical, oil and solvent imbibing properties of

composites were also investigated with respect to filler loading. Cure properties like optimum cure and scorch time decreased with an increase in the concentration of nanoparticles. Mechanical properties like tensile and tear strength have been found to increase up to a threshold loading (7phr), followed by a decrease in tensile and tear resistance at a still higher loading. The elongation at break, resilience and compression set values decreased with the addition of ZnS nanoparticles. The AC conductivity and dielectric properties were found to be maximum at 7 phr loading of ZnS. Composite with 7 phr loading absorbed less oils and solvent compared to those of other composites and with pure Cl-SBR, indicating a better interaction between filler and rubber. Transport behavior of samples in aromatic and industrial solvents at different temperatures was analysed. Transport properties such as diffusion coefficient, sorption coefficient and permeation coefficient have been estimated with respect to loading of nanoparticles, nature of solvent and temperature. The mechanism of diffusion was found to be Fickian in nature for Cl-SBR, while in the nanoparticles filled composites, it was anomalous.

5.1 Introduction

Scientists and technologists are highly motivated in the fabrication of polymer under composites; afford fantastic properties in addition to macro or microparticles [189]. The polymer composites filled with particles are excellent in properties due to its wide application and very low cost. Nanoparticles will reinforce polymer matrix in its physical properties like mechanical strength, modulus and hardness [220, 238]. This shows the mechanical properties of polymer composites are mainly determined by size, shape and the way in which the filler particles are dispersed in the polymer matrix and also the interfacial interaction between the filler and polymer matrix. The large interfacial area per unit volume of nanoparticles and its low weight will impart the distinguished reinforcement of nanocomposites. Generally polymers are good insulators, though it is used as insulating materials in electric wire, however the addition of inorganic nanofillers into the elastomer the leads the polymer composite with excellent electrical properties [178]. Today nanoparticle has many applications, and has more attraction in various fields. Among these, nano-clay has been extensively used in the nanocomposite preparation.

The synthetic and amorphous elastomer such as styrene butadiene rubber (SBR) with filler particles will help a stand up in thermal, transport and electrical properties of new composites. Manganous tungstate ($MnWO_4$) is an important metal oxide with excellent properties such as photo catalysts, optical fibres, photo sensors, humidity sensor and multi-ferroic materials etc. [239, 240]. It has an important role in the fabrication of various electronic devices due to its specific structure and properties. In the present study, $MnWO_4$ is used as reinforcing filler for the fabrication of styrene

butadiene rubber (SBR) composite. $MnWO_4$ was mixed with SBR in a two-roll mill mixing in the presence of phase transfer catalyst in order to minimize agglomeration. The fabricated composites were characterized by FTIR, UV- visible spectroscopy, scanning electron microscopy and X-ray diffraction analysis. Thermal stability and glass transition temperature of the composites were carried out by DSC and TGA respectively. The effect of metal nanoparticles on processing characteristics and mechanical properties of the nanocomposite has been investigated. Variation in AC conductivity and dielectric constant was studied with respect to the different content of $MnWO_4$ nanoparticles. Also, the transport characteristics of aromatic hydrocarbons and petroleum fuels were studied through the compounds to evaluate the reinforcement of the SBR matrix by the nanoparticles.

5.2 Results and discussions

5.2.1 FTIR- analysis

FTIR spectrum of SBR, $MnWO_4$ and SBR/$MnWO_4$ composite are given in **figure 5.1**. The intense peak at 2912 and 2836 cm^{-1} are the characteristic peaks of C-H stretching of the aromatic ring in SBR. The peak at 696 cm^{-1} corresponds to the styrene unit present in SBR [160, 228]. FTIR spectra of pure $MnWO_4$ shows the characteristic vibrations of the W-O bond at 708 and 590 cm^{-1} and a broad peak at 3448 cm^{-1}, attributed to the water molecule adsorbed on the surface of $MnWO_4$ particles. The absorption peak located at 850 cm^{-1} is responsible for WO_2 groups having symmetric stretching vibrations. The IR spectra of SBR/$MnWO_4$ composite contain all the characteristic peak of SBR and the metal nanoparticles at 559 cm^{-1}. It is seen that the reinforcement of

nanoparticles in SBR induces some justifiable changes in the spectrum of nanocomposite as compared to pure SBR. Also, the intensity and broadness of the composite is higher than the pure SBR and this is due to the strong interaction between SBR and the $MnWO_4$ nanoparticles.

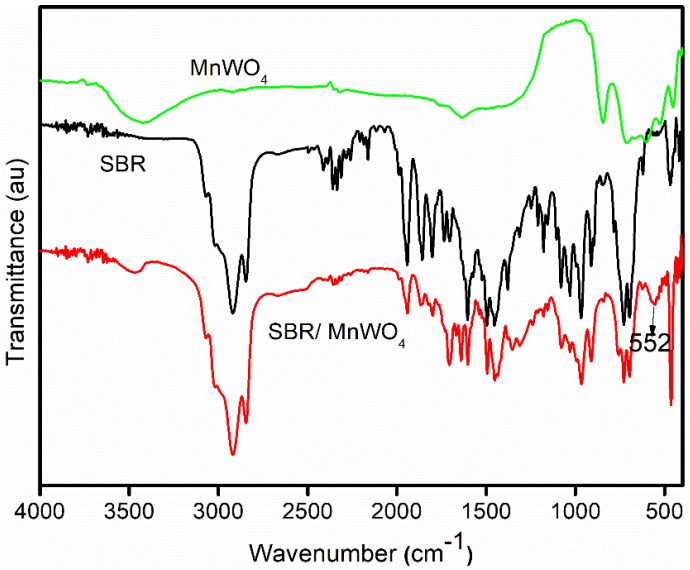

Figure 5.1 FTIR spectra of $MnWO_4$, SBR and SBR/$MnWO_4$ nanocomposite

5.2.2 UV-Visible spectrum

UV-visible spectra of SBR and SBR with different content of $MnWO_4$ are given in **figure 5.2**. In the UV spectrum of SBR, the absorption peak appeared at 294 nm, which is responsible for the π-π* transition. It is noted that as the concentration of the $MnWO_4$ nanoparticles increases, the absorption band shifted to higher wavelength region (i.e. from 294 nm to 303 nm). This indicates the encapsulation of the $MnWO_4$ nanoparticles, which can modify the electronic and spectral properties of composite materials [160]. It is interesting to observe that the absorbance of SBR/$MnWO_4$ composite is greater than the pure

SBR. The higher absorption is due to the interfacial interaction between the nanoparticles and the macromolecular chain of SBR. Among the composites, 10 phr of $MnWO_4$ nanoparticles/SBR shows the maximum absorbance and the efficiency of absorption decreases with the further addition of nanoparticles. Also the absorption edge of all composite is higher than pure SBR. The shifting of the absorption edge of the composite to higher wavelength region is a good indication for the formation of nanoparticles in the SBR matrix. The decrease in absorption at higher content of nanoparticle in SBR is due to the formation of clusters (aggregation of nanoparticles), which restrict the movement of polymer segment.

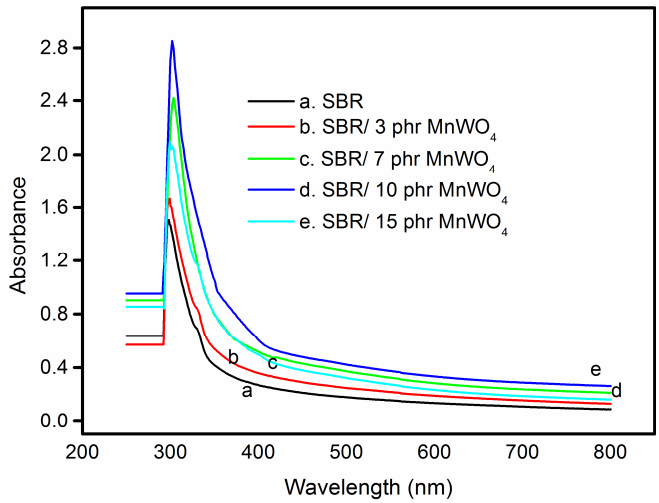

Figure 5.2 UV-Visible spectra of SBR and SBR/$MnWO_4$ nanocomposites

5.2.3 X-ray Diffraction Analysis (XRD)

The XRD profile of $MnWO_4$, SBR and SBR with 5 and 15 phr $MnWO_4$ filled SBR nanocomposites are presented in **figure 5.3**. The crystalline peaks of $MnWO_4$ are appeared at several regions in the

XRD curve indicating the highly crystalline nature of the metal nanoparticles [241]. SBR shows a broad peak at 2θ=20.7° indicating its amorphous nature. The XRD pattern of nanoparticles shows most of the crystalline peaks of $MnWO_4$ along with an amorphous peak of SBR. It is important to mention here that the broadness of the amorphous peak of SBR is found to decreases with increase in the concentration of nanoparticles. And the position of the amorphous peak is slightly shifted to lower XRD region (i.e., from 2θ = 20.7° to 17.88° for 5 phr composite). The decrease in amorphous nature of nanocomposite with diffraction angle is due to the strong interfacial interaction between the nanoparticles and polymer chain. Hence it can be inferred that the introduction of $MnWO_4$ nanoparticles into SBR collapse the amorphous structure of the polymer matrix.

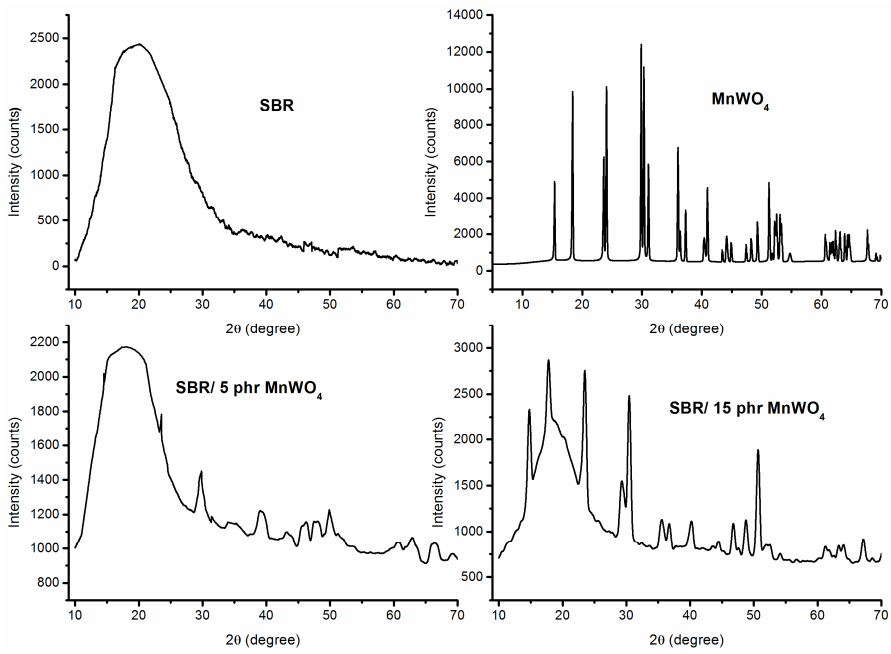

Figure 5.3 XRD of SBR, $MnWO_4$ and SBR/$MnWO_4$ nanocomposites

5.2.4 Morphological studies

The SEM images of SBR and SBR/ $MnWO_4$ composites are given in **figure 5.4**. The pure SBR (Fig. 4 a) showed the smooth surface indicating the homogenous surface of the elastomer. In the case of nanocomposite, it is observed that the $MnWO_4$ nanoparticles are well distributed in the polymer matrix. However, the regular structure of elastomer is totally destroyed when the loading of nanoparticles became 15 phr. The polymer interaction with the filler is too less at higher loading and also the particle to particle distance reduces, leads to a stress on the elastomer composite (i.e., agglomeration of nanoparticles).

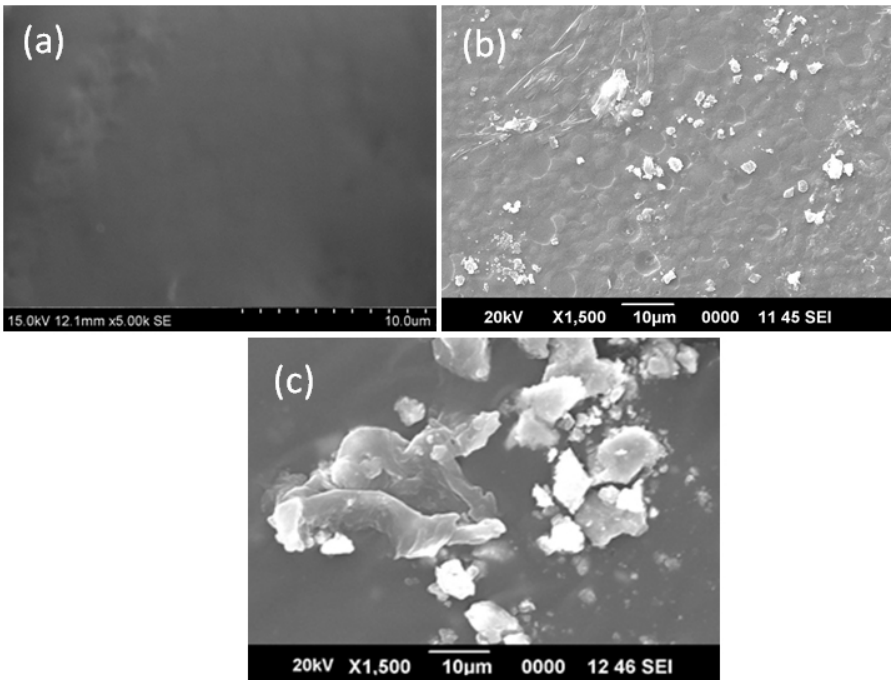

Figure 5.4 SEM images of (a) SBR (b) SBR/ 5 phr $MnWO_4$ and (c) SBR/15 phr $MnWO_4$

5.2.5 Thermal properties

5.2.5.1 Differential scanning calorimetry (DSC)

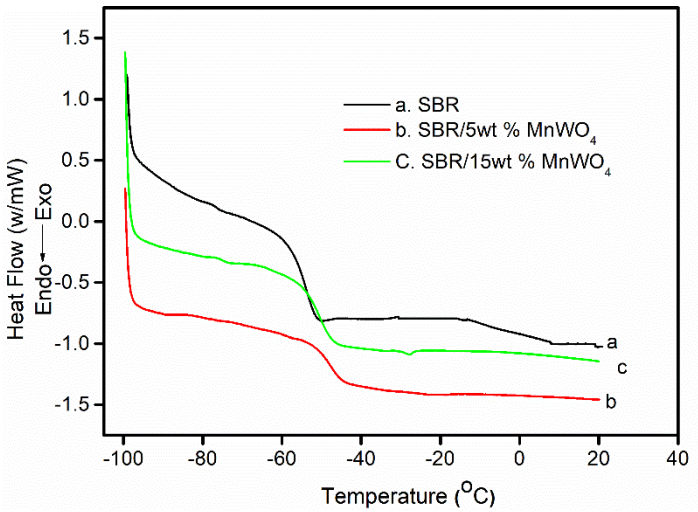

Figure 5.5 DSC plots of SBR and SBR/$MnWO_4$ nanocomposites

For the DSC analysis, about 5 mg of the samples are heated from -80°C to 40°C under the nitrogen atmosphere with a programmed heating rate of 5°C/min. The effect of $MnWO_4$ on the glass transition temperature (T_g) of SBR and SBR with $MnWO_4$ nanoparticles are presented in **figure 5.5**. SBR shows the Tg at -56°C. The composite with 7 and 15 phr of $MnWO_4$ shows the glass transition temperature at -52.5°C and -49.7°C respectively. The increase in T_g of composite is due to high interfacial adhesion between filler particles and SBR segments and that inhibits the free rotational motion of the chain. It is clear from XRD studies that on increasing filler content compactness of matrix increases and also free volume inside the composite reduces, which cause restricted motion of polymer chains [242].

5.2.5.2 Thermogravimetric analysis (TGA)

TGA curve of the thermal degradation behavior of SBR with 5, 10 and 15 phr of $MnWO_4$ nanoparticles are shown in **figure 5.6**. The results show that the thermal stability of the nanocomposites is clearly enhanced by the incorporation of nanoparticles and all the samples show a single stage decomposition pattern. The thermal degradation of SBR is appeared at 401°C. The composite with 5, 10 and 15 phr is undergoing thermal decomposition at 411, 422 and 429°C respectively. The decomposition temperature of 10 phr of the composite is raised by 21°C than that of pure SBR. The increase in thermal stability on increase in loading of the nanoparticle is due to the higher interfacial interaction between nanoparticles and the polymer chain. Since the nanoparticles with the large surface area can effectively interact with SBR and this interaction leads to a protective layer on the surface of polymer matrix which restricts further thermal degradation of composite materials. Moreover, the final char residue left after 700°C for pure SBR is only 9.21%, while the composite with 5, 10 and 15 phr composite at 700°C are accompanied at 14.11, 18.09 and 13.52 % respectively. The increased value of char residue is an indication of the improved flame resistance of polymer composite [243].

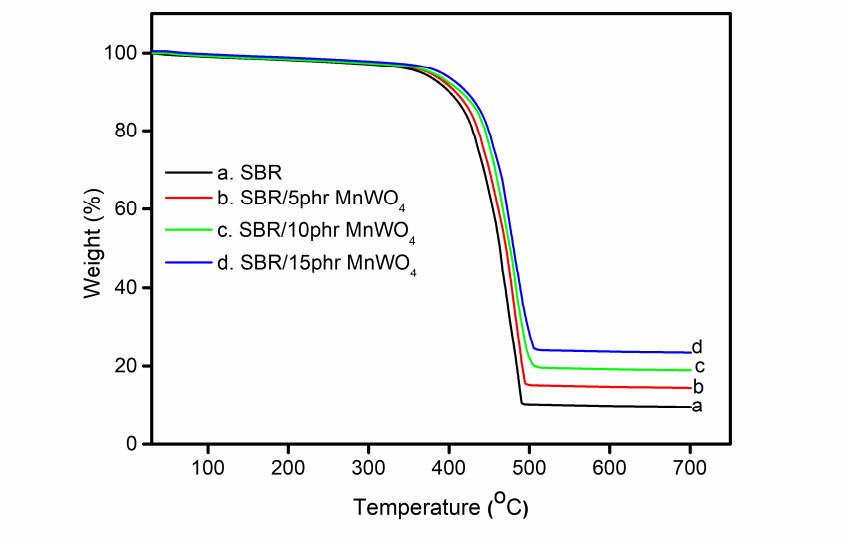

Figure 5.6 TGA SBR and SBR/$MnWO_4$ nanocomposites

5.2.6 Processing Characteristics

Table 5.1 represents the effect of different content of $MnWO_4$ nanoparticles on the curing or processing characteristics of SBR. It is clear that the scorch time and optimum cure time decreases with increase in loading of metal oxide nanoparticles in SBR. The decrease in cure properties as compared to pure SBR is due to the increased conducting nature of metal particles present in the composite. Also, the polymer matrix becomes more viscous and heated with the addition of nanoparticles which shortens the optimum cure time. The variation of torque (maximum and minimum torque) increases significantly with increase in loading of nanoparticles in SBR. The increase in rheometric torque is an indication of the crosslinking of the nanocomposite [244]. It is interesting to observe that the increase in torque is more pronounced at 10 phr filler loading and thereafter the torque value

decreases with the further addition of nanoparticles. It is well known that the maximum torque depends on the crosslink density which is directly related to the greater interaction between the filler and rubber matrix. The decrease in torque value at higher loading is attributed to the formation of the individual cluster in the polymer composite.

Table 5.1 Processing characteristics of SBR and SBR/$MnWO_4$ nanocomposites

Sample code	Cure time, t_{90} (min)	Scorch time, t_2 (min)	Maximum torque (dNm)	Minimum torque (dNm)
SM_0	15.7	4.8	29	6.9
SM_3	15.0	4.5	31	7.3
SM_5	14.3	4.13	34	7.7
SM_7	13.8	3.84	36	7.9
SM_{10}	13.2	3.52	39	8.3
SM_{15}	12.8	3.22	38	8.2

Table 5.2 Mechanical properties of SBR and SBR/ $MnWO_4$ nanocomposites

Properties	Loading of $MnWO_4$ nanoparticles (phr)					
	0	3	5	7	10	15
Tensile strength (MPa)	2.13	2.87	3.65	4.54	5.69	5.33
Elongation @ break (%)	425	412	399	383	370	351
Modulus (300%)	1.94	2.32	3.18	4.09	5.23	4.85
Tear strength (kN/m)	18	22	27	30	34	32
Hardness (Shore A)	33	35	36	37	39	42
Heat build-up (^oC)	10	11	12.3	13.5	14.9	16.4
Compression set (%)	19.8	18.9	18.01	17.6	17.0	16.2
Abrasion loss (mm^3)	66.8	66.4	66.2	66.0	65.7	65.9
Resilience (%)	46.24	45.89	44.96	44.05	43.59	43.01

5.2.7 Mechanical Properties

Tensile strength measurement has a major role among the other mechanical properties because the composite having higher tensile strength seem to perform well in daily service. The effect of $MnWO_4$ nanoparticles on the mechanical properties of SBR are summarised in **table 5.2**. The tensile strength and modulus (at 300% elongation)of composite increased with the loading of nanoparticles up to 10 phr. Higher tensile strength and tensile modulus of nanocomposite is due to the homogeneous dispersion of nanoparticles in SBR. However, a slight decrease in mechanical strength and modulus are observed for 15 phr loading and this is arises from the agglomeration of filler particles. These results are in good agreement with the SEM analysis. It can be seen that the elongation at break drops with increasing loading of nanoparticles and the reduction in elongation at break is considered as the criteria for higher reinforcement of nanoparticles [234]. Tear strength is an important property that reflects the resistance of composite towards crack growth. **Table 5.2** showed an increase in tear strength up to 10 phr of $MnWO_4$ and then showed a decrease with the further loading of nanoparticles. This means that 10 phr loading provides a large interfacial area of contact, resulting in better interfacial adhesion. The abrasion resistance of SBR with different content of metal oxide nanoparticles are reported in **table 5.2**. The abrasion resistance increases with increase in loading of nanoparticles. The crystalline nanoparticles arrest the cracks or voids in the tip and thus increase the abrasion resistance. Better abrasion resistance is observed for 10 phr loading and this improvement is probably due to

the greater surface area and better filler-rubber interfacial adhesion resulting in an improved abrasion resistance. Rebound resilience of unfilled SBR is high as compared to filled composite and the resilience decreases continuously with the addition of nanoparticles. It is well known that the addition of inorganic fillers reduces the resilience. The hardness of composite material is a complex property and it depends on the concentration of filler particles in the polymer. The variation in hardness of composite given in **table 5.2** indicates that the hardness of materials increases progressively with increasing loading of nanoparticles. The hardness of unfilled rubber is least in the series. Generally, a non-reinforcing filler shows lower compression set values as compared to a reinforcing particulate filler [245]. The compression set values of SBR/$MnWO_4$ composite increases with increase in loading of filler particles and this can be attributed to the higher crosslink density of composite. Heat build-up of an elastomer generated from the internal friction in the compounds. It can be seen from the table that the heat build-up increases with the loading of nanoparticles and this is because of the increased friction between the filler and elastomer.

5.2.8 Electrical properties

5.2.8.1 AC conductivity

Figure 5.7 shows the AC electrical properties of SBR and SBR with different content of $MnWO_4$ nanoparticles at various frequencies. It is found that the AC conductivity of all the composite material is much higher than pure SBR. The AC conductivity of all the samples

increases with increase in frequency. The frequency dependence AC conductivity is explained on the basis of Maxwell- Wagner two layer models and the highly crystalline structure of $MnWO_4$ nanoparticles. It is well clear from the figure that the increasing trend of AC conductivity is steeper at higher frequencies and this is related to the conductive grains present in the system. The overall AC conductivity of nanocomposite increases with increase in loading of nanoparticles. In the case of nanocomposite, the higher conductivity is either due to hopping of charge carriers between Mn^{3+} and Mn^{2+} ions and the hopping of charge carrier increases not only with frequencies but also with the loading of filler particles. Hence it can be inferred that the addition of $MnWO_4$ nanoparticles into the rubber matrix can impart bulk conductivity to SBR and the bulk conductivity depends on the concentration, filler-polymer interaction and the dispersion of nanoparticles [246]. The maximum conductivity is noted for 10 phr of nanocomposite. This means that the nanoparticles are effectively interact with the SBR chain. As the interfacial adhesion increases in the composites, the nanoparticles are more tightly packed and pressed against each other which lead to the uniform orientation of nanoparticles within the polymer chain. The decrease in AC conductivity beyond 10 phr loading is due to the increase in net resistance, resulting from the poor adhesion between filler and polymer. Moreover, the heterogeneous structure developed from the aggregate or clusters like morphology resist the hopping of electron throughout the matrix and thereby cause a decrease in poor conductivity.

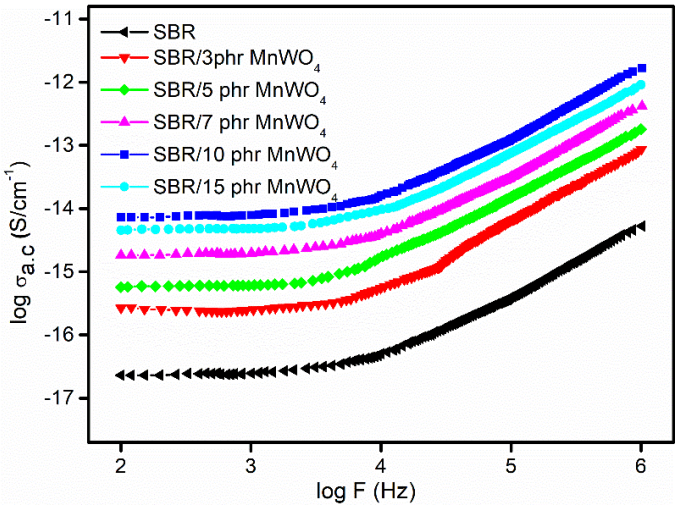

Figure 5.7 conductivity of SBR and SBR/$MnWO_4$ nanocomposites

5.2.8.2 Dielectric constant

The dielectric constant (ε_r) is an evaluation of the material to be polarized or it is an evaluation of how much energy from an external electric field is stored in the material. The dielectric constant (ε_r) of SBR and SBR with different contents of $MnWO_4$ nanoparticles at room temperature is given in **figure 5.8**. Generally, the dielectric constant of a material arises from the polarization of molecules. It is seen that the dielectric constant of SBR is increases by the addition of $MnWO_4$. The dielectric constant of the nanocomposite increases with increase in the nanoparticle content up to 10 phr loading and thereafter the values decreases. This means that the dipole orientation and interfacial polarization is higherin10 phr of composite. Moreover, the crystalline nature of nanoparticle imparts some regular orientation of nanoparticles within the elastomer and this is already confirmed from XRD and UV studies. The lower dielectric

property beyond 10 phr loading is attributed to the poor interfacial interaction between the polymer chain and $MnWO_4$ and this leads to the agglomeration of filler particles within macromolecular chains [166].

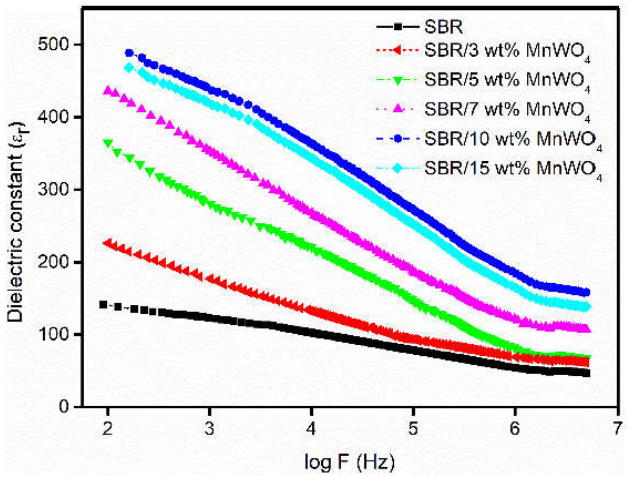

Figure 5.8 Dielectric constant of SBR and SBR/ $MnWO_4$ nanocomposites

5.2.8.3 Dielectric loss tangent (Tan δ)

The dissipation factor of SBR/$MnWO_4$ nanocomposite was observed by plotting the tan δ *Vs* frequency with different loading of nanoparticles is shown in **figure 5.9.** The dissipation factor of nanocomposite is higher than pure SBR and the tan δ value increases with the loading of nano-fillers. The increase in tan δ value is mainly attributed to the formation of interfacial polarisation by the addition of $MnWO_4$ particles. Tan δ value found to decreases steeply with increase in frequency and reaches a constant value at 10^4 Hz for all samples in the present investigation. At lower frequencies, the inertia of molecules and the binding forces are low and therefore charge carriers easily flow

by the application of electric field. Hence the dielectric loss shows a large tan δ value at lower frequency. However at higher frequencies, the charge carriers do not get enough time for long range hopping before field reversal, so the tan δ decreases as the signal frequency increases [247]. It can be seen from the figure that the dielectric loss increases with increase in concentration of filler particles up to 10 phr of loading. This indicates that the electron exchange between Mn^{3+} and Mn^{2+} ions in the composite affect the local displacement of electrons in the direction of applied field, results in an enhanced polarisation at this loading. This interaction is responsible for the higher tan δ value of 10 phr composite. The decrease in tan δ value above 10 phr loading is due to the presence of aggregate or cluster in the nanocomposites (which is well clear from the SEM images) and these aggregates reduces the hopping of charge carriers in the polymer matrix.

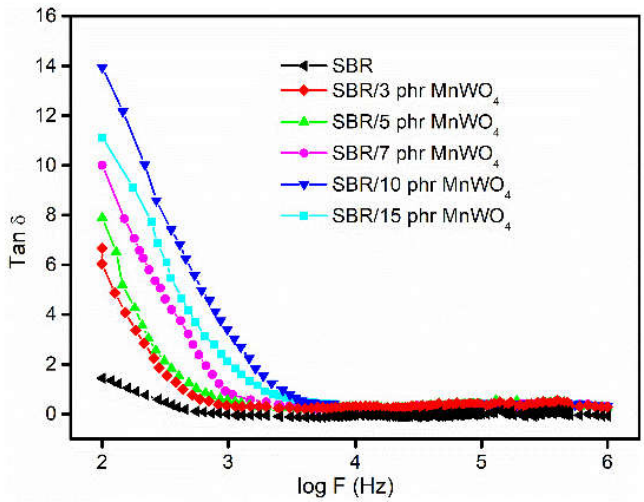

Figure 5.9 Dielectric loss tangent plots of SBR and SBR/$MnWO_4$ nanocomposite

5.2.9 Diffusion Studies

5.2.9.1 Mol % uptake of aromatic and petroleum fuels

The sorption data of SBR/$MnWO_4$ with different filler loading in different solvents were calculated, and is expressed as mol percentage uptake (Q_t %) of solvent and is calculated using **equation 3.1**

The effect of filler loading on mol % uptake

The mole percentage uptake of SBR/$MnWO_4$ composites was carried out in both aromatic and industrial solvents. The effect of filler loafing is studied using benzene and petrol is shown in **figure 5.10** and **5.11**. It is clear that with increasing the filler loading, sorption is found to be decreased in both cases. It is clearly seen that the solvent uptake of SBR is higher than SBR/ $MnWO_4$ nanocomposite. The composite with 10 phr loading shows the minimum solvent uptake. All the sorption experiments were conducted in aromatic (benzene, toluene and xylene) and industrial (petrol, diesel and kerosene) solvents.

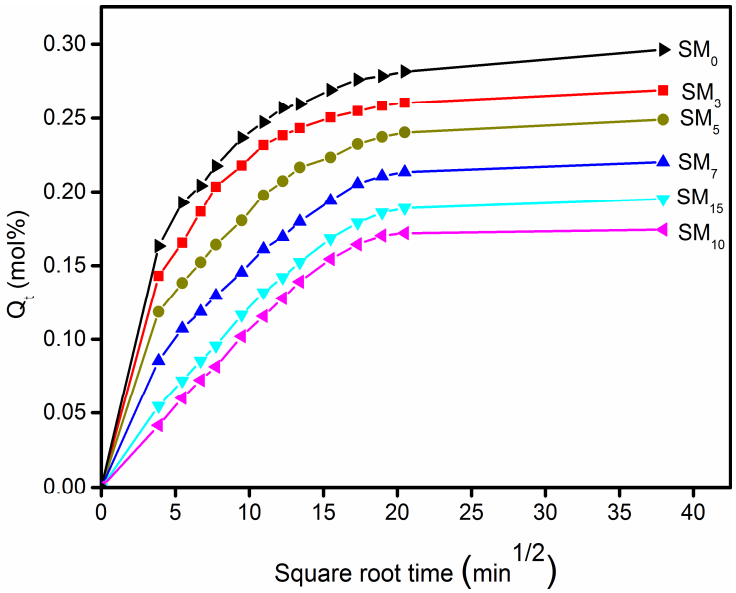

Figure 5.10 Sorption curves of SBR/ $MnWO_4$ nanocomposites in benzene

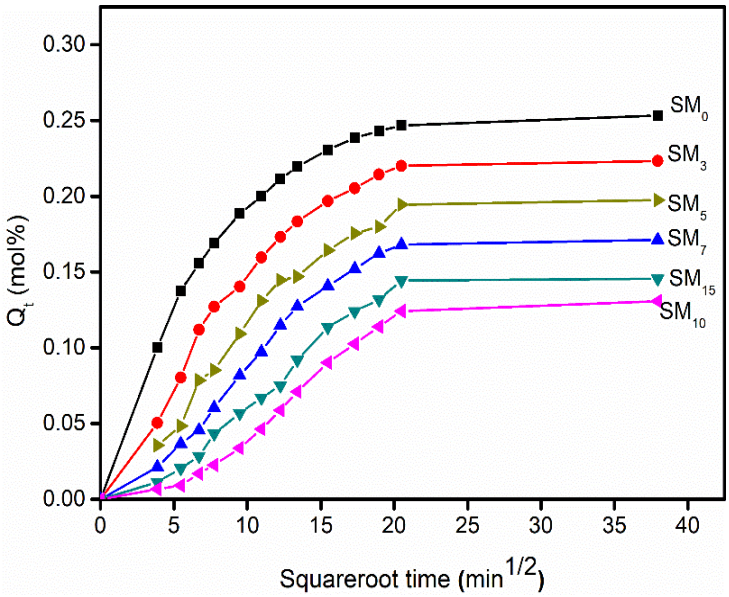

Figure 5.11 Sorption curves of SBR/ $MnWO_4$ nanocomposites in petrol

The solvent uptake of all the solvent followed the same diffusion trend. The minimum solvent uptake nanocomposite is mainly due to the formation of rigid regions in the matrix, which prevents the flexibility of the polymer [201]. Also, the strong polymer-filler interaction leads to an orientation of nanoparticles within the polymer matrix (well clear from SEM analysis) and that reduce the solvent sensitivity of composite. The penetration of solvent molecule through polymer composite also depends on the free volume of the polymer matrix. When the loading of nanoparticles reached 15 phr, the solvent uptake slightly increases as compared to 10 phr composite. The increase in solvent uptake is due to the poor dispersion of nanoparticles within SBR and that results in the agglomeration of nanoparticles in the matrix. This result is in good agreement with the SEM analysis.

Effect of solvent on mol uptake

The effect of various solvent uptakes is investigated for composite with 10 phr of the sample and this is given in **figure 5.12** and **5.13**. There is a systematic trend in the sorption behavior of both aromatic and petroleum fuels with different molecular weight of solvent. The Q_t decreases with increase in molecular weight of solvent is due to the high activation energy needed for the penetration of solvent molecule. The decrease in solvent uptake with an increase in molar volume of penetrant has been reported by many researchers [248]. The diffusion rate is strongly depending on the easy exchange of solvent with polymer chains. So the easiness of exchange becomes less as the penetrant size increases. Among the various petroleum fuels, petrol shows the maximum and diesel shows minimum value of Q_t. In the

case of aromatic solvents benzene shows maximum and xylene shows a minimum of solvent uptake.

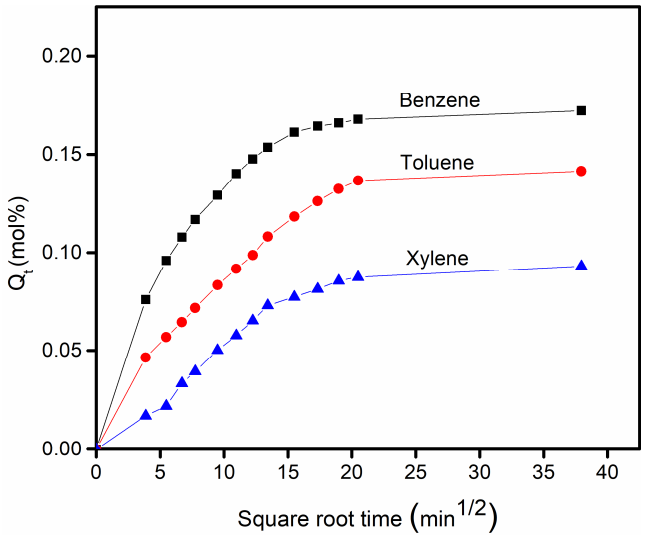

Figure 5.12 Solvent uptake of SBR/10 phr $MnWO_4$ in aromatic solvents

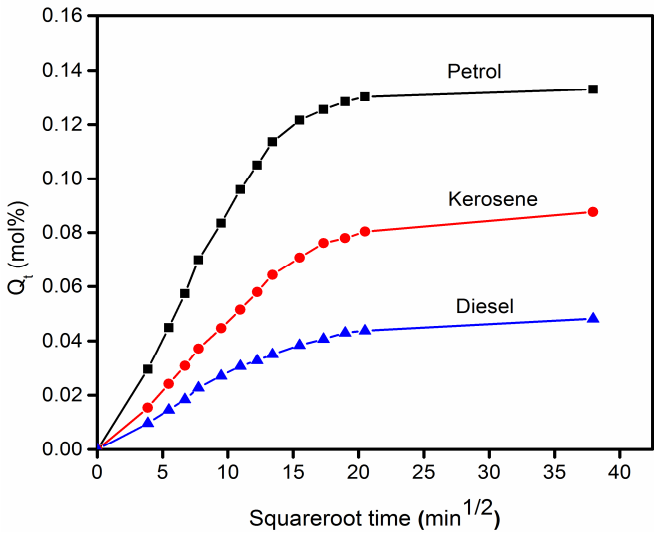

Figure 5.13 Solvent uptake of SBR/10 phr $MnWO_4$ in industrial solvents

Effect of temperature on transport properties

Here we select the composite with 10 phr for studying the effect of temperature on the solvent uptake and this is because of the better solvent resistance of composite at room temperature. Using benzene and petrol the effect of temperature on sorption and diffusion behavior of SBR/10 phr $MnWO_4$ composite were studied and are shown in **figure 5.14** and **5.15**.

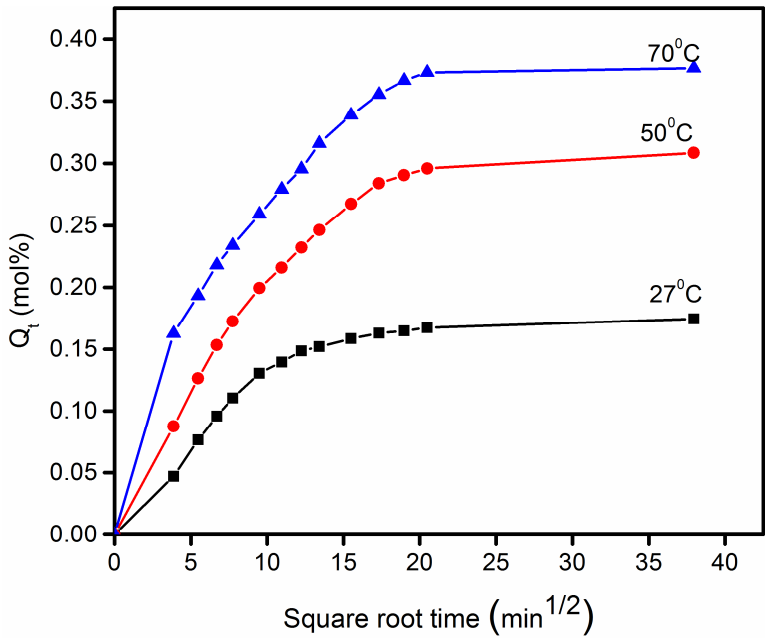

Figure 5.14 The mole uptake of SBR and SBR/10 phr $MnWO_4$ in benzene at different temperature

Figures indicate that the rate of diffusion and the solvent uptake increases on temperature. Moreover, the slope of the linear position of the swelling curve increases with temperature proves that the transport process is temperature dependent. This is because of the segmental motion of the polymer chain increases with temperature, which leads

to increase in free volume in the matrix [249]. The temperature also enhances the collision of molecules and thereby increases the kinetic energy of the system. All the composites show the same pattern with all solvents.

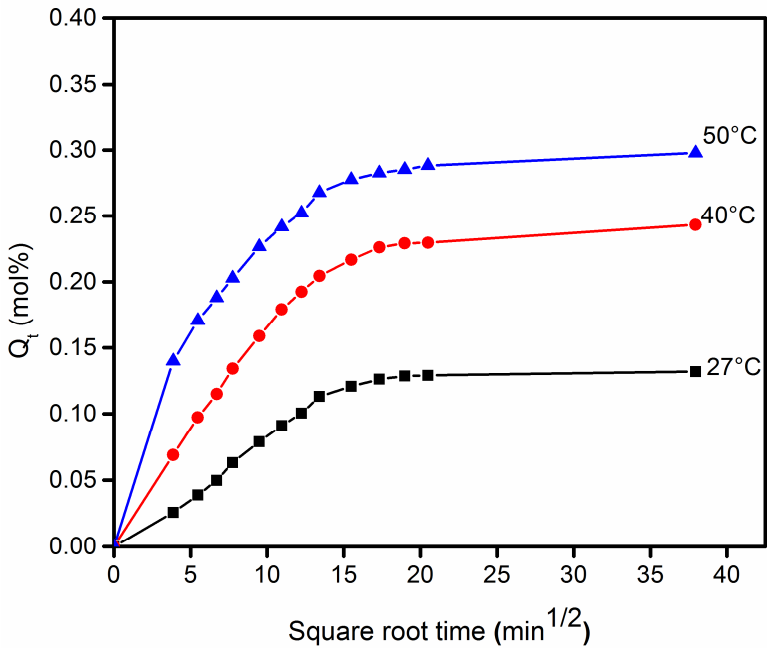

Figure 5.14 The mole uptake of SBR and SBR/10 phr $MnWO_4$ in petrol at different temperature

5.2.9.2 Sorption, diffusion and permeation coefficient

The sorption, diffusion and permeation coefficient of composites in different solvents at room temperature is given in **table 5.3** and **5.4**. The diffusion coefficient is a measure of better dispersion of nanoparticles in the polymer matrix. On increasing the $MnWO_4$ the free volume of the composite decreases, hence the diffusion coefficient decreases with filler loading. This is due to better dispersion of nanoparticles in composites, which is well understood from SEM

images. The increased interfacial interaction between polymer and nanoparticles are revealed from the diffusion coefficient values. Its value decreases with increase in penetrant size is also explained on the basis of activation energy, that is high activation energy is needed for high density solvents. On comparing the diffusivity of SBR with 10 phr of $MnWO_4$ in different solvents, the diffusivity is decreasing with increasing penetrant size, which well explained from **figure 5.12** and **5.13**. The sorption coefficient S is also shows similar trend as diffusion coefficient. Sorption coefficient is the measure of the ratio of mass of the solvent at equilibrium swelling and the initial mass of polymer sample. The permeation coefficient depends on both diffusion coefficient and sorption coefficient, which is the amount of solvent permeated in to the composite in unit area per second. And is calculated P=D.S. from the table it is clear that D, S and P values are decreases on loading, and the minimum value is exhibited by SBR/ $MnWO_4$ composite with10 phr of nanoparticles. The slight increase in value is again explained according to the agglomeration found in SEM analysis.

Table 5.3 D, S and P values of SBR/$MnWO_4$ nanocomposites in aromatic solvents

Samples	Diffusion coefficient D x 10^5 (cm^2/s)			Sorption coefficient S			Permeation coefficient P x 10^5(cm^2/s)		
	Benzene	Toluene	Xylene	Benzene	Toluene	Xylene	Benzene	Toluene	Xylene
SM_0	1.89	1.75	1.46	1.23	1.18	1.16	2.32	2.07	1.69
SM_3	1.86	1.58	1.43	1.22	1.15	1.13	2.26	1.82	1.62
SM_5	1.83	1.57	1.36	1.19	1.13	1.11	2.18	1.77	1.51
SM_7	1.81	1.52	1.32	1.18	1.12	1.1	1.18	1.7	1.45
SM_{10}	1.44	1.22	0.91	1.13	1.09	1.08	1.62	1.33	0.98
SM_{15}	1.72	1.47	1.21	1.17	1.11	1.09	2.01	1.63	1.32

Table 5.4 D, S and P values of SBR $MnWO_4$ nanocomposites in industrial solvents

Samples	Diffusion coefficient D x 10^5 (cm^2/s)			Sorption coefficient S			Permeation coefficient P x 10^5(cm^2/s)		
	Petrol	Kerosene	Diesel	Petrol	Kerosene	Diesel	Petrol	Kerosene	Diesel
SM_0	1.53	1.39	1.28	1.20	1.19	1.17	1.83	1.65	1.49
SM_3	1.41	1.28	1.22	1.18	1.16	1.15	1.66	1.48	1.41
S M_5	1.36	1.21	1.18	1.13	1.11	1.09	1.53	1.34	1.28
SM_7	1.22	1.17	1.14	1.12	1.08	1.08	1.36	1.26	1.23
SM_{10}	1.03	0.99	0.91	1.05	1.02	0.92	1.08	1.01	0.83
SM_{15}	1.09	1.07	1.03	1.09	1.06	1.02	1.18	1.13	1.05

5.2.9.3 Mechanism of transport

From **table 5.5** and **5.6** it is seen that the majority of the composites approaches an anomalous mode of transport, all the values are found to be greater than 0.6. The variation from Fickian to anomalous mode indicates that the increased swelling stress associated with the reinforcement.

Table 5.5 Values of n and k of SBR/$MnWO_4$ nanocomposites in aromatic solvents

Samples	Benzene		Toluene		Xylene	
	n	$Kx10^2$ (min^{-1})	n	$Kx10^2$ (min^{-1})	n	$Kx10^2$ (min^{-1})
SM_0	0.49	0.28	0.67	0.17	0.78	0.13
SM_3	0.58	0.20	0.72	0.15	0.81	0.12
SM_5	0.66	0.16	0.75	0.13	0.82	0.11
SM_7	0.67	0.15	0.77	0.12	0.81	0.12
SM_{10}	0.66	0.16	0.78	0.12	0.83	0.11
SM_{15}	0.71	0.11	0.79	0.14	0.81	0.12

Table 5.6 n and k values of SBR/$MnWO_4$ nanocomposites in industrial solvents

Samples	Petrol		Kerosene		Diesel	
	n	$Kx10^2$ (min^{-1})	n	$kx10^2$ (min^{-1})	n	$Kx10^2$ (min^{-1})
SM_0	0.32	0.32	0.56	0.21	0.62	0.19
SM_3	0.44	0.31	0.73	0.14	0.76	0.12
SM_5	0.63	0.18	0.61	0.19	0.69	0.16
SM_7	0.63	0.18	0.58	0.20	0.65	0.17
SM_{10}	0.63	0.18	0.56	0.21	0.63	0.18
SM_{15}	0.75	0.13	0.49	0.27	0.62	0.19

On increasing the amount of filler, the restriction towards the rearrangement of polymer chain increases. Slow polymer chain relaxation leads to an anomalous mode of transport. This proves the improved interfacial interaction between polymer matrix and nanoparticles. The value of k reveals the structural properties of the polymer, and gives an idea about the solvent-polymer interaction. Upon the addition of filler, the value of k is decreasing and that proves the strong interaction between polymer and filler, which will reduce polymer-solvent interaction [250].

5.2.9.4 Activation energy of diffusion (E_D) and permeation (E_P)

From **table 5.7** and **5.8** the values of E_P and E_D in different aromatic and industrial solvents are found to be increased on increasing the amount of nanoparticles and also increased with the size of the penetrant molecule. To create larger space for larger molecules inside the polymer composite, high activation energy is needed. The better distribution of nanoparticles induces a higher resistance to solvent

interaction. Hence here the better activation energy is obtained for SBR with 10 phr of $MnWO_4$. The least value is noted for pure SBR.

Table 5.7 E_D and E_P (kJ/mol) values of SBR/$MnWO_4$ nanocomposites in aromatic solvents

Samples	Benzene		Toluene		Xylene	
	E_P	E_D	E_P	E_D	E_P	E_D
SM_0	6.12	4.92	6.34	5.16	6.57	5.38
SM_3	6.25	5.14	6.48	5.28	6.78	5.42
SM_5	6.39	5.26	6.59	5.33	6.84	5.49
SM_7	6.4	5.29	6.62	5.37	6.85	5.51
SM_{10}	6.48	5.45	6.67	5.49	6.91	5.57
SM_{15}	6.42	5.32	6.64	5.41	6.86	5.54

Table 5.8 E_D and E_P (kJ mol^{-1}) values of SBR/$MnWO_4$ nanocomposites in industrial solvents

	Petrol		Kerosene		Diesel	
Sample	E_P	E_P	E_P	E_D	E_P	E_D
SM_0	4.19	3.55	4.69	3.93	5.42	4.6
SM_3	5.37	4.39	5.39	4.49	6.11	4.56
SM_5	7.01	5.87	7.42	6.11	8.87	7.01
SM_7	7.24	5.89	7.65	6.27	9.05	7.13
SM_{10}	7.46	6.20	8.28	6.44	9.58	7.56
SM_{15}	7.28	6.09	7.78	6.32	9.12	7.24

5.2.9.5 Thermodynamic parameters

Table 5.9 and **5.10** shows the thermodynamic properties of SBR and SBR/$MnWO_4$ composite with various filler loadings in different aromatic and industrial solvents. It is observed from the table that all the samples in all solvent show positive ΔH values, this assures the endothermic mode of sorption. According to Henry's law, the sorption

occurs on the creation of new holes or free space in the polymer matrix [79]. The entropy change (ΔS) values are positive, and it is seen that on increasing the amount of $MnWO_4$ concentration, ΔS values decreases which are due to the increased interfacial interaction between polymer matrix and nanoparticles. It causes the reduced entropy and reduces the solvent transport. The ΔG values are increased from pure SBR to its composites, and the maximum value is for SBR with 10 phr of $MnWO_4$ nanoparticles. So the sorption is more spontaneous in pure SBR and on-going from SBR to its composites the spontaneity lowers and is least for 10 phr of the composite. All these thermodynamic properties revealed the better distribution and strong interaction of polymer and nanoparticles.

Table 5.9 ΔH, ΔS and ΔG (kJ/mol) of SBR/$MnWO_4$ nanocomposites in aromatic solvents

Samples	ΔH			ΔS			-ΔG		
	Benzene	Toluene	Xylene	Benzene	Toluene	Xylene	Benzene	Toluene	Xylene
SM_0	0.682	0.694	0.792	0.077	0.064	0.059	22.41	18.51	16.91
SM_3	0.694	0.708	0.812	0.071	0.061	0.042	20.61	17.59	11.79
SM_5	0.712	0.718	0.825	0.068	0.054	0.032	19.68	15.48	8.77
SM_7	0.717	0.721	0.827	0.064	0.051	0.029	18.48	14.58	7.87
SM_{10}	0.729	0.731	0.839	0.058	0.043	0.024	16.67	12.17	6.36
SM_{15}	0.721	0.726	0.828	0.062	0.047	0.027	17.89	13.38	7.27

Table 5.10 ΔH, ΔS and ΔG (kJ/mol) values of SBR/$MnWO_4$ nanocomposites in industrial solvents

	ΔH			ΔS			-ΔG		
Samples	Petrol	Kerosene	Diesel	Petrol	Kerosene	Diesel	Petrol	Kerosene	Diesel
S_0	0.632	0.664	0.95	0.072	0.052	0.049	15.28	14.94	13.75
SM3	0.811	0.88	0.98	0.062	0.051	0.041	14.49	14.42	13.72
SM_5	0.885	.998	1.14	0.051	0.038	0.029	14.41	10.402	7.56
SM_7	0.891	1.12	1.21	0.048	0.035	0.024	13.51	9.38	5.99
SM_{10}	0.999	1.32	1.49	0.033	0.027	0.018	8.901	6.78	3.91
SM_{15}	0.917	1.26	1.33	0.041	0.031	0.021	11.38	8.04	4.97

5.3 CONCLUSIONS

In this study styrene butadiene rubber with different content of manganous tungstate nanocomposites were prepared by a simple two roll mixing mill. The FTIR studies verify the presence of $MnWO_4$ nanoparticles in the SBR matrix at 559 cm^{-1}. UV-Visible spectroscopy proved the enhanced interfacial interaction between nanoparticles and the elastomeric chain and the composite with 10 phr shows the maximum UV absorption. This study investigated the effect of $MnWO_4$ nanoparticles on the morphology, crystalline nature, thermal stability, processability, mechanical and electrical properties. The interaction with solvents using aromatic and industrial solvents were also studied. The XRD pattern of nanocomposite showed the decrease in amorphous peak of SBR by the interaction with $MnWO_4$. The uniform dispersion of nanoparticles in SBR decreased with an increase in the nanoparticles loading. The interaction of nanoparticles with polymer can effectively enhanced the thermal stability of SBR. Processing characteristics such as optimum cure time and scorch time decreases with loading of $MnWO_4$, whereas the rheometric torque

increased with loading of nanoparticles up to 10 phr. Addition of nanoparticles to SBR increases the tensile strength, modulus, tear and abrasion resistance, hardness and heat build-up, while elongation at break, resilience and compression set were decreased. AC electrical conductivity and dielectric property of nanocomposites were higher than SBR and the maximum electrical property was obtained for 10 phr of composite and above this loading, the electrical properties were found to be decreases. The liquid transport characteristics of nanocomposite were analysed using aromatic and industrial solvent molecules and the results were compared with unfilled SBR. Nanocomposites showed a reduced penetration of solvent due to the interaction between nanoparticles and SBR components. The solvent uptake was lower for 10 phr loading and the solvent uptake tendency increased at higher filler loading, which results from the poor interaction between the matrix and that leads to the aggregation of nanoparticles. The sorption coefficient and activation parameter showed a dependence on the size of penetrant molecules. The transport phenomenon was found to follow anomalous type mechanism in all the cases. So, the SBR/ $MnWO_4$ composite show the significant variation in mechanical electrical and solvent sorption properties when small amounts of fillers (10 phr loading) were incorporated.

6.1 Introduction

Academic and industrial research works, worldwide have paid great energy and money to the fascinating field of polymer nanocomposites. The main reason for this is obviously the superior performance to weight ratio, which is unique for these materials [5,251]. Polymers, reinforced with nanomaterial exhibited mechanical strength, modulus, high thermal stability, improved barrier properties and flame resistance [252–254]. They offer superior performance and durability compared to conventional composites. This wide range of properties is determined by various factors of the reinforcing filler, such as size, shape, surface morphology and the effectiveness filler particles distribution in the polymer matrix. In other words, the polymer nanofiller interface plays the major role in deciding these useful properties. The large interfacial area per unit volume and low weight will impart the distinguished reinforcement of nanocomposites [255]. Owing to the requirement of the market for novel semiconducting material with easy processability, polymeric insulating material filled with electrically conducting metal nanoparticles have gained much attraction in recent years [256]. Researchers, in specific cases [257] revealed that the electrical conductivity of polymer nanocomposites depend on nature of filler and polymer, loading of filler, dispersion of nanoparticles and crystallinity of nanoparticles. In this scenario, use of elastomers, which are of low modulus, easily processable, curable and compliant is most promising. Several polymers have been used for preparing polymer nanocomposites such as natural rubber, epoxidized natural rubber, SBR and chloroprene rubber [258]. Among these, SBR is unique due to its purely synthetic nature and resulting well-defined properties and possibilities for further

chemical modification of the unsaturation in its butadiene repeating unit.

Styrene butadiene rubber (SBR) is widely employed in the tire industry, healthcare products and cables [180, 259]. Despite its high abrasion resistance SBR suffers from poor tensile strength, flame retardancy and very low oil resistance. Research focusing on the reinforcement of SBR with nanoparticles also did not give fruitful results due to the poor mechanical properties resulting from the weak interface formed between the elastomer and nanoparticles. One of the many strategies to enhance the interfacial interaction between SBR and nanofiller is by the incorporation of polar functional group in the rubber. Our previous research showed that chemically modified SBR (chlorinated SBR) has excellent tensile strength, tear property and flame retardant behavior. Chlorination improved its oil resistance superior to that of chloroprene rubber and equal to that of nitrile rubber [167, 221].

Polymer nanocomposites can be prepared by many methods such as solution mixing, melt mixing or by using simple but efficient two roll open mill mixer. Solution mixing give uniform dispersion of nanofiller in the elastomer matrix but the occlusion of solvent in the matrix, reduces the glass transition temperature of the nanocomposite, plasticize the sample, and deteriorates its properties, so as to affect health and thereby limiting industrial applications. The problem with melt mixing is the possible rupture of the polymer chain, and the resulting reduction in molecular weight and degradation in the random mode. Compared to these methods, simple two roll mill mixing method is relatively quick and easy and results in a superior performance of the final product [115, 260].

In this study, we report preparation of elastomer nanocomposites based on chlorinated SBR and $MnWO_4$. A simple open two roll mixing mill is used for the preparation of the sample. The main objectives of the present investigation are to analyse the effect of $MnWO_4$ nanoparticles on the structural, morphological, thermal, curing properties, mechanical and electrical properties of the resulting nanocomposite. This study is also focused on the effect of manganous tungstate nanofiller on the absorption of ASTM oils and on the transport of aromatic and petroleum fuels through vulcanized chlorinated SBR at different temperatures, thus calculating the overall performance of the nanocomposites.

6.2 Result and Discussions

6.2.1 FT-IR spectroscopy

Figure 6.1 shows the FTIR spectra of $MnWO_4$, Cl-SBR and $MnWO_4$ filled Cl-SBR nanocomposites. The FTIR spectra of pure $MnWO_4$ (**Figure 6.1** (a)) shows the characteristic vibrations of the W-O bond at 708 and 590 cm^{-1} [261, 262]. The absorption of moisture on the metal oxide surface causes a broad peak at 3439 cm^{-1}. The C-H stretching of Cl-SBR (Figure 1 (b)) is observed at 2930 and 2853cm^{-1}. The *trans* C=C stretching and the CH_2 in plane deformation appear at 968 and1443 cm^{-1} respectively. The IR peak at 700 cm^{-1} is due to the presence of an aromatic ring of SBR. The C-Cl stretching of chlorinated SBR is visible at 804 cm^{-1} along with the cyclopropyl ring at 1067 cm^{-1} [263]. The IR spectrum of Cl-SBR/$MnWO_4$ (**Figure 6.1** (c)) exhibits all the characteristic peaks of chlorinated SBR. Additionally, a new peak at 575 cm^{-1} is the characteristic of $MnWO_4$ stretching indicates the presence of metal oxide in Cl-SBR. It is

interesting to observe from the figure that the C-H stretching vibrations of SBR at 2930 and 2853 cm^{-1} are merged into a broad IR peak at 2898 cm^{-1}. Also, interestingly the sharp peak of Cl-SBR at 1443 cm^{-1} is found to be shifted to broad absorption peak at 1408 cm^{-1}. These shifts in the IR peak of nanocomposite with respect to pure Cl-SBR is due to the intermolecular interactions between halogenated segment of the elastomer and the nanoparticles. Therefore, it can be inferred that the nanoparticles are well inserted into the macromolecular structure of Cl-SBR.

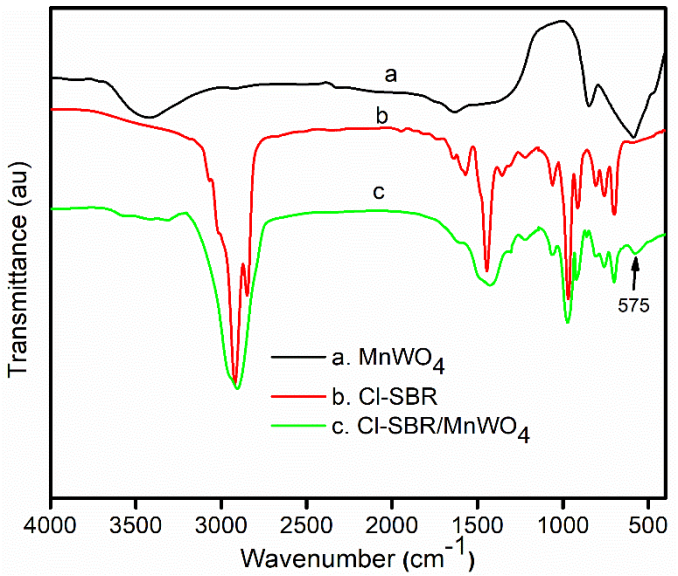

Figure 6.1 FTIR of a) $MnWO_4$ b) Cl-SBR and c) Cl-SBR/$MnWO_4$

6.2.2 UV-Vis spectra

The optical properties of Cl-SBR and Cl-SBR containing various loading of $MnWO_4$ particles are given in **figure 6.2**. The absorption maxima of Cl-SBR at 287 nm is attributed to the π to π* transition of the polymer. It can be seen from the figure that the π to

π* transition of the all the rubber composite materials is changed to slightly a higher wavelength region [261]. For example, 7 phr composite shows a higher UV absorption peak at 295 nm. Also the intensity and broadness of the absorption peaks of all the composites are higher than that of pure Cl-SBR. Moreover, the broadness and intensity of the elastomer composite increase with the loading of nanoparticles up to 7 phr and beyond this loading, the intensity of UV peak decreases. Higher absorption of 7 phr composite indicates the strong intermolecular interactions and the uniform distribution of nanoparticles in Cl-SBR matrix. The decrease in UV absorbance above 7 phr loading is due to the poor interaction of nanoparticles with the elastomer matrix, resulting from the agglomeration of nanoparticles.

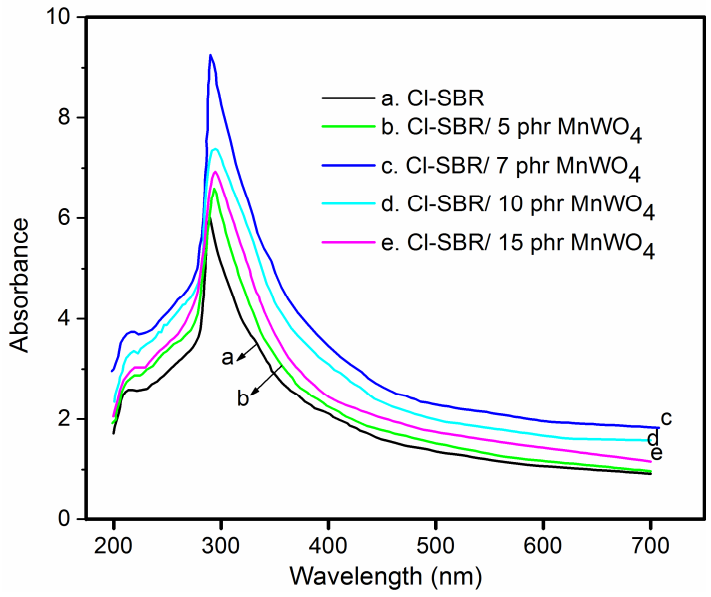

Figure 6.2 UV spectroscopy of Cl-SBR and Cl-SBR/$MnWO_4$ nanocomposites

6.2.3 X-ray Diffraction Analysis (XRD)

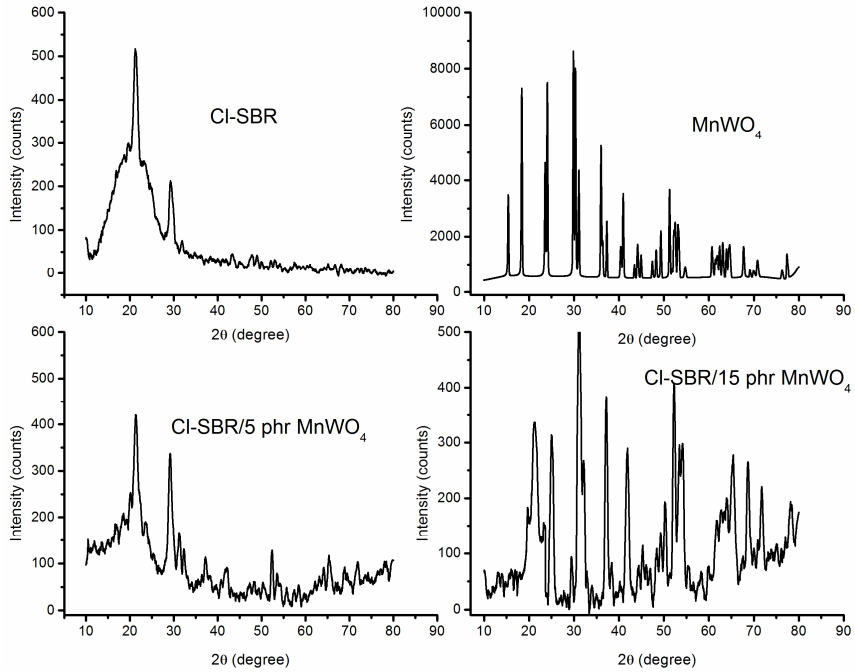

Figure 6.3 XRD pattern of Cl-SBR, $MnWO_4$ and Cl-SBR/$MnWO_4$ nanocomposites

X-ray diffraction patterns of $MnWO_4$, Cl-SBR and Cl-SBR/$MnWO_4$ nanocomposites are displayed in **figure 6.3**. Many crystalline peaks of $MnWO_4$ are observed from the XRD which corresponds to monoclinic wolframite tungstate structure and this is consistent with JCPDS Card Number: 80-0133. The XRD pattern of Cl-SBR shows the broad peak centered at 2θ=21.2° indicating the amorphous nature of the polymer and a weak XRD peak at 2θ=29.36° associated with the crystalline unit of the Cl-SBR. The prepared Cl-SBR/$MnWO_4$ composite contains most of the diffraction peaks of $MnWO_4$ and Cl-SBR. It is clear from the figures that the amorphous nature of Cl-SBR has decreased with the addition of $MnWO_4$ nanoparticles. In addition to this it can be seen

from a comparison of figures that the diffraction peaks $MnWO_4$ in the polymer matrix is slightly shifted from lower diffraction angle to higher one. This indicates the structural changes of composites by the interaction of elastomer with the nanoparticles [262].

6.2.4 Scanning Electron Microscopy (SEM)

Figure 6.4 shows the SEM images of Cl-SBR elastomer and the elastomer with different contents of $MnWO_4$ nanoparticles. As shown in the SEM image file (Figure 6.4 (a)), the Cl-SBR has surface irregularity with few crack propagations. The micrograph obtained from the 3 phr composite reveals (Figure 6.4 (b)) a smooth surface with the incorporation of some small nanoparticles. As the loading of nanoparticles in Cl-SBR increases to 7 phr (Figure 6.4 (c)), the nanoparticles are uniformly arranged in the rubber with uniformly shaped particles.

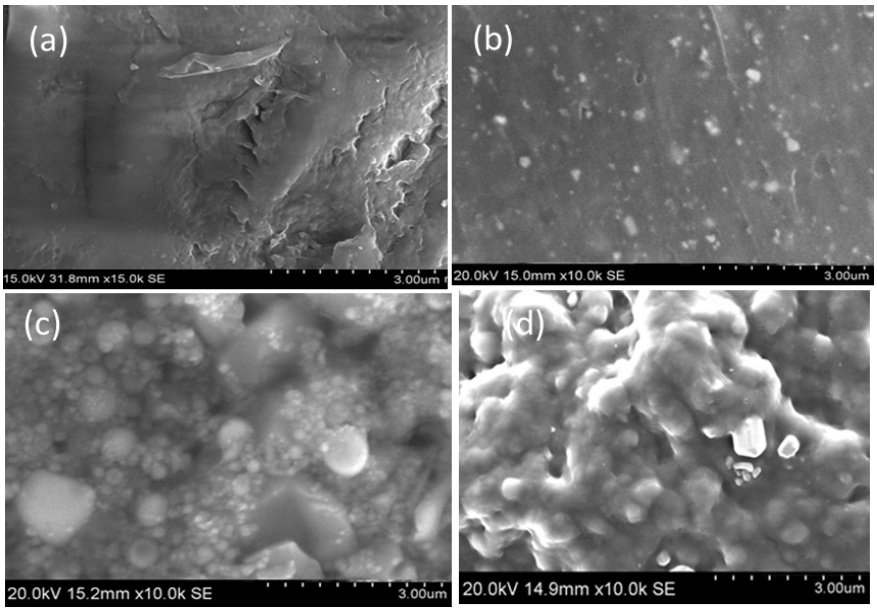

Figure 6.4 SEM images of (a) Cl-SBR (b) Cl-SBR with 3, (c) 7 and (d) 15 phr $MnWO_4$ nanoparticles

The functional $MnWO_4$ nanoparticles having large surface area can strongly adhere with the polar segments of Cl-SBR which leads to the encapsulation by growth process of the polymer matrix. However, at higher loading of nanoparticles (Figure 6.4 (d)), the surface morphology is remarkably changed into a rough structure. At higher loadings, the particle to particle distance is too short which generates more and more stress in the polymer matrix leading to the formation of agglomerates in the polymer.

6.2.5 Thermal analysis

6.2.5.1 Differential scanning calorimetry (DSC)

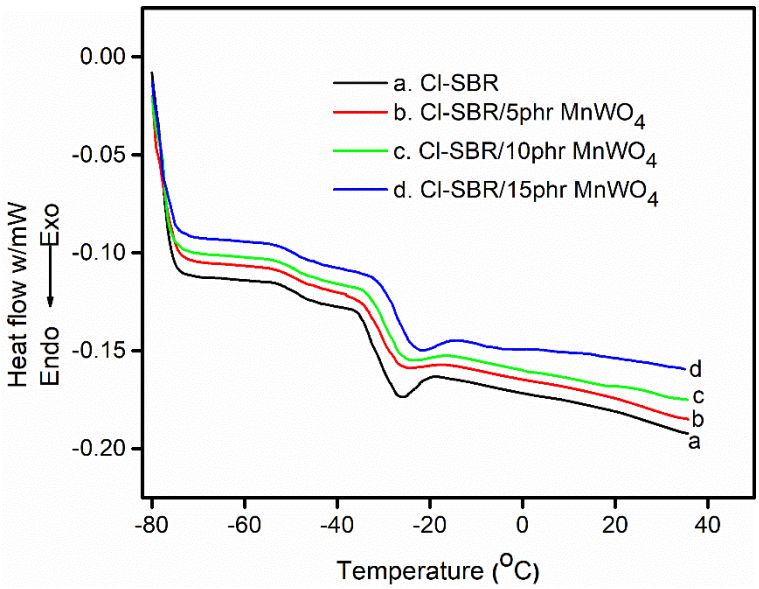

Figure 6.5 DSC thermorgams of Cl-SBR and Cl-SBR/$MnWO_4$nanocomposites

Glass transition temperature (T_g) is of great importance in deciding the range of service temperature of polymeric materials and is used for

evaluating the flexibility of a polymer molecule. The DSC thermograms of Cl-SBR and Cl-SBR with different content of $MnWO_4$ nanoparticles are given in **figure 6.5**. All the samples show two glass transition temperatures. The first thermal transition observed at -53°C is attributing to the glass transition temperature of SBR and second Tg appears at -35.1°C is assigned to the chlorinated segment of SBR. It is well recognized that the Tg of polymer composite depends on the overall flexibility of the chains resulting from the interfacial interactions between the nanofiller and the polymer, crystallinity and polarity of filler particles. It is clear from the figure that the glass transition temperatures of all nanocomposites are higher than that of pure Cl-SBR. This confirms the reduced flexibility of Cl-SBR chains resulting from its reinforcement by $MnWO_4$ nanoparticles. The composites with 5, 10 and 10 phr samples showed the TG at -33.9°C, -32.8°C and -29.39°C, respectively. The rise in Tg of nanocomposites is due to the strong intermolecular interactions between the nanoparticles and the polymer chains. At higher loading, the segmental movement of polymer chains is restricted, which causes an enhancement in the Tg of polymer composites [224]. It is important to mention here that the loading of nanoparticles does not affect the glass transition temperature of SBR units at -53°C. This suggests that the efficient interfacial interaction is taking place between the chlorinated polar units of SBR with $MnWO_4$.

6.2.5.2 Thermogravimetric analysis (TGA)

Figure 6.6 shows the TGA profile of chlorinated styrene butadiene rubber and its composites filled with $MnWO_4$ nanoparticles. The TGA

curves of all the samples show well defined two step decomposition patterns. The first weight loss is related to the loss of compounding ingredients and the removal of hydrogen chloride from the elastomeric chain. The second thermal decomposition is assigned to the degradation of SBR units [225].

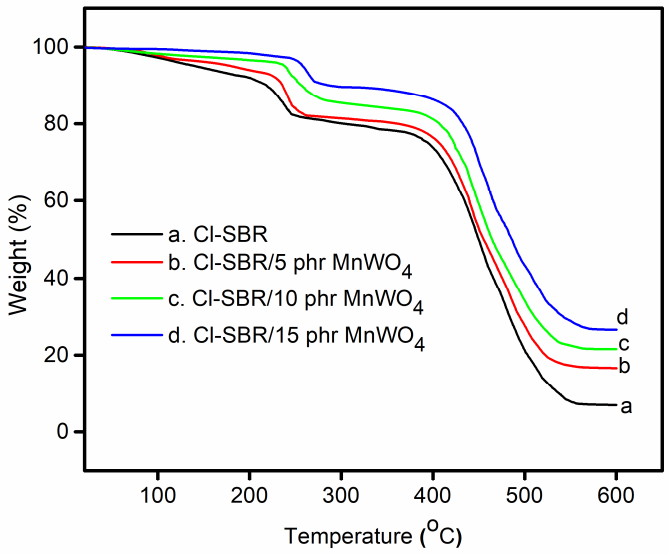

Figure 6.6 TGA of Cl-SBR and Cl-SBR/$MnWO_4$ nanocomposites

The nanocomposites filled with $MnWO_4$ nanoparticles displayed better thermal resistance than that of the pristine Cl-SBR. The second degradation step of Cl-SBR is observed at 392°C, while the composite with 5, 10 and 15 phr of $MnWO_4$/Cl-SBR shows the second degradation at 402, 410 and 423°C, respectively. The improved thermal stability of nanocomposites is due the thermal barrier effect of metal nanoparticles and also from the strong intermolecular interaction between Cl-SBR and $MnWO_4$ particles. It is clear from the result that the $MnWO_4$ nanoparticles can effectively shield the composite material

from thermal degradation and following combustion process. The flame resistance of all the nanocomposite samples can be clearly understood from the final char residue. The Cl-SBR shows 6.87% final char residue at 600°C, whereas the composite with 5, 10 and 15 phr samples shows the final char residue around 16.94, 21.89 and 26.88% respectively at the same temperature. The char residue formed during thermal degradation acts as a protective layer on the surface of nanocomposite and thereby increases the flame resistance.

6.2.6 Flame retardancy

The ignitability and inflammation resistance of polymeric system can analysed by the limiting oxygen index (LOI). The LOI value is the percentage of oxygen required to support combustion of polymer. The amount of oxygen present in air is approximately 21%, so any material with an LOI of less than 21 will support burning in an open air condition [227]. The LOI values of Cl-SBR with various contents of $MnWO_4$ nanoparticles are given in **figure 6.7**. The chloro functional groups present in Cl-SBR influence the chemical reactions during combustion process. Since the combustion of halogenated polymers produces heavy gases that suppress the access of oxygen to the burning site, produce a masking effect and consequently reduces the flammability of Cl-SBR. From the figure it can be seen that the LOI value of composites increase regularly with the addition of $MnWO_4$ nanoparticles.

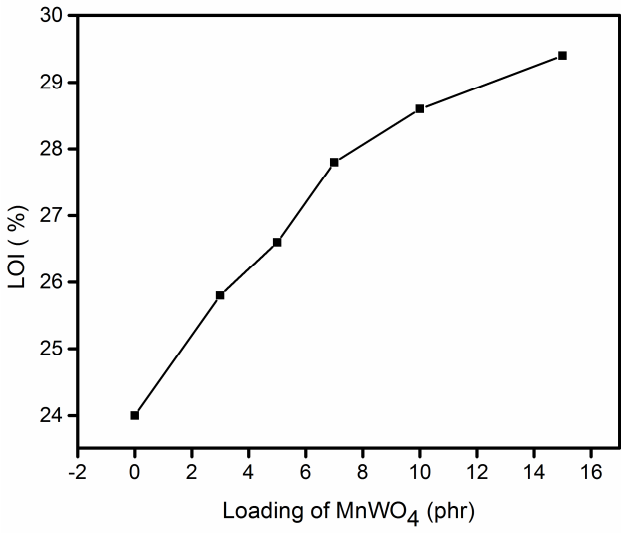

Figure 6.7 Flame resistance of Cl-SBR and Cl SBR/$MnWO_4$ nanocomposites

It can be seen that the pure Cl-SBR has LOI value of 22.1 which increases to 28.1 at 15 phr loading of $MnWO_4$. This means that in order to keep the sample burning, more concentration of oxygen in a mixture of oxygen and nitrogen is needed. This indicates an improvement in flame resistance or decrease in flammability of nanocomposites. The incorporation of metal nanoparticles in the polymer matrix generates a protective layer during burning process [228]. During the burning process, the viscosity of the molten Cl-SBR/ $MnWO_4$ nanocomposite decreases and this facilitates the migration of the nanoparticles to the burning front. The nanoparticles adhere to the surface of the composite materials act as a protective barrier to prevent the heat transfer through the halogen containing rubbery material. This reduces the chance of further degradation of sample and the volatilization of the degradable by-products.

6.2.7 Cure Characteristics

The cure characteristics of the different Cl-SBR/$MnWO_4$ nanocomposites are shown in **table 6.1**. The minimum torque value M_L is considered as the measure of viscosity resulting from the filler content in the polymer matrix. It is always expected to increase with the loading of nanoparticles and the same observation can be seen here. The maximum torque value (M_H) is the measure of the combined effect of physical reinforcement of filler in polymer and the crosslink density of the vulcanizate [264]. It can be seen that both maximum and minimum torque values of the uncured Cl-SBR/$MnWO_4$ composites increases with the loading of nanoparticle up to 7 phr. This indicates the maximum polymer filler adhesion at 7 phr loading of nanofiller, due to strong intermolecular interaction. The decrease in rheometric torques with further loading is attributed to the diluent effect and agglomeration of nanoparticles resulting in poor cross-links between the Cl-SBR and $MnWO_4$ nanoparticles. Scorch time is the time required for the torque value to increase by 5 units above the minimum torque value and it is a direct measure of the scorch (premature vulcanization time) safety of the nanocomposite samples. The optimum cure time t_{90} is the time for the vulcanization form 90% of the cross-links to get better physical properties.

Table 6.1 Processing characteristics of Cl-SBR and Cl-SBR/$MnWO_4$ nanocomposites

Sample code	Cure time, t_{90} (min)	Scorch time, t_2 (min)	Maximum torque- M_H (dNm)	Minimum torque -M_L (dNm)
CSM_0	14	4.0	34	9.25
CSM_3	12.7	3.82	36.5	10.2
CSM_5	11.8	3.60	40.4	11.3
CSM_7	11.0	3.48	45.0	12.2
CSM_{10}	10.0	3.29	43.6	11.6
CSM_{15}	9.2	3.05	42.8	10.3

It can be seen from the table that both scorch and optimum cure time decreases regularly with increase in the concentration of $MnWO_4$ nanoparticles. This is because of the dual role of metal nanoparticles primarily as co-activators and secondarily facilitating the heat transfer in the system creating more interaction with the curing agent. These factors ultimately lead to better cross-linking in the Cl-SBR matrix. The reduction in optimum cure time is advantages because it can enhance the production rate of articles made from these nanocomposite elastomer compounds.

Table 6.2 Mechanical properties of Cl-SBR and Cl-SBR/$MnWO_4$ nanocomposites

Properties	Loading of $MnWO_4$ nanoparticles (phr)					
	0	**3**	**5**	**7**	**10**	**15**
Tensile strength (MPa)	7.45	9.66	13.21	18.01	16.34	13.02
Elongation @ break (%)	398	366	348	335	319	292
Modulus (300%)	2.44	3.16	5.72	8.02	7.69	6.51
Tear strength (kN/m)	27.3	29.3	32.9	37.0	35.9	34.4
Hardness (Shore A)	35	36	37	38	41	43
Heat build-up (^oC)	12.3	13.0	14.4	15.5	16.6	17.0
Compression set (%)	12.6	13.8	15.1	15.5	15.1	14.3
Abrasion loss (mm^3)	77.0	76.1	75.6	75.2	74.7	74.0
Resilience (%)	36.3	34.7	31.9	29.6	28.1	26.5

6.2.8 Mechanical properties

The incorporation of nanoparticles into a weak elastomer matrix such as SBR is highly effective technique to improve its mechanical properties. The tensile strength, modulus, elongation at break, tear resistance, hardness, abrasion loss, resilience and heat build-up of Cl-SBR with different loading of $MnWO_4$ nanoparticles are given in **table 6.2**. The tensile properties of polymer/nanofiller vulcanizates depend on several factors such the uniform dispersion of nanoparticles, the compatibility between filler and polymer, polarity and crystalline nature of fillers [230]. For Cl-SBR/$MnWO_4$

nanocomposites, tensile strength, modulus at 300% and tear resistance increased with increase in the concentration of $MnWO_4$ reaching the maximum value up to 7 phr loading. Further addition of nanofillers reduces these values. The higher tensile, tear and modulus values at 7 phr loading of $MnWO_4$ is due to the uniform dispersion of the nano-filler and the strong interaction of nanoparticles with the elastomeric chains at this loading. The optimization of interaction between the chlorinated moieties in Cl-SBR and $MnWO_4$ filler particles bring excellent compatibility between the chain segments and nanoparticles. The decrease in tensile and tear properties beyond 7 phr loading is due to the combined influence of the clustering tendency and a possible dilution effect. The force applied to pull the vulcanizate apart is measured to determine the elongation at break (EB) and the values of EB is given in **table 6.2**. The EB decreases with the addition of nanoparticles in all the systems and it is well recognized that the decreased EB is an indication of the higher reinforcement of nanoparticles in the polymer matrix [265]. Shore hardness becomes an important property when the surface property of nanocomposite becomes relevant. The hardness of the Cl-SBR/$MnWO_4$ nanocomposite is also given in **table 6.2**. It shows a progressive increase in hardness of compound with the loading of nanoparticles. This is usual to expect from the addition of a high modulus material to a low modulus material such as Cl-SBR. Abrasion resistance is the material property to prevent the rubbing or scraping that tends to remove material from its surface and the abrasion resistance value of elastomeric composite is given in the same table (table 6.2). Nanoparticles incorporated polymer has lower abrasion loss than the

pure Cl-SBR and good abrasion resistance is noted for 7 phr loading. Rebound resilience is the compound ability to retain its original dimensions and shape after temporary deformation. Resilience values of Cl-SBR with different loading $MnWO_4$ filler are given in table 6.2. The resilience decreases with the loading of nanoparticles as expected. Heat build-up is the increase in temperature of the specimen when it is subjected to an oscillating compressive stress cycle in a controlled environment. The heat build-up values of Cl-SBR and Cl-SBR/ $MnWO_4$ nanocomposites are shown in table 6.2. The heat build-up of composite increases with increase in loading of nanoparticles due to more extensive cross-linking achieved through better thermal conductivity.

6.2.9 Electrical properties

6.2.9.1 AC Conductivity studies

Figure 6.8 represents the frequency dependence of alternating current (AC) conductivity of Cl-SBR and Cl-SBR/$MnWO_4$ nanocomposites with different filler loading. It is clear that the conductivity of nanocomposites is greater than that of pure Cl-SBR. The conductivity shows an increasing in trend with an increasing frequency for all the samples. The randomly oriented macromolecular chains of Cl-SBR (confirmed from XRD) provide a poor compactness of the polymer, leading to its low conductivity. The conduction mechanism of polymer composite normally occurs in two ways: (1) tunnelling effect between the conductive fillers separated by the polymer layer and (2) through the flow of electrons through the conductive network. Generally the

observed enhancement in conductivity is attributed to the tunnelling effect of the polymeric system [266].

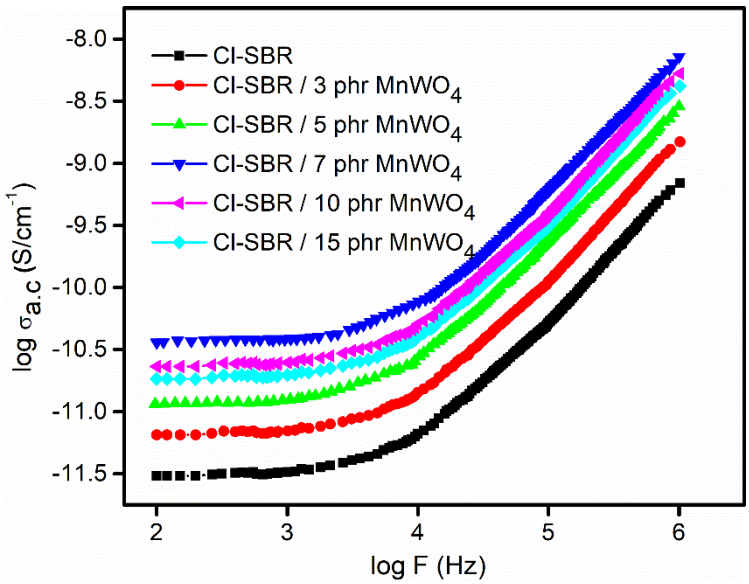

Figure 6.8 AC conductivity of Cl-SBR and Cl-SBR/ $MnWO_4$ nanocomposites

Moreover, uniform dispersion of nanoparticles in the polymer and the interfacial polarization between the nanoparticles and polymer chain are also affecting the electrical conductivity of polymer composites. Also the conductivity increases steadily with the loading of nanoparticles up to 7 phr loading. The higher conductivity of nanocomposite at 7 phr loading is due to the strong intermolecular interaction between the nanoparticles and the chlorinated segments of SBR. Due to these strong interactions, the crystalline $MnWO_4$ impart a structural order in the composites and thereby leading to a higher conductivity. As the loading of nanoparticles increased above 7 phr, the AC conductivity of nanocompositeis found to be decreasing. At

higher loading, the nanoparticles are oriented irregularly making the linkage between the polymer matrixes very poor which leads to poor conductivity. This is clear from the SEM photos presented earlier.

6.2.9.2 Dielectric constant

Figure 6.9 presents the dielectric constant of Cl-SBR and Cl-SBR containing different loadings of $MnWO_4$ nanoparticles. Dielectric constant is the ability of the material to store a charge when the material is subjected to an electric field. It can be found that the dielectric constant increased with the loading of nanoparticles over the entire range of frequencies. The significant increase in dielectric property of nanocomposite is mainly ascribed to the homogeneous dispersion of $MnWO_4$ particles followed by the continuous formation of micro-capacitor network with the loading of fillers [267]. The magnitude of its increase is higher at lower frequencies and marginal at high frequencies. This behavior is associated with the interfacial polarization suggested by Maxwell-Wagner model which is in well line with Koop's theory [268]. According to this theory, heterogeneous composite materials as in the present case contain well conducting grain boundaries separated by highly resistive thin grains. Here the conducting metal-polymer interfaces are separated by the insulating elastomer phase creating inhomogeneity in the system which leads to a frequency dependent polarization. At low frequencies, the orientation of the molecules completely follows the alternation in the external applied field. This leads to higher interfacial polarization and result in high dielectric constant. But at higher frequencies, alternation in the field applied externally becomes fast and therefore charge carriers

cannot follow this. This leads to poor interfacial polarization of the polymer matrix. It is evident from the figure that Cl-SBR/ $MnWO_4$ composite with 7 phr nanofiller loading exhibit the maximum dielectric constant and beyond this loading, the dielectric constant decreases. This means that the interfacial polarization is the maximum in 7 phr loading, and is due to the strong polar-polar interaction between the nanoparticles and chlorinated SBR matrix. These molecular interactions induce the orientation of dipoles in the elastomer. The poor dielectric constant of nanocomposite at higher loading (above 7 phr) is attributed to the heterogeneous conduction in polymer matrix which arises from the agglomeration of filler particles within the macromolecular chain of chlorinated SBR.

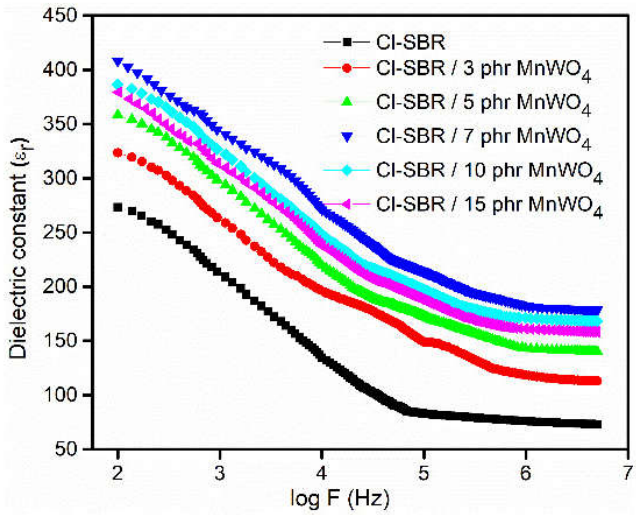

Figure 6.9 Dielectric constant of Cl-SBR and Cl-SBR/$MnWO_4$ nanocomposites

6.2.9.3 Dielectric loss tangent (Tan δ)

The variation of dielectric loss as a function of frequency for Cl-SBR and Cl-SBR/$MnWO_4$ nanocomposites at room temperature is shown in **figure 6.10**. It has been observed that the values of Tan δ decreases in the low frequency region from 10^2 to 10^4 Hz and remains constant for all the composites up to the applied frequency above 10^4 Hz. Generally more energy is required for the polarization of grain boundaries at lower frequency and therefore the energy loss is higher for the composite materials [269]. However, the polarization between the grain boundaries is minimum at higher frequencies which either lowers the Tan δ value is low or stabilizes it. It can be seen from the figure that the tangent loss increases with the loading of nanoparticles up to 7 phr loading due to the strong interaction between polymer and the nanoparticles. Thereafter the value decreases with further addition of nanoparticles. Generally, the maximum tangent loss (tan δ) occurred when the migration and accumulation of charge carriers is maximum at the interface between nanofiller and polymer matrix. Nanoparticles undergoes agglomerations at higher loading (above 7 phr), which resist the migration and accumulation of charge carriers leading to a poor interfacial polarization. Therefore, the dielectric loss tangent decreases.

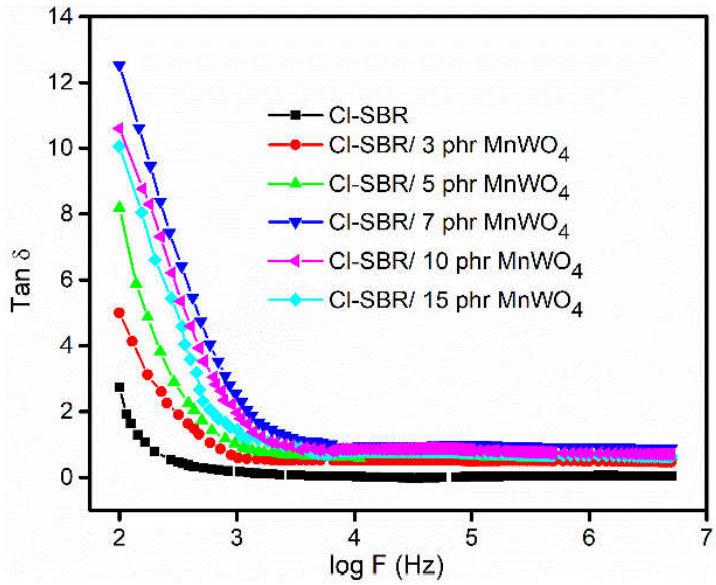

Figure 6.10 Dielectric loss tangent of Cl-SBR and Cl-SBR/$MnWO_4$ nanocomposite

6.2.10 Oil Resistance

Fuel and oil resistant elastomeric compounds and nanocomposites are promising materials for automotive industry. Without coming in contact with fuels, greases and oils, the life cycle of an automotive product will not be completed. The solvent and oil resistance properties are inherent rubbers containing polar functional groups. These include chloroprene, chlorinated SBR and NBR. The oil resistance (ASTM oil # 1, 2 and 3) shown by Cl-SBR and its nanocomposites at various temperatures are given in **figure 6.11**. All the composite shows higher oil resistance values than the Cl-SBR control sample. Among the nanocomposites, vulcanizate containing 7 phr $MnWO_4$ nanofiller shows the maximum oil resistance at 25 and at

100°C. Various factors such as the electro-negativity of rubber compounds, crosslink density and crystallinity play an important role in deciding the oil resistance of samples [259].

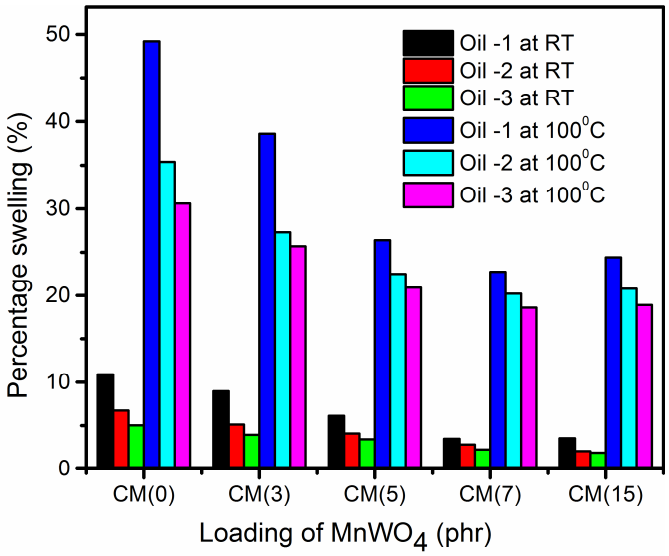

Figure 6.11 Oil resistance of Cl-SBR/$MnWO_4$ nanocomposites

The higher oil resistance of nanocomposite in the present study is due to the uniform dispersion of crystalline $MnWO_4$ particles. The clustering of nanoparticles in Cl-SBR matrix beyond 7 phr decreases crosslink density of the polymer matrix. The oil resistance of all the samples decreases with increasing temperatures due to easy penetration of oil into the thermally relaxed polymeric matrix. It is clear from the figure that the penetration of oil is more pronounced in ASTM oil # 3 than oil # 1 and oil # 2. This is because the aniline point of ASTM oil # 3 is significantly lower and therefore it diffuses more easily into the nanocomposites

6.2.11 Diffusion studies

6.2.11.1 Mol % uptake of aromatic and petroleum fuels

Effect of filler loading

The effect of filler contents on swelling properties of Cl-SBR and Cl-SBR/$MnWO_4$ in benzene and petrol at 27°C is shown in **figure 6.12** and **6.13.** It can be seen that all the plots are sigmoidal in nature signifying the initial high uptake of the solvent followed by the slow uptake that slowly reaches the equilibrium. As the filler concentration increases, the solvent uptake decreases as expected from the reinforcement. The composite with 7 phr of $MnWO_4$ possesses very low rate of uptake. The free volume inside the Cl-SBR matrix decreases with the addition of nanoparticles, hence the mobility of solvent inside the polymer chain is restricted and this decreases the mol uptake [270]. At a higher loading of nanoparticles above (7 phr), the solvent uptake increases due to agglomeration of $MnWO_4$. All the curves at room temperature, in petrol, diesel and kerosene show the same trends.

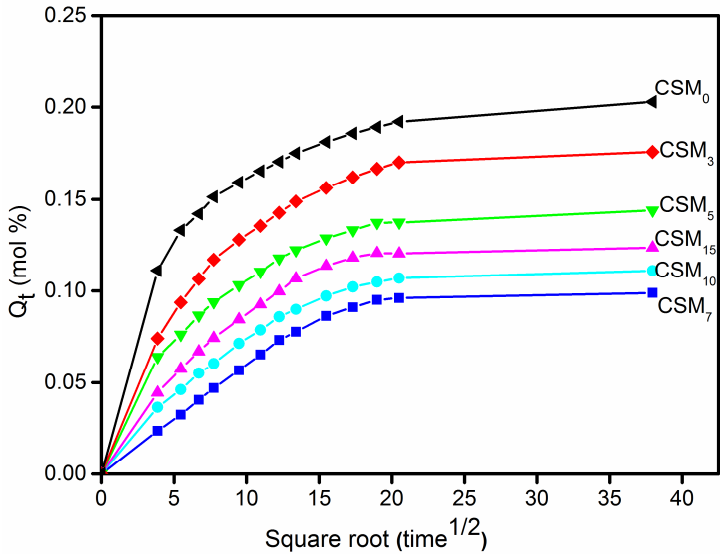

Figure 6.12 Sorption curves of Cl-SBR/$MnWO_4$ nanocomposite in benzene

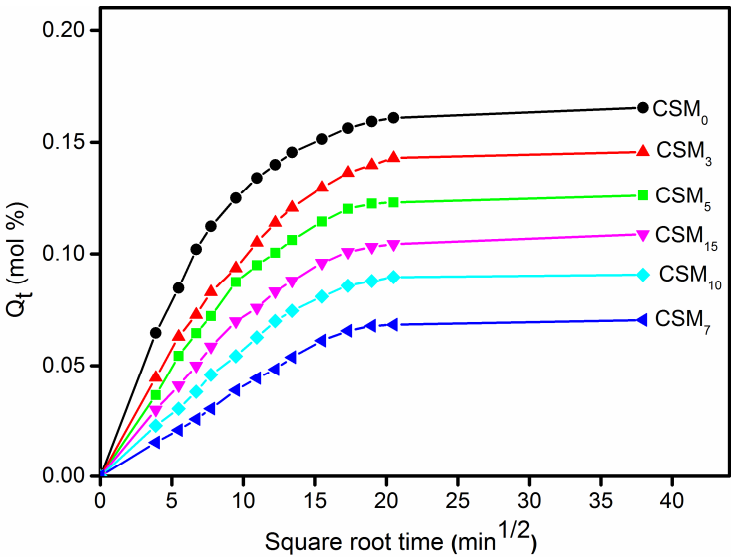

Figure 6.13 Sorption curves of Cl-SBR/$MnWO_4$ nanocomposite in petrol

Effect of solvent on mol uptake

The effect of solvent on sorption mainly depends on the structure, molecular weight and polarity of solvent molecules. **Figure 6.14** and **6.15** shows the effect of various solvents such as aromatic (benzene, toluene and xylene) and petroleum fuels (petrol, diesel and kerosene) in the mol uptake of Cl-SBR/7 phr $MnWO_4$. It is clear that the solvent uptake decreases on increasing the size of the penetrant molecules. This can be explained on the basis of free volume theory, according to which the diffusion rate of penetrant molecules depends on the ability of polymer segments to exchange their voids to the penetrant molecules [271]. Owing to the presence of reinforcing fillers, the exchange of positions in macromolecular chain becomes very difficult for large penetrant molecules.

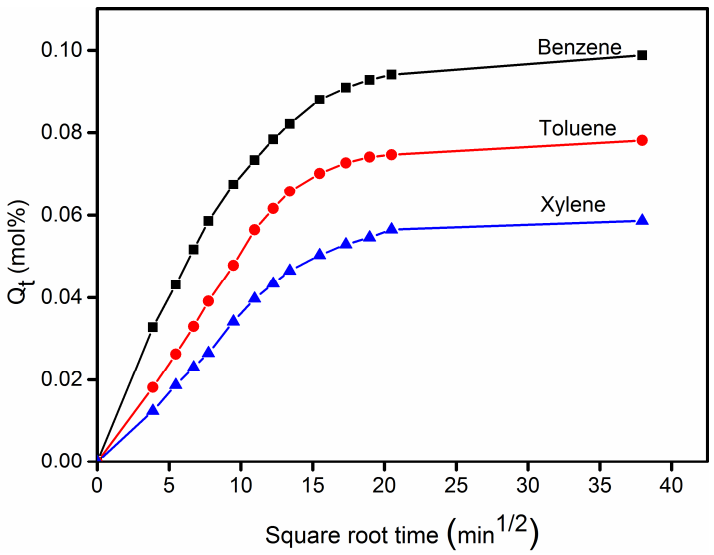

Figure 6.14 Solvent uptake of Cl-SBR with 7 phr of $MnWO_4$ in aromatic solvents

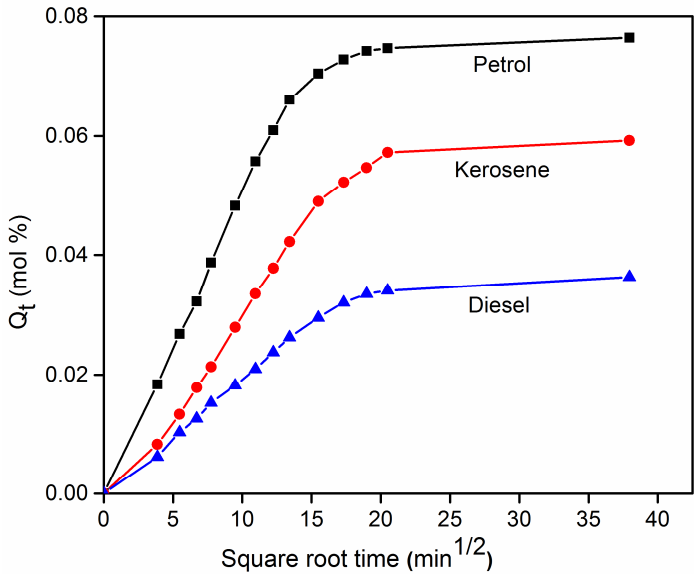

Figure 6.15 Solvent uptake of Cl-SBR with 7 phr of $MnWO_4$ in industrial solvents

Effect of temperature on mol uptake

The increase in temperature as expected can enhance the solvent uptake. **Figure 6.16 and 6.17** shows the effect of temperature on mol uptake of benzene and petrol respectively. The composite having maximum solvent resistant property (7 phr of filler) is selected to analyse the effect of temperature. An increase in solvent uptake with the increase in temperature can be observed; it is due to the gain in kinetic energy of polymer chain; which causes increased segmental mobility of matrix.

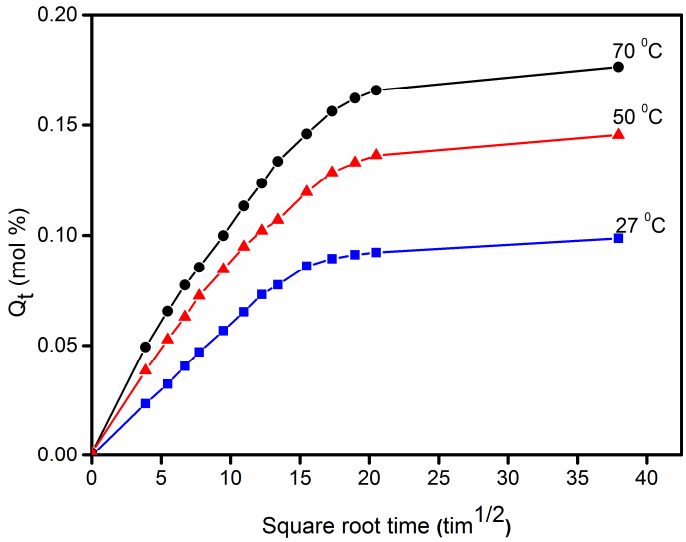

Figure 6.16 The mole uptake of Cl-SBR and SBR with 7 phr of $MnWO_4$ in benzene at different temperature

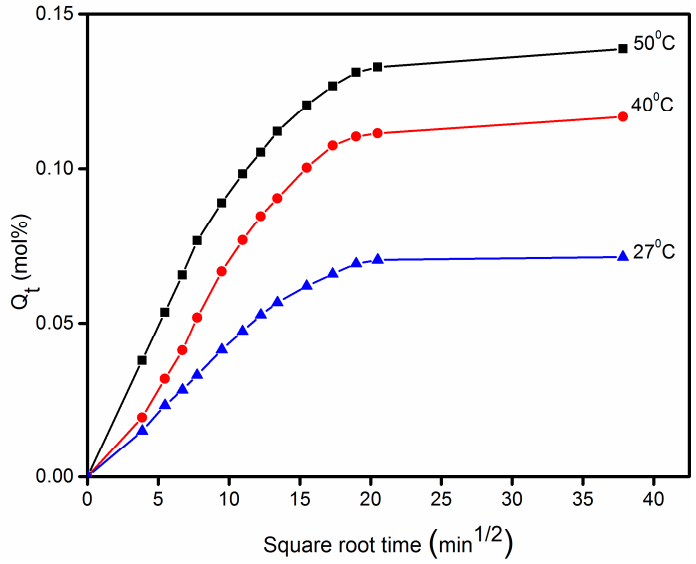

Figure 6.17 The mole uptake of Cl-SBR and SBR with 7 phr of $MnWO_4$ in petrol at different temperature

6.2.11.2 Diffusion (D), sorption (S) and permeation (P) coefficients

From **table 6.3** and **6.4**, it is seen that the D values decreases with increase in the amount of $MnWO_4$ nanofiller. Upon addition of nanofillers to Cl-SBR matrix, the compactness of the sample increases, and the improvement in the interfacial interaction between the polymer and filler restrict the local movement of polymer chains. This reduces the equilibrium uptake and hence diffusion coefficient decreases with increase in filler loading [272]. The Cl-SBR/7 phr $MnWO_4$ nanocomposite has the minimum solvent uptake and hence the minimum D value due to the strong and effective interaction between Cl-SBR matrix and $MnWO_4$ nanofiller. Diffusion coefficient also shows the variation with the nature of solvents, i.e., petrol has maximum and diesel has the least penetrating effect. The decrease in D values in accordance with the molar volume of solvents can be explained on the basis of free volume theory. For large molecules, higher activation energy is needed for the exchange of voids in between the macromolecular chain of Cl-SBR and selected solvent [207].

Table 6.3 D, S and P values of Cl-SBR and Cl-SBR/$MnWO_4$ nanocomposites in aromatic solvents

Samples	Diffusion coefficient D x 10^5 (cm^2/s)			Sorption coefficient S			Permeation coefficient P x 10^5(cm^2/s)		
	Benzene	Toluene	Xylene	Benzene	Toluene	Xylene	Benzene	Toluene	Xylene
CSM_0	1.64	1.52	1.41	1.18	1.15	1.13	1.93	1.75	1.59
CSM_3	1.61	1.46	1.32	1.15	1.12	1.09	1.85	1.63	1.43
CSM_5	1.52	1.37	1.24	1.12	1.09	1.06	1.70	1.49	1.31
CSM_7	1.21	1.14	1.09	1.07	1.03	1.01	1.29	1.17	1.10
CSM_{10}	1.43	1.32	1.17	1.09	1.06	1.03	1.55	1.39	1.21
CSM_{15}	1.48	1.35	1.21	1.11	1.07	1.05	1.64	1.44	1.27

Table 6.4 D, S and P values of Cl-SBR and Cl-SBR/$MnWO_4$ nanocomposites in industrial solvents

Samples	Diffusion coefficient D x 10^5 (cm^2/s)			Sorption coefficient S			Permeation coefficient P x 10^5(cm^2/s)		
	Petrol	Kerosene	Diesel	Petrol	Kerosene	Diesel	Petrol	Kerosene	Diesel
CSM_0	1.46	1.41	1.32	1.15	1.12	1.09	1.68	1.58	1.44
CSM_3	1.41	1.37	1.22	1.12	1.07	1.06	1.58	1.47	1.29
CS M_5	1.35	1.32	1.18	1.08	1.03	1.01	1.46	1.35	1.19
CSM_7	1.21	1.19	1.08	1.01	0.91	0.86	1.22	1.08	0.93
CSM_{10}	1.25	1.23	1.14	1.05	0.96	0.89	1.31	1.18	1.01
CSM_{15}	1.27	1.25	1.16	1.06	0.99	0.92	1.34	1.23	1.06

The sorption coefficient also registers a decrease with the addition of $MnWO_4$ nanoparticles and the composite containing 7 phr of filler shows the minimum value of sorption coefficient. Here from the **table 6.3 and 6.4** it is clear that the sorption coefficient shows the same trend as that of diffusion coefficients in both aromatic and petroleum fuels. The amount of solvent permeated through the unit area of polymer matrix per second is the permeation coefficient. It signifies the solvent transport through successive layers in polymer sample. It is obtained on multiplication of sorption coefficient and diffusion coefficient. **Table 6.3** and **6.4** depicts the decrease in permeation coefficient values with increasing the $MnWO_4$ nanofiller loading. Mathematically, this is due to the decrease in D and the physical reason is the restriction to the permeation process of the solvent created by the strong interface in filled Cl-SBR samples. The composite containing 7 phr of $MnWO_4$ and the gum sample (Cl-SBR

without filler) exhibits the minimum and maximum permeation coefficients respectively.

6.2.11.3 Activation energy of diffusion(E_D) and permeation (E_P)

In order to take place diffusion or permeation of solvents, there should be free volume inside the matrix, or a diffusional jump occurs in the presence of free voids inside the matrix [206]. It requires high activation energy and is obtained from the slopes of the curve plotted as log D versus 1/T. From the **table 6.5** and **6.6**, the E_P and E_D values are found increasing in accordance with the filler loading and penetrant size.

Table 6.5 E_D, and E_P (kJ mol^{-1}) values of Cl-SBR and Cl-SBR/$MnWO_4$ nanocomposites in aromatic solvents

Samples	Benzene		Toluene		Xylene	
	E_D	E_P	E_D	E_P	E_D	E_P
CSM_0	6.28	5.17	6.38	5.21	6.69	5.44
CSM_3	6.34	5.21	6.42	5.27	6.74	5.53
CSM_5	6.39	5.28	6.45	5.32	6.83	5.58
CSM_7	6.54	5.39	6.68	5.44	6.95	5.72
CSM_{10}	6.46	5.35	6.57	5.37	6.89	5.64
CSM_{15}	6.43	5.32	6.53	5.34	6.86	5.62

Table 6.6 E_D and E_P (kJ mol^{-1}) values of Cl-SBR and Cl-SBR/ $MnWO_4$ nanocomposites in industrial solvents

Samples	Petrol		Kerosene		Diesel	
	E_D	E_P	E_D	E_P	E_D	E_P
CSM_0	6.52	5.29	6.64	5.38	6.82	5.52
CSM_3	6.58	5.34	6.69	5.43	6.94	5.58
CSM_5	6.73	5.41	6.77	5.49	6.99	5.63
CSM_7	6.92	5.59	7.08	5.69	7.23	5.77
CSM_{10}	6.81	5.47	6.89	5.56	7.12	5.71
CSM_{15}	6.77	5.45	6.81	5.51	7.08	5.67

In the case of aromatic solvents xylene and diesel in the case of petroleum fuels; due to the large molecular size they require more activation energy to penetrate. On increasing the filler content, the free volume inside the polymer decreases due to high compactness and this result in higher activation energy. Here from the table, it is clear that the Cl-SBR without filler has a minimum activation energy of diffusion and permeation, and the composite with 7 phr of $MnWO_4$ shows highest activation energy. There is a decrease in activation energy upon further addition of nanoparticles beyond 7 phr.

6.2.11.4 Thermodynamic parameters

Thermodynamic parameters are given in **table 6.7** and **6.8,** and is seen that all the composites in all solvents show an endothermic enthalpy change (positive ΔH_s). The enthalpy change increases from benzene to xylene and also from petrol to diesel; and the results obtained are in good agreement with the values obtained from E_P and E_D ($\Delta H=E_P - E_D$). The entropy change of diffusion is also found positive and on increasing filler loading the entropy change decreases.

Table 6.7 ΔH, ΔS and ΔG (kJ/mol) of Cl-SBR and Cl-SB/$MnWO_4$ nanocomposites in aromatic solvents

Samples	ΔH			ΔS			$-\Delta G$		
	Benzene	Toluene	Xylene	Benzene	Toluene	Xylene	Benzene	Toluene	Xylene
CSM_0	1.17	1.22	1.27	0.061	0.058	0.042	17.13	16.18	11.33
CSM_3	1.22	1.26	1.32	0.052	0.047	0.038	14.38	11.33	10.08
CSM_5	1.27	1.29	1.38	0.047	0.041	0.022	12.83	11.01	5.22
CSM_7	1.46	1.53	1.59	0.039	0.022	0.010	10.24	5.07	1.41
CSM_{10}	1.36	1.38	1.47	0.042	0.034	0.014	11.24	8.82	2.73
CSM_{15}	1.32	1.35	1.43	0.044	0.038	0.017	11.6	10.05	3.67

Table 6.7 ΔH, ΔS and ΔG (kJ/mol) of Cl-SBR and Cl-SBR/$MnWO_4$ nanocomposites in industrial solvents

Samples	ΔH			ΔS			-ΔG		
	Petrol	Kerosene	Diesel	Petrol	Kerosene	Diesel	Petrol	Kerosene	Diesel
CSM_0	1.24	1.29	1.36	0.051	0.046	0.037	14.06	12.51	9.74
CSM_3	1.27	1.36	1.47	0.048	0.037	0.031	13.13	9.74	7.83
CSM_5	1.32	1.43	1.52	0.042	0.032	0.025	11.28	8.17	5.98
CSM_7	1.54	1.69	1.73	0.021	0.018	0.012	4.76	3.44	1.87
CSM_{10}	1.44	1.56	1.66	0.032	0.024	0.019	8.16	5.64	4.04
CSM_{15}	1.39	1.51	1.62	0.039	0.029	0.021	10.31	7.19	4.68

The composite filled with 7 phr of $MnWO_4$ has strong interfacial interaction between polymer and filler, hence it shows minimum entropy. By using the values of ΔH_s and ΔS_s the Gibbs free energy can be calculated ($\Delta G_s = \Delta H_s - T\Delta S_s$). It is found that the free energy of diffusion enhanced by increasing the amount of $MnWO_4$, hence the Cl-SBR without filler and with 7 phr of filler shows the minimum and maximum free energy of sorption. The values obtained reveals the fact that the spontaneity in the diffusion solvent decreases upon reinforcement with nanoparticles [201].

6.2.11.5 Transport mechanism

The value of n indicates the mode of transport, and when the value of n is 0.5 mode of transport is said to be Fickian, if it is in between 0.5 and 1 then it is in anomalous mode. It may be due to the coupling of Fickian and non-Fickian mode of transport [237]. Here reinforcement of Cl-SBR matrix with nanoparticles makes the chain relaxation very slow due to high viscosity. Hence the mode of transport becomes

anomalous as indicated by 'n' values in **table 6.9** and **6.10** for aromatic and industrial solvents respectively. It is very clear from the table that the structural parameter k is decreased with increase in $MnWO_4$ nanofiller loading; this is a clear evidence for reinforcement. From the k values obtained, we can see that in the presence of nanoparticles the solvent matrix interaction become very weak as compared to the pure Cl-SBR matrix. The lowest value of k is shown by the composite with 7 phr of $MnWO_4$ nanoparticles which can be a strong support for the uniform distribution of nanoparticles. This is supported by SEM micrographs also. It also ensures the compactness of the samples upon reinforcement. Owing to the same reason the value of k decreases on increasing the molar mass of the solvents [168].

Table 6.9 n and k values of Cl-SBR and Cl-SBR/$MnWO_4$ nanocomposites in aromatic solvents

Samples	Benzene		Toluene		Xylene	
	n	$kx10^2$ (min^{-1})	n	$kx10^2$ (min^{-1})	n	$kx10^2$ (min^{-1})
CSM_0	0.69	0.24	0.72	0.19	0.81	0.15
CSM_3	0.71	0.21	0.76	0.17	0.82	0.14
CSM_5	0.71	0.18	0.78	0.16	0.85	0.13
CSM_7	0.72	0.15	0.81	0.12	0.89	0.09
CSM_{10}	0.67	0.16	0.79	0.14	0.87	0.11
CSM_{15}	0.67	0.17	0.78	0.15	0.86	0.12

Table 6.10 n and k values of Cl-SBR and Cl-SBR/$MnWO_4$ nanocomposites in industrial solvents

Samples	Petrol		Kerosene		Diesel	
	n	$kx10^2(min^{-1})$	n	$kx10^2(min^{-1})$	n	$kx10^2(min^{-1})$
CSM_0	0.75	0.22	0.76	0.21	0.82	0.19
CSM_3	0.77	0.21	0.83	0.19	0.86	0.18
CSM_5	0.78	0.18	0.81	0.17	0.89	0.16
CSM_7	0.78	0.16	0.87	0.14	0.94	0.12
CSM_{10}	0.73	0.17	0.86	0.16	0.93	0.14
CSM_{15}	0.75	0.18	0.79	0.17	0.92	0.15

6.3 Conclusions

Composites of Cl-SBR with different contents of $MnWO_4$ nanoparticles were prepared and characterized by FT-IR, UV, XRD, SEM, DSC, TGA and flame resistance studies. The interaction of nanoparticles with the elastomer was confirmed from spectroscopic studies through the shift in the absorption peaks of the nanocomposites. The semi-crystalline behavior and the uniform dispersion of nanoparticles were revealed from XRD and SEM analysis respectively. The addition of nanofiller to Cl-SBR reduces the amorphous nature of Cl-SBR. Scanning electron microscope pictures, in fact reveals that this is due to the uniform distribution of the nanoparticles in the Cl-SBR matrix at 7 phr. The increased compactness of or reduced flexibility of the samples increased the glass transition temperature of Cl-SBR from -35°C to -29°C. The thermal stability and flame resistance of nanocomposites were greater than that of pure Cl-SBR and these properties increased with the loading of nanoparticles. The processability, mechanical, electrical

properties, oil and solvent diffusion of composites were also studied with respect to different loading of nanoparticles. The reduction in optimum cure time of Cl-SBR, noted with the increasing loading of nanoparticles proved to be beneficial to enhance the production rate of articles using these compositions. The improved tensile strength, modulus and tear strength values with the loading of nanoparticles up to 7 phr was attributed to the formation of a strong interface with the large interfacial area. In addition, the electrical conductivity was also found to be highest at this loading thus opening the possibility to use these materials as future semiconducting materials with easy processability. The studies based on the absorption of ASTM oils as well as petroleum fuels supports the excellent reinforcement of Cl-SBR matrix at 7 phr loading of $MnWO_4$ particles; meanwhile reflecting the reduced absorption of solvent with higher molecular weight and size. Overall, an anomalous diffusion mechanism was revealed from the study of solvent transport in Cl-SBR and its nanocomposites.

7.1 Conclusions

In order to improve the processing characteristics, mechanical properties and to reduce the cost, the use of fillers in elastomers has been in practice for many decades. In fact, polymers filled with inorganic particles show excellent electrical and thermal properties. Compared to conventional polymer composite containing micro sized inorganic particles as fillers, the incorporation of even lower weight percent of nanoparticles (<15 phr) has tremendous improvement in properties. The advantages of polymer nanocomposites are its high strength, low cost, lightweight, elasticity, toughness and easy processability to a desired and useful shape by using different fabrication methods. Owing to their nano-size, the surface energy of nanoparticles is very high which result in better interfacial area, adhesion and superior mechanical properties. However, nanoparticles have a tendency to undergo agglomeration in most cases due to their high surface energy and therefore nanoparticles cannot uniformly distribute into the macromolecular chain. The clustered or agglomerated nanoparticles create stress concentration in the polymer matrix and this deteriorates the mechanical performance of the resulting polymer nanocomposite.

Styrene butadiene rubber (SBR), a purely synthetic elastomer with well-defined and carefully optimized properties such as molecular weight, molecular weight distribution, viscosity, green and gum strength etc. Owing to the high abrasion resistance, it finds use in automobile sector, and mainly in tires. However, nanocomposite based on SBR has very poor oil, ozone and flame resistance and this restricts

their use in many applications requiring high performance. The tensile strength, oil and flame resistance of SBR was enhanced by the introduction of polar group in the rubber such as chloro functional group. Halogenated polymers are widely applicable in engineering applications due to the improved physico-mechanical properties, high dielectric characteristics, resistant to chemicals, oil, and good adhesion to metals. The reaction of alkenes with dichlorocarbene generated from the in situ reaction of chloroform with alkali is a simple route of introducing chlorine atoms into polymer macromolecules; in fact this is a simple alternative to chlorination and hydro-chlorination. This method is comparatively greener because it allows the production of halogenated polymers without any aggressive chemical reagent such as halogen and hydrogen chloride. Our previous work showed that chemically modified SBR (chlorinated SBR) prepared by the alkaline hydrolysis of chloroform shows excellent tensile strength, flame retardant and resistance to oil. This is a novel strategy because as per literature polar functional groups in SBR (chlorinated SBR) play a vital role to enhance interaction between the nanoparticles and the elastomeric matrix. The major problem associated with the reinforcement of SBR with nanoparticles is the poor interaction of hydrocarbon rubber with the nanoparticles.

Generally, the nanocomposites are prepared by the addition of nanofillers to polymers through solution blending or melt blending. The main disadvantage of the solution mixing is the poor dispersion of nanoparticles and inability to remove trace of solvent completely, which limits the applicability of the solution mixing in industrial

sector. Even though the melt mixing technique is effective to produce good filler dispersion, the higher temperature involved in the process causes deterioration in mechanical properties. Compared to these methods, a simple two roll mill mixing technique offers many advantages such as satisfactory filler dispersion, absence of any organic solvent, moderate temperature during mixing and time saving factor.

Chapter 3 deals with the preparation and characterization of SBR/ZnS nanocomposites using a simple and environmentally-friendly two-roll mill mixing technique. The composites were characterized by FT-IR, UV, XRD, SEM, DSC and TGA. The interaction of nanoparticles with SBR was confirmed from the spectroscopic studies through the shift in absorption peaks of the nanocomposite. The XRD showed the ordered arrangement of filler particles in SBR and the amorphous nature of composite decreased with an increase in content of nanoparticles. The SEM images showed a uniform dispersion of the fillers in SBR. The glass transition temperature of the composites increased with the loading of metal sulphide nanoparticles. TGA results showed an increase in thermal stability of nanocomposites upon increasing filler content. The processability, mechanical properties, electrical properties and solvent penetration studies of the composites were studied with respect to different loading of nanofiller. Despite the reduction in scorch safety, the compounded SBR/ZnS samples indicated higher production rate resulting from lowering of optimum cure time. Mechanical properties such as tensile, tear strength, modulus, hardness, abrasion resistance, heat build-up and compression

set were in agreement with the reinforcement by ZnS particles. This is advantages because elastomer nanocomposite with improved mechanical properties tends to be high performing and durable in-service life. The AC conductivity of SBR was significantly enhanced by the addition of ZnS nanoparticles. Dielectric properties of composites were greater than pure SBR and the maximum dielectric properties were obtained for 10 phr composite. Diffusion and sorption of aromatic and industrial solvents through SBR/ZnS nanocomposites was studied at different temperatures. The diffusion results were explained in terms of the size of liquid molecules and the diffusion mechanism was found to follow the anomalous in trend. The diffusion and permeation coefficient values decreased with an increase in the molar volume of the solvent. The enhanced dielectric property of the elastomeric nanocomposites can be used in various applications such as electromagnetic shielding, flexible energy storage and other nanoelectronic devices.

Cl-SBR/ZnS nanocomposites were prepared by a two-roll mill mixing method is discussed in chapter 4. The composites with different loading of ZnS nanoparticles and characterized by FTIR, UV, XRD, SEM, TEM, DSC and TGA analysis. The intermolecular interaction between nanoparticles and Cl-SBR was confirmed from FTIR and UV spectrum by the shift in the absorption peaks of the polymer matrix. The XRD results indicated that the amorphous nature of Cl-SBR was decreased with the addition of nanoparticles. The TEM and SEM images revealed the presence of ZnS nanoparticles which were uniformly distributed in the elastomer at 7 phr loading. The thermal

stability and flame retardancy were greatly enhanced with the addition of ZnS nanoparticles. The processability, mechanical, electrical, oil and solvent imbibing properties of composites were also investigated with respect to filler loading. Cure properties like optimum cure and scorch time decreased with an increase in the concentration of nanoparticles. Mechanical properties like tensile and tear strength have been found to increase up to a threshold loading (7 phr), followed by a decrease in tensile and tear resistance at a still higher loading. The elongation at break, resilience and compression set values decreased with the addition of ZnS nanoparticles. The AC conductivity and dielectric properties were found to be maximum at 7 phr loading of ZnS. Composite with 7 phr loading absorbed less oils and solvent compared to those of other composites and with pure Cl-SBR, indicating a better interaction between filler and rubber. Transport behavior of samples in aromatic and industrial solvents at different temperatures was analysed. Transport properties such as diffusion coefficient, sorption coefficient and permeation coefficient have been estimated with respect to loading of nanoparticles, nature of solvent and temperature. The mechanism of diffusion was found to be Fickian in nature for Cl-SBR, while in the nanoparticles filled composites, it was anomalous.

In chapter 5 styrene butadiene rubber with different content of manganous tungstate nanocomposites were prepared by a simple two roll mixing mill. The FTIR studies verify the presence of $MnWO_4$ nanoparticles in the SBR matrix at 559 cm^{-1}. UV-Visible spectroscopy proved the enhanced interfacial interaction between nanoparticles and

the elastomeric chain and the composite with 10 phr shows the maximum UV absorption. This study investigated the effect of $MnWO_4$ nanoparticles on the morphology, crystalline nature, thermal stability, processability, mechanical and electrical properties. The interaction with solvents using aromatic and industrial solvents were also studied. The XRD pattern of nano composite showed the decrease in amorphous peak of SBR by the interaction with $MnWO_4$. The uniform dispersion of nanoparticles in SBR decreased with an increase in the nanoparticles loading. The interaction of nanoparticles with polymer can effectively enhanced the thermal stability of SBR. Processing characteristics such as optimum cure time and scorch time decreases with loading of $MnWO_4$, whereas the rheometric torque increased with loading of nanoparticles up to 10 phr. Addition of nanoparticles to SBR increases the tensile strength, modulus, tear and abrasion resistance, hardness and heat build-up, while elongation at break, resilience and compression set were decreased. AC electrical conductivity and dielectric property of nanocomposites were higher than SBR and the maximum electrical property was obtained for 10 phr of composite and above this loading, the electrical properties were found to be decreases. The liquid transport characteristics of nanocomposite were analysed using aromatic and industrial solvent molecules and the results were compared with unfilled SBR. Nanocomposites showed a reduced penetration of solvent due to the interaction between nanoparticles and SBR components. The solvent uptake was lower for 10 phr loading and the solvent uptake tendency increased at higher filler loading, which results from the poor interaction between the matrix and that leads to the aggregation of

nanoparticles. The sorption coefficient and activation parameter showed a dependence on the size of penetrant molecules. The transport phenomenon was found to follow anomalous type mechanism in all the cases. So, the SBR/ $MnWO_4$ composite show the significant variation in mechanical electrical and solvent sorption properties when small amounts of fillers (10 phr loading) were incorporated.

Composites of Cl-SBR with different contents of $MnWO_4$ nanoparticles were prepared and characterized by FT-IR, UV, XRD, SEM, DSC, TGA and flame resistance studies and are discussed in chapter 6. The interaction of nanoparticles with the elastomer was confirmed from spectroscopic studies through the shift in the absorption peaks of the nanocomposites. The semi-crystalline behavior and the uniform dispersion of nanoparticles were revealed from XRD and SEM analysis respectively. The addition of nano-filler to Cl-SBR reduces the amorphous nature of Cl-SBR. Scanning electron microscope pictures, in fact reveals that this is due to the uniform distribution of the nanoparticles in the Cl-SBR matrix at 7 phr. The increased compactness of or reduced flexibility of the samples increased the glass transition temperature of Cl-SBR from -35°C to -29°C. The thermal stability and flame resistance of nanocomposites were greater than that of pure Cl-SBR and these properties increased with the loading of nanoparticles. The processability, mechanical, electrical properties, oil and solvent diffusion of composites were also studied with respect to different loading of nanoparticles. The reduction in optimum cure time of Cl-SBR, noted with the increasing loading of nanoparticles proved to be beneficial to enhance the

production rate of articles using these compositions. The improved tensile strength, modulus and tear strength values with the loading of nanoparticles up to 7 phr was attributed to the formation of a strong interface with the large interfacial area. In addition, the electrical conductivity was also found to be highest at this loading thus opening the possibility to use these materials as future semiconducting materials with easy processability. The studies based on the absorption of ASTM oils as well as petroleum fuels supports the excellent reinforcement of Cl-SBR matrix at 7 phr loading of $MnWO_4$ particles; meanwhile reflecting the reduced absorption of solvent with higher molecular weight and size. Overall, an anomalous diffusion mechanism was revealed from the study of solvent transport in Cl-SBR and its nanocomposites.

7.2 Future outlook

The present investigation on reinforcement of SBR and its chlorinated forms opens many future possibilities for research innovations. These include;

- Preparation of SBR and chlorinated SBR nanocomposites using nano-fillers like NiO, FeO and magnetite.
- Investigation of the magnetic properties of nanocomposites and identifying the specialties in magnetic behavior, including magnetic hysteresis.
- Exploration of the SBR and chlorinated SBR nanocomposite membranes with varying type and extent of cross-links for

solvent mixture separation using pervaporation, development of prototypes for online separation or purification.

- Development of prototypes based on SBR and chlorinated SBR nanocomposite membranes for separation of chemical purification and as fuel hoses, oil seals and gaskets.

- Development of better fire and weather resistant polymer coatings.

1. M.Barz, R. Luxenhofer, R. Zentel and M.J. Vicent, Polym. Chem. **2**, 1900 (2011).

2. C. J. Biermann, Handb. Pulping Papermak. (Second Ed.), pp. 395–402 (1996).

3. S. Ramakrishna, J. Mayer, E. Wintermantel and K. W. Leong, Compos. Sci. Technol. **61**, 1189 (2001).

4. C. Sanchez, P. Belleville, M. Popall and L. Nicole, Chem. Soc. Rev. **40**, 696 (2011).

5. Z. Tang, C. He, H. Tian, J. Ding, B. S. Hsiao, B. Chu, and X. Chen, Prog. Polym. Sci. **60**, 86 (2016).

6. A. P. Leber, Chem. Biol. Interact. pp. 169–173 (2001).

7. W. H. Jo, K. H. Nam, and J. C. Cho, J. Polym. Sci. Part B Polym. Phys. **34**, 2169 (1996).

8. F.A. Bovcy and F.H. Winslow, Macromolecules. **18**, 549 (1979).

9. S. Berthumeyrie, S. Collin, P. O. Bussiere and S. Therias, J. Hazard. Mater. **272**, 137 (2014).

10. G. Mathew, R. P. Singh, N. R. Nair and S. Thomas, Polymer. **42**, 2137 (2001).

11. Á. Fernández De La Ossa, M. Torre, and C. García-Ruiz, Adv. Mater. Sci. Res. (2012), pp. 201–220.

12. J.A. Reilly, J. Am. Insti. Conser. **30**, 145 (1991).

13. D. Feldman, Designed Monomers and Polymers. **11,** 1–15 (2008).

14. M. Wang, M. Leitch and C. Xu, Eur. Polym. J. **45**, 3380 (2009).

15. K. A. Günay, P. Theato, and H. A. Klok, J. Polym. Sci. Part A Polym. Chem. **51**, 1 (2013).

16. V. Pintus, S. Wei, and M. Schreiner, Microchem. J. **124**, 949 (2016).

17. W. H. Carothers, J. Am. Chem. Soc. **51**, 2548 (1929).

18. D. Chao, X. Ma, X. Lu, L. Cui, H. Mao, W. Zhang, and Y. Wei, Macromol. Chem. Phys. **208**, 658 (2007).

19. A. Viswanathan, World Pat. Inf. **32**, 300 (2010).

20. H. M. James and E. Guth, J. Chem. Phys. **11**, 455 (1943).

21. D. J. Merline, S. Vukusic, and A. A. Abdala, Polym. J. **45**, 413 (2013).

22. M. Morton, J. Macromol. Sci. Part A - Chem. **15**, 1289 (1981).

23. H. M. James and E. Guth, J. Chem. Phys. **11**, 455 (1943).

24. P. J. Flory, J. Am. Chem. Soc. **59**, 241 (1937).

25. P. J. Flory, Principles of Polymer Chemistry. Cornell Univ. Press (1953).

26. G. W. Coates, P. D. Hustad and S. Reinartz, Angew. Chemie - Int. Ed. **41**, 2236 (2002).

27. V. Busico, G. Talarico, and R. Cipullo, Macromol. Symp.**226**, 1 (2005).

28. H. Sinn and W. Kaminsky, Adv. Organomet. Chem. **18**, 99 (1980).

29. V.R. Gowarikar, V.N. Viswanathan and T. Sreedhar, Polymer Science, Wiley-Eastern Ltd, (1995).

30. Y. Gnanou and M. Fontanille, Organic and Physical Chemistry of Polymers (2007).

31. F. W. Harris, Am. Chem. Soc. Polym. Prepr. Div. Polym. Chem.**26**, 287 (1985).

32. D. Le Corre, J. Bras, and A. Dufresne, Biomacromolecules **11**, 1139 (2010).

33. R. J. W. Reynolds, Polymer. **19**, 1477 (1978).

34. A. He, B. Huang, S. Jiao and Y. Hu, J. Appl. Polym. Sci.**89**, 1800 (2003).

35. C. Kow, M. Morton, L. J. Fetters, and N. Hadjichristidis, Rubber Chem. Technol. **55**, 245 (1982).

36. S. Toki, B. S. Hsiao, S. Amnuaypornsri, and J. Sakdapipanich, Polymer . **50**, 2142 (2009).

37. N. Phewthongin, P. Saeoui, and C. Sirisinha, Polym. Test. **24**, 227 (2005).

38. M. A. Mansilla, J. L. Valentín, M. A. L. Manchado, A. G. Jiménez and A. J. Marzocca, Eur. Polym. J. **81**, 365 (2016).

39. P. R. Hornsby, Adv. Polym. Sci. **139**, 155 (1999).

40. L. Bokobza, Macromol. Mater. Eng. **289**, 607 (2004).

41. S. Joly, G. Garnaud, R. Ollitrault, and L. Bokobza,Chem. Mater. **14**,pp 4202 (2002).

42. S. Venkatanarasimhan and D. Raghavachari, J. Mater. Chem. A **1**, 868 (2013).

43. K. Singha, J. Safety Eng.**1**, 7(2012).

44. B. Longstreth, Ind. Eng. Chem. **32**, 1156 (1940).

45. J. Karger-Kocsis, L. Mészáros and T. Bárány, J. Mater. Sci. **48**, 1 (2013).

46. M. T. Ramesan, R. Alex and N. V. Khanh, React. Funct. Polym. **62**, 41 (2005).

47. A. Malas and C. K. Das, Compos. Part B Eng. **79**, 639 (2015).

48. P. B. Smith, A. J. Pasztor, M. L. McKelvy, D. M. Meunier, S. W. Froelicher and F. C.Y. Wang, Anal. Chem. **71**, 61 (1999).

49. S. O. A. Gomez, C. Erisken, L.K.U. Yilmazer and F. Pekel, J. Appl. Polym. Sci. **67**, (1998).

50. C. Oommen and S. R. Jain and J. Hazard. Mater. **67**, 253 (1999).

51. S. A. Rashkovskii, Y. M. Milekhin and A. V. Fedorychev, Combustion, Explosion, and Shock Waves. **53,** 652 (2017).

52. S. R. Jain, J. Sci. Ind. Res. **61**, 899 (2002).

53. N. K. Hamadi, X. D. Chen, M. M. Farid and M. G. Q. Lu, Chem. Engi. J. **84**, 95 (2001).

54. M. Norouzi, Y. Zare, and P. Kiany, Polym. Rev. **55**, 531 (2015).

55. N. Rattanasom, U. Thammasiripong, and K. Suchiva, J. Appl. Polym. Sci. **97**, 1139 (2005).

56. A. Zubov, J. Pokorny, and J. Kosek, Chem. Eng. J. **207**–**208**, 414 (2012).

57. A. Ciesielski, An Introd. to Rubber Technol. iSmithers Rapra Publishing. **44**, 0 (1999).

58. J. V. Vanderhoff, J. Polym. Sci. Polym. Symp. **72**, 161 (1985).

59. A. B. Luximon, D. Jhurry, N. Spassky, S. Pensec and J. Belleney, Polymer. **42**, 9651 (2001).

60. V. M. Il'in and A. K. Rezova, Int. Polym. Sci. Technol. **42**, 35 (2015).

61. G. W. Harding and A. J. Van Reenen, Eur. Polym. J. **47**, 70 (2011).

62. J. Herzberger, K. Niederer, H. Pohlit, J. Seiwert, M. Worm, F. R. Wurm and H. Frey, Chem. Rev. **116**, 2170 (2016).

63. K. Sahakaro, N. Naskar, R. N. Datta and J. W. M. Noordermeer, J. Appl. Polym. Sci. **103**, 2538 (2007).

64. L. Qu, G. Huang, P. Zhang, Y. Nie, G. Weng and J. Wu, Polym. Int. **59**, 1397 (2010).

65. H. Ismail and H. S. Ahmad, J. Elastomers Plast. **46**, 483 (2014).

66. J. X. Li and C. M. Chan, Polymer. **42**, 6833 (2001).

67. A. Choudhury, A. K. Bhowmick and M. Soddemann, J. Appl. Polym. Sci. **128**, 2556 (2013).

68. Y. Liang, W. Cao, Z. Li, Y. Wang, Y. Wu and L. Zhang, Polym. Test. **27**, 270 (2008).

69. Y. Li, Y. Zhang and Y. X. Zhang, Polym. Test. **22**, 859 (2003).

70. D. Bodas, J. Y. Rauch and C. K. Malek, Eur. Polym. J. **44**, 2130 (2008).

71. A. Wilford, T. C. P. Lee and T. J. Kemp, Int. J. Adhes. Adhes. **12**, 171 (1992).

72. G. Marković, B. Radovanović, J. B. Simendić, and M. M. Cincović, J. Serbian Chem. Soc. **70**, 695 (2005).

73. J. Shu, R. Xia, J. Qian, J. Miao, L. Su, M. Cao, H. Lin, P. Chen and J. Chen, Macromol. Res. **24**, 640 (2016).

74. Q. Ma and K. L. Wooley, J. Polym. Sci. Part A Polym. Chem. **38**, 4805 (2000).

75. O. Colombani, M. Ruppel and F. Schubert, Macromolecules **40**, 4338 (2007).

76. B. P. Michalak, R. Lisowska and A. Balas, J. Elastomers Plast. **26**, 327 (1994).

77. S. C. G. Da Costa and M. I. Felisberti, J. Appl. Polym. Sci. **72**, 1835 (1999).

78. J.C.Brosse, I.Campistron, D.Derouet, A.E.Hamdaoui, S.Houdayer, D.Reyx andS.R. Gillier, J.ofAppl. Polym.Sci.**78**,1461(2000).

79. R. Stephen, S. Varghese, K. Joseph, Z. Oommen, and S. Thomas, J. Memb. Sci. **282**, 162 (2006).

80. M. T. Ramesan, React. Funct. Polym. **59**, 267 (2004).

81. P.M. Berthalot, Bull. La Soc. Chime Fr. **11**, 33 (1869).

82. K. Simma, G. L. Rempel and P. Prasassarakich, Polym. Degrad. Stab. **94**, 1914 (2009).

83. K. I. Elizabeth, R. Alex, B. Kuriakose, S. Varghese and N. R. Peethambaran, J. Appl. Polym. Sci. **101**, 4401 (2006).

84. N. K. Singha, S. Bhattacharjee and S. Sivaram, Rubber Chem. Technol. **70**, 309 (1997).

85. K. Ongwongsakul, G. L. Rempel, S. Poompradub and N. Hinchiranan, J. Appl. Polym. Sci. **134**, (2017).

86. C.O. Weber, Chem. Ber. **33**, 779 (1900).

87. C.D. Harries, Chem. Ber. **56**, 1048 (1923).

88. F.W. Hinrichsen, H. Quensell and Kindschen, Cheische Berichte **46**, 1283 (1913).

89. C.D. Harries, Chem. Ber. **46**, 733 (1913).

90. DHE. Tom, J.Appl.Polm.Sci **20**, 381 (1956).

91. R. Pummerer and P.A. Burkard, Chem. Ber. **55**, 3458 (1922).

92. C. Rouse, R. Pautrat, R. Cheriatat, F. Lederan, J. C. Danijard, R.Pautrat and R.Cheriatat, J.Appl.Polm.Sci. Part C **16**, 4687 (1969).

93. I. R. Gelling and N. J. Morrison, Rubber Chem. Technol. **58**, 243 (1985).

94. Y. Tanaka and L. Tarachiwin, Rubber Chem. Technol. **82**, 283 (2009).

95. G. T. Knight, B. Pepper, Tetrahedron **27**, 6201 (1971).

96. D. Barnard, Rubber Dev. **28**, 58 (1975).

97. R.G. Bacon and E.H Farmer, Rubb.Chem.Technol **12**, 200 (1939).

98. C.Pinazzi, J.C. Danjard and R.Pautrat, Rubb.Chem.Technol **36**, 282 (1963).

99. C. Nakason, S. Saiwaree, S. Tatun, and A. Kaesaman, Polym. Test. **25**, 656 (2006).

100. M.A Goulb, J.Appl.Polm.Sci **25**, 373 (1957).

101. C. W. Bedford and H. A. Wilkinson, Syst. Surv. Rubber Chem. Chem. Cat. Co. New York (1923).

102. J. Tangpakdee Sakdapipanich, T. Kowitteerawut, S. Kawahara and Y. Tanaka, J. Rubb. Res **4**, 1 (2001).

103. D. Derouet, P. Intharapat, Q. N. Tran, F. Gohier and C. Nakason, Eur. Polym. J. **45**, 820 (2009).

104. D.C. Blackley, Polymer Lattices, Chapman Hall London **2**, ch: 14 (1997).

105. D. Roy, M. Semsarilar, J. T. Guthrie and S. Perrier, Chem. Soc. Rev. **38**, 2046 (2009).

106. R.S. Lehrle and S.L Willis, Polymer. **38**, 5937 (1997).

107. X. Fukushima , Y. Kawahara s Tanaka, J Rubb Res **1**, 154 (1988).

108. H. Hashim, N. I. Adam, N. H. M. Zaki, Z. S. Mahmud, C. M. S. Said, M. Z. A. Yahya, and A. M. M. Ali,Int. Conf. Sci. Soc. Res. pp. 485–488 (2010).

109. D. J. Hourston and J. Romaine, J. Appl. Polym. Sci. **43**, 2207 (1991).

110. N. Subramaniam, M. J. Monteiro, J. R. Taylor, A. S. Gomes and R. G. Gilbert, Macromol. Symp. **152**, 43 (2000).

111. F. P. La Mantia and M. Morreale, Compos. Part A Appl. Sci. Manuf. **42**, 579 (2011).

112. Gibson, F.A. Ronald, O.W. Emmanuel and Y. Feng, Compos. Sci. Technol. **67**, 1 (2007).

113. A. J. Crosby and J. Lee, Polym. Rev. **47**, 217 (2007).

114. R. Hemanth, B. Suresha and M. Sekar, J. Comp. Mat. **49**, 2217 (2014).

115. J. Cho, A. R. Boccaccini and M. S. P. Shaffer, J. Mater. Sci. **44**, 1934 (2009).

116. N. Saheb, Z. Iqbal, A. Khalil, A. S. Hakeem, N. Al Aqeeli, T. Laoui, A. Al-Qutub and R. Kirchner, J. Nanomater. **2012**, (2012).

117. Q. Yuan and R. D. K. Misra, Mater. Sci. Technol. **22**, 742 (2006).

118. M. Z. Rong, M. Q. Zhang and W. H. Ruan, Mater. Sci. Technol. **22**, 787 (2006).

119. L. M. Hamming, R. Qiao, P. B. Messersmith and L. Catherine Brinson, Compos. Sci. Technol. **69**, 1880 (2009).

120. D. Ciprari, K. Jacob and R. Tannenbaum, Macromolecules **39**, 6565 (2006).

121. V. Mittal, Macromol. Mater. Eng. **299**, 906 (2014).

122. H. Liu and L. C. Brinson, Compos. Sci. Technol. **68**, 1502 (2008).

123. E. P. Giannelis, Adv. Mater. **8**, 29 (1996).

124. D. R. Paul and L. M. Robeson, Polymer. **49**, 3187 (2008).

125. R. Rudolf, P. Mitschang, and M. Neitzel, Compos. Part A Appl. Sci. Manuf. **31**, 1191 (2000).

126. E. J. Garcia, D. S. Saito, L. Megalini, a J. Hart, R. G. De Villoria, and B. L. Wardle, Composites **1**, 1 (2009).

127. Kim, J. K. Pal, Koushik and V. Sridhar, Adv. Struct. Mater. **9**, 3 (2011).

128. Y. P. Wu, Q. X. Jia, D. S. Yu and L. Q. Zhang, J. Appl. Polym. Sci. **89**, 3855 (2003).

129. J. T. Kim, T. S. Oh and D. H. Lee, Polym. Int. **52**, 1058 (2003).

130. M. A. Kader, K. Kim, Y. S. Lee, and C. Nah, J. Mater. Sci. **41**, 7341 (2006).

131. A. Das, R. Jurk, K. W. Stöckelhuber, P. Sen Majumder, T. Engelhardt, J. Fritzsche, M. Klüppel and G. Heinrich, J. Macromol. Sci. Part A **46**, 7 (2008).

132. S. M. R. Paran, G. Naderi, and M. H. R. Ghoreishy, Appl. Surf. Sci. **382**, 63 (2016).

133. J. Fritzsche, A. Das, R. Jurk, K. W. Stöckelhuber, G. Heinrich and M. Klüppel, Express Polym. Lett. **2**, 373 (2008).

134. M. Salehi and M. R. Kashani, J. Appl. Polym. Sci. **126**, 253 (2012).

135. L. Zhang, Y. Wang, Y. Wang, Y. Sui, and D. Yu, Polymer. 1873 (2000).

136. L. Ji, T. Zhang, K. L. Milliken, J. Qu, and X. Zhang, Appl. Geochemistry **27**, 2533 (2012).

137. M. S. Zoromba, A. A. M. Belal, A. E. M. Ali, F. M. Helaly, A. A. A. El-Hakim and A. S. Badran, Polym. - Plast. Technol. Eng. **46**, 529 (2007).

138. L. E. Yahaya, K. O. Adebowale, A. R. R. Menon, and S. Rugmini, Afr. J. Pure Appl. Chem. **4**, 198 (2010).

139. L. D. Perez, M. A. Zuluaga, T. Kyu, J. E. Mark and B. L. Lopez, Polym. Eng. Sci. **49**, 866 (2009).

140. P. Verge, S. Peeterbroeck, L. Bonnaud and P. Dubois, Compos. Sci. Technol. **70**, 1453 (2010).

141. X.H. Chen, and Song H.H, New Carbon Mater. **19**, 204 (2004).

142. X. Zhou, Y. Zhu, Q. Gong and J. Liang, Mater. Lett. **60**, 3769 (2006).

143. Y. Zhan, J. Wu, H. Xia, H.N. Yan, G. Fei, and G. Yuan, Macromol. Mater. Eng. **296,** 590 (2011).

144. B. Ozbas, S. Toki, B. S. Hsiao, B. Chu, R. A. Register, I. A.

Aksay, R. K. P. Homme and D. H. Adamson, J. Polym. Sci. Part B Polym. Phys. **50**, 718 (2012).

145. L.L Wang, L.Q Zang and M Tian, Wear **85**, 276 (1912).

146. M. Tanahashi, Materials. **3**, 1593 (2010).

147. M. Alexandre and P. Dubois, Mater. Sci. Eng. R: Reports **28**, 1 (2000).

148. H. O. Pierson, Handb. Carbon, Graph. Diam. Fullerenes. 25 (1993).

149. S. Lijima and T. Ichihashi, Nature **363**, 603 (1993).

150. D. Zhang, L. Shi, J. Fang, X. Li and K. Dai, Mater. Lett. **59**, 4044 (2005).

151. Y. H. Liu, F. Wang, J. Hoy, V. L. Wayman, L. K. Steinberg, R. A. Loomis, and W. E. Buhro, J. Am. Chem. Soc. **134**, 18797 (2012).

152. P. C. Sercel and K. J. Vahala, Phys. Rev. B **42**, 3690 (1990).

153. M. Z. Jacobson, Nature **409**, 695 (2001).

154. Sun, J.T. Hong and C.Y. Pan, Polym. Chem. **2**, 998 (2011).

155. J. A. Rogers, Nat. Nanotechnol **3**, 254 (2008).

156. K.J. Yu, Z. Yan, M. Han and J.A. Rogers, npj Flexible Electronics. **4**, 1 (2017).

157. K. Taniguchi, N. Abe, T. Takenobu, Y. Iwasa, and T. Arima, Phys. Rev. Lett. **97**, (2006).

158. S. Dey, R. a. Ricciardo, H. L. Cuthbert, and P. M. Woodward, Inorg. Chem. **53**, 4394 (2014).

159. M. T. Ramesan, V. P. Abdu Raheem, P. Jayakrishnan, and P. P. Pradyumnan, AIP Conf. Proc. **1620**, 3 (2014).

160. S. Saranyaa, R. K. Selvana and N. Priyadharsisni, Appl. Surf. Sci. **258**, 4881 (2012).

161. J.Y. Liao and K.C. Ho, Sol. Energy Mater. Sol. Cell, **86**, 229 (2005).

162. Y. Li, X. He, and M. Cao, Mater. Res. Bull. **43**, 3100 (2008).

163. A.J. Hoffman and G. Mills, J. Phys. Chem. **96**, 5546-5552, (1992).

164. X. Wang, H. Huang, B. Liang, Z. Liu, D. Chen and G. Shen, Crit. Rev. Solid State Mater. Sci. **38**, 57 (2013).

165. M. T. Ramesan, A. Nihmath and J. Francis, AIP Conf. Proc. **1536**, 255 (2013).

166. V. C. Jasna and M. T. Ramesan, J. Inorg. Organomet. Polym. Mater. **27**, 968 (2017).

167. M. T. Ramesan and R. Alex, J. Appl. Polym. Sci. **68**,153(1998).

168. H. J. Maria, N. Lyczko, A. Nzihou, C. Mathew, S. C. George, K. Joseph, and S. Thomas, J. Mater. Sci. **48**, 5373 (2013).

169. Q. Liu, Y. Zhang, and H. Xu, Appl. Clay Sci. **42**, 232 (2008).

170. M. Jacob, K. T. Varughese, and S. Thomas, J. Mater. Sci. **41**, 5538 (2006).

171. K. Suhailath and M. T. Ramesan, J. Mater. Sci. Mater. Electron. **28**, 13797 (2017).

172. H. N. Pazhooh, R. Bagheri and A. Adloo, Polym. (United Kingdom) **108**, 135 (2017).

173. P. Jayakrishnan and M. T. Ramesan, Polym. Bull. **74**, 3179 (2017).

174. E. Jayamani, S. Hamdan, M. R. Rahman and M. K. Bin Bakri, Mater. Today Proc. **2**, 2757 (2015).

175. B. Seentrakoon, B. Junhasavasdikul and W. Chavasiri, Polym. Degrad. Stab. **98**, 566 (2013).

176. M. J. Jiang, Z. M. Dang, and H. P. Xu, Eur. Polym. J. **43**, 4924 (2007).

177. M. T. Ramesan, V. Nidhisha and P. Jayakrishnan, Mater. Sci. Semicond. Process. **63**, 253 (2017).

178. Y. Zhang, Q. Zhang, Q. Liu, H. Cheng and R. L. Frost, J. Therm. Anal. Calorim. **115**, 1013 (2014).

179. A. Zanchet, L. N. Carli, M. Giovanela, R. N. Brandalise and J. S. Crespo, Mater. Des. **39**, 437 (2012).

180. L. Guo, G. Huang, J. Zheng and G. Li, J. Therm. Anal. Calorim. **116**, 359 (2014).

181. H. H. Hassan, E. Ateia, N. A. Darwish, S. F. Halim and A. K. Abd El-Aziz, Mater. Des. **34**, 533 (2012).

182. S. Mishra and N. G. Shimpi, J. Appl. Polym. Sci. **98**, 2563 (2005).

183. D. R. Paul and L.M. Robeson, Polymer. **49**, 3187 (2008).

184. M. Liu, Z. Jia, D. Jia and C. Zhou, Prog. Polym. Sci. **39**, 1498 (2014).

185. M. T. Ramesan, Int. J. Plast. Technol. **19**, 368 (2015).

186. Q. T. Nguyen and D. G. Baird, Adv. Polym. Technol. **25**, 270 (2006).

187. B. Xu, Q. Zheng, Y. Song, and Y. Shangguan, Polymer. **47**, 2904 (2006).

188. A. Sorrentino, M. Tortora and V. Vittoria, J. Polym. Sci. Part B Polym. Phys. **44**, 265 (2006).

189. V. C. Jasna and M. T. Ramesan, AIP Conf. Proc. **1849**, 020044-1 (2017).

190. S. Kango, S. Kalia, A. Celli, J. Njuguna, Y. Habibi and R. Kumar, Prog. Polym. Sci. **38**, 1232 (2013).

191. A. Stroyuk, A. Raevskaya, A. Korzhak and S. Kuchmii, J. Nanoparticle Res. **9**, 1027 (2007).

192. S. Mitra, S. Chattopadhyay and A. K. Bhowmick, Polym. Compos. **32**, 103 (2011).

193. L. Flandin, A. Chang, S. Nazarenko, A. Hiltner, and E. Baer, J. Appl. Polym. Sci. **76**, 894 (2000).

194. M. T. Ramesan and T. Sampreeth, J. Mater. Sci. Mater. Electron. **28**, 16181 (2017).

195. A. Dasari, Z. Z. Yu, Y. W. Mai and S. Liu, Nanotechnology **18**, 445602- 1 (2007).

196. D. W. van Krevelen, Polymer. **16**, 615 (1975).

197. T. Johnson and S. Thomas, Polymer. **41**, 7511 (2000).

198. M. T. Ramesan and K. Surya, Polym. Compos. (2016).

199. K. Suhailath, M. T. Ramesan, B. Naufal, P. Periyat, V. C. Jasna and P. Jayakrishnan, Polym. Bull. **74**, 671 (2017).

200. S. George, K. T. Varughese and S. Thomas, Polymer. **41**, 579 (2000).

201. C. Sareena, M. T. Ramesan and E. Purushothaman, Fibers Polym. **14**, 1674 (2013).

202. S. K. Sen, B. Dasgupta and S. Banerjee, J. Memb. Sci. **343**, 97 (2009).

203. V. C. Jasna and M. T. Ramesan, J. Mater. Sci. **53**, 8250 (2018).

204. G. Unnikrishnan, S. Thomas and S. Varghese, Polymer. **37**, 2687 (1996).

205. R. Stephen, K. Joseph, Z. Oommen and S. Thomas, Compos. Sci. Technol. **67**, 1187 (2007).

206. C. Sareena, M. P. Sreejith, M. T. Ramesan and E. Purushothaman, Polym. Bull. **72**, 1683 (2015).

207. S. Padhi, P. G. R. Achary and N. C. Nayak, Bull. Mater. Sci. **38**, 925 (2015).

208. M. Farshad and A. Benine, Polym. Test. **23**, 347 (2004).

209. A. Ladhar, M. Arous, H. Kaddami, M. Raihane, A. Kallel, M. P. F. Graça and L. C. Costa, J. Mol. Liq. **196**, 187 (2014).

210. A. Gannoruwa, M. Sumita and S. Kawahara, Polymer. **126**, 40 (2017).

211. X.W. Zhou, Y.F. Zhu and J. Liang, Mater. Res. Bull. **42**, 456 (2007).

212. Y. Meng, J. Chu, C. Liu, Z. Wei and L. Zhang, J. Appl. Polym. Sci. **131**, 1 (2014).

213. W. Chonkaew, W. Mingvanish, U. Kungliean, N. Rochanawipart and W. Brostow, J. of Nanosci. and Nanotech. **11**, 2018 (2011).

214. J. Abraham, H. J. Maria, S. C. George, N. Kalarikkal and S. Thomas, Phys. Chem. Chem. Phys. **17**, 11217 (2015).

215. I. O. Igwe and O. E. Ezeani, Int. J. Polym. Sci. **2012**, (2012).

216. Y. P. Mamunya, V. V. Davydenko, P. Pissis and E. V. Lebedev, Eur. Polym. J. **38**, 1887 (2002).

217. I. M. Alwaan and A. Hassan, Iran. Polym. J. **23**, 277 (2014).

218. C. A. Olivati, A. J. F. Carvalho, D. T. Balogh and R. M. Faria, J. Mater. Sci. **41**, 2767 (2006).

219. X. Cheng, Q. Zhao, Y. Yang, S. C. Tjong and R. K. Y. Li, J. Mater. Sci. **45**, 777 (2010).

220. M. T. Ramesan and T. Anil Kumar, J. Chil. Chem. Soc. **54**, 23 (2009).

221. M. T. Ramesan and R. Alex, Kautsch. Gummi Kunstst.**53**, 596 (2000).

222. A. Pich, J. Hain, Y. Prots and H. J. Adler, Polymer. **46**, 7931 (2005).

223. Y. Zhang, F. Lu, Z. Wang, H. Wang, M. Kong, X. Zhu and L. Zhang, Cryst. Growth Des. **7**, 1459 (2007).

224. G. Bussu and A. Lazzeri, J. Mater. Sci. **41**, 6072 (2006).

225. N. Z. Noriman and H. Ismail, J. Appl. Polym. Sci. **123**, 779 (2012).

226. M. T. Ramesan, Pet. Sci. Technol. **32**, 1775 (2014).

227. F. Laoutid, L. Bonnaud, M. Alexandre, J. M. Lopez-Cuesta, and P. Dubois, Mater. Sci. Eng. R Reports **63**, 100 (2009).

228. M. T. Ramesan, Pet. Sci. Technol. **32**, 1775 (2014).

229. W.G. Hwang, K.H. Wei and C.M. Wu, Polym. Eng. Sci. **44**, 2117 (2004).

230. X. L. Ji, J. K. Jing, W. Jiang and B. Z. Jiang, Polym. Eng. Sci. **42**, 983 (2002).

231. F. Stadlbauer, T. Koch, F. Planitzer, W. Fidi and V. M. Archodoulaki, Polym. Test. **32**, 1045 (2013).

232. M. M. Badawy and G. M. Nasr, Polym. Test. **16**, 155 (1997).

233. P. Jayakrishnan and M. T. Ramesan, J. Inorg. Organomet. Polym. Mater. **27**, 323 (2017).

234. M. T. Ramesan, J. Elastomers Plast. **46**, 303 (2014).

235. I. C. Chukwujike, C. M. Ewulonu and M. Chukwu, Int. J. Multidiscip. Res. Dev. **2**, 154 (2015).

236. Mariyamma george, Polym. Polym. Compos. **23**, 85 (2015).

237. M. Balachandran and S. S. Bhagawan, J. Polym. Res. **19**, 9809 (2012).

238. D. C. D. Nath, S. Bandyopadhyay, A. Yu, D. Blackburn and C. White, J. Mater. Sci. **45**, 1354 (2010).

239. A.M.E.S. Raj, C. Mallika, OM Sreedharan, K.S. Nagaraja, Mater. Lett. **53**, 316 (2002).

240. L. Zhang, C. Lu, Y. Wang, and Y. Cheng, Mater. Chem. Phys. **103**, 433 (2007).

241. S. Muthamizh, R. Suresh, K. Giribabu, R. Manigandan, S. Praveen Kumar, S. Munusamy and V. Narayanan, J. Alloys Compd. **619**, 601 (2015).

242. A. Nihmath and M. T. Ramesan, AIP Conf. Proc. **1620**, 353 (2014).

243. J.W. Gilman, Appl. Clay. Sci. **15**, 31 (1999).

244. S. Chakraborty, S. Kar, S. Dasgupta, R. Mukhopadhyay, S. Bandyopadhyay, M. Joshi and S. C. Ameta, Polym. Test. **29**, 181 (2010).

245. E. Osabohien and S. H. Egboh, J. Appl. Sci. Environ. Manag. **11**, 43 (2007).

246. P. Jayakrishnan and M. T. Ramesan, Mater. Chem. Phys. **186**, 513 (2017).

247. G. C. Psarras, Compos. Part A Appl. Sci. Manuf. **37**, 1545 (2006).

248. A. B. Oskouyi, U. Sundararaj, and P. Mertiny, Materials. **7**, 2501 (2014).

249. C. Sareena, M. T. Ramesan, and E. Purushothaman, J. Appl. Polym. Sci. **125**, 2322 (2012).

250. A. Sujith and G. Unnikrishnan, J. Mater. Sci. **40**, 4625 (2005).

251. J. Wang, W. Wu, W. Wang and J. Zhang, J. Polym. Res. **18**, 1023 (2011).

252. S. Kar, P. K. Maji and A. K. Bhowmick, J. Mater. Sci. **45**, 64 (2010).

253. M. Gómez, B. Diego, P. Humberto and R. Quijada, Polym. Int. **64**, 1245 (2015).

254. H. J. Ye, W. Z. Shao and L. Zhen, J. Appl. Polym. Sci. **129**, 2940 (2013).

255. C. Wan and B. Chen, J. Mater. Chem. **22**, 3637 (2012).

256. K. Lee, Carbon N. Y. **9**, 5235 (2004).

257. U. Schubert, Polym. Int. **58**, 317 (2009).

258. Y. Changjie, Q. Zhang, G. Junwei, Z. Junping, S. Youqiang and W. Yuhang, J. Polym. Res. **18**, 2487 (2011).

259. H. Li, J. Sun, Y. Song and Q. Zheng, J. Mater. Sci. **44**, 1881 (2009).

260. M. Ahmadi and A. Shojaei, Polym. Int. **64**, 1627 (2015).

261. M. F. H. Al-Kadhemy, R. Hussein and A. A. D. Al-Zuky, J. Phys. Sci. **23**, 89 (2012).

262. V. C. Jasna, T. Anilkumar, G. Mathew and M. T. Ramesan, **53**, 9861 (2018).

263. M. T. Ramesan and R. Alex, PolymInt.**50,** 1298(2001).

264. S. Lakshminarayanan, G. A. Gelves and U. Sundararaj, J. Appl. Polym. Sci. **124**, 5056 (2012).

265. L. Jong, Eur. Polym. J. **74**, 136 (2016).

266. T. Sampreeth, M. A. Al-Maghrabi, B. K. Bahuleyan and M. T. Ramesan, J. Mater. Sci. **53**, 591 (2017).

267. M.T. Ramesan, J. Thermoplast. Compos. Mater.**28**, 1286 (2015).

268. C. G. Koops, Phys. Rev. **83**, 121 (1951).

269. M. T. Ramesan and V. Santhi, J. Mater. Sci. Mater. Electron. **28**, 18804 (2017).

270. S. C. George, M. Knörgen, and S. Thomas, J. Memb. Sci. **163**, 1 (1999).

271. K. A. Moly, S. S. Bhagawan, S. C. George, and S. Thomas, J. Mater. Sci. **42**, 4552 (2007).

272. V. G. Geethamma and S. Thomas, Polym. Compos. **26**, 136 (2005).

LIST OF PUBLICATIONS

1. V. C. Jasna and M. T. Ramesan, Fabrication of novel nanocomposites from styrene butadiene rubber/zinc sulphide nanoparticles, J. Mater. Sci. **53**, 8250 (2018).

2. V. C. Jasna, T. Anilkumar and M. T. Ramesan, Nanocomposite materials based on zinc sulfide nanoparticles reinforced chlorinated styrene butadiene rubber, J. Appl. Polym. Sci. **135**, 46538, (2018).

3. V. C. Jasna, T. Anilkumar, Adarsh A. Naik and M. T. Ramesan, Chlorinated Styrene Butadiene Rubber/ Zinc Sulfide: Novel Nanocomposites with Unique Properties- Structural, Flame Retardant, Transport and Dielectric Properties, J. Polym. Res.**25,**144 (2018).

4. V. C. Jasna and M. T. Ramesan, Studies on the Mechanical, Electrical Properties and Interaction of Petroleum Fuels with SBR/ Manganous Tungstate Nanocomposites, J. Inorg. Organomet. Polym. Mater. **27**, 968 (2017).

5. V. C. Jasna and M. T. Ramesan, Preparation, characterization, dielectric properties and diffusion studies of styrene butadiene rubber (SBR)/manganous tungstate (MnWO4) nanocomposites, AIP Conf. Proc. **1849**, (2017).

6. V. C. Jasna, T. Anilkumar, G. Mathew and M.T. Ramesan, Novel nanocomposites based on chlorinated styrene butadiene

rubber and manganous tungstate: focus on curing, mechanical, electrical and solvent transport properties, J. Mater. Sci. **53**, 9861 (2018).

7. V. C. Jasna, K. Priyanka, G. Mathew, and M. T. Ramesan, Evaluation of Spectral, Thermal, Flame Retardant, Dielectric, Solvent Diffusion, and Transport Behavior of Novel Nanocomposite Derived from Chlorinated Styrene Butadiene Rubber and Manganous Tungstate, Polym. Compos. DOI 10.1002/pc.24846(2018).

8. V. C. Jasna and M. T. Ramesan, Preparation, Characterization, dielectric properties and solvent imbibing behavior of styrene butadiene rubber/zinc sulfide nanocomposites, Int. J. Plast. Tech. **22**, 217-233 (2018).

9. V. C. Jasna and M. T. Ramesan, Diffusion and transport of aromatic hydrocarbons through SBR/chemically modified fly ash composites, J. Chem. Pharm. Sci., special issue. **45** (2016).

10. M. T. Ramesan, V. C. Jasna, J. Francis, A. R. V P, and M. Subburaj, Preparation of Zinc and Calcium Silicate Modified Fly Ash/Styrene Butadiene Rubber Composites, The Chemist, **88**, 1 (2015).

11. K. Suhailath, P. Jayakrishnan, B. Naufal, P. Periyat, V. C. Jasna, and M. T. Ramesan, Synthesis by In Situ-Free Radical Polymerization, Characterization, and Properties of Poly (n-butyl methacrylate)/Samarium-Doped Titanium Dioxide

Nanoparticles Composites, Adv. Polym. Technol. DOI10.1002/adv.21770(2016).

12. K. Suhailath, M. T. Ramesan, B. Naufal, P. Periyat, V. C. Jasna, and P. Jayakrishnan, Synthesis, characterisation and flame, thermal and electrical properties of poly (n-butyl methacrylate)/ titanium dioxide nanocomposites, Polym. Bull. **74**, 671 (2017).

Presentations

1. V. C. Jasna and M. T. Ramesan, Diffusion and transport of aromatic hydrocarbons through SBR/chemically modified fly ash composites, **UGC Sponsered National Seminar on** "Crystallography: Special Emphasis on Applications in Chemistry". N.S.S. College, Manjeri on 6th and 7th January 2016.

2. V. C. Jasna and M. T. Ramesan, Preparation, characterization, dielectric properties and diffusion studies of styrene butadiene rubber (SBR)/manganous tungstate (MnWO4) nanocomposites, ***Optics '17, A Conference on Light***. NIT Calicut, 9-11th January, 2017.